Universidad de Málaga
Facultad de Ciencias
Departamento de Ingeniería Química
Doctoral thesis

Bifunctional activated carbon-based catalysts for raw bio-oil hydrodeoxygenation

Author:
Tomás Cordero-Lanzac

Supervisors:
Prof. José Rodríguez-Mirasol
Prof. Javier Bilbao

Programa de doctorado:
Química y Tecnologías Químicas. Materiales y Nanotecnología

2021

UNIVERSIDAD
DE MÁLAGA

UNIVERSIDAD
DE MÁLAGA

AUTOR: Tomás Cordero Lanzac

https://orcid.org/0000-0002-1365-931X

EDITA: Publicaciones y Divulgación Científica. Universidad de Málaga

BY NC ND

Esta obra está bajo una licencia de Creative Commons Reconocimiento-NoComercial-SinObraDerivada 4.0 Internacional:
http://creativecommons.org/licenses/by-nc-nd/4.0/legalcode
Cualquier parte de esta obra se puede reproducir sin autorización
pero con el reconocimiento y atribución de los autores.
No se puede hacer uso comercial de la obra y no se puede alterar, transformar o hacer obras derivadas.

Esta Tesis Doctoral está depositada en el Repositorio Institucional de la Universidad de Málaga (RIUMA): riuma.uma.es

UNIVERSIDAD
DE MÁLAGA

UNIVERSIDAD
DE MÁLAGA

ANDALUCÍA TECH
Campus de Excelencia Internacional

Escuela de Doctorado

DECLARACIÓN DE AUTORÍA Y ORIGINALIDAD DE LA TESIS PRESENTADA PARA OBTENER EL TÍTULO DE DOCTOR

D./Dña TOMÁS CORDERO LANZAC
Estudiante del programa de doctorado QUIMICA Y TECNOLOGÍA QUÍMICA, MATERIALES Y NANOTECNOLOGÍA de la Universidad de Málaga, autor/a de la tesis, presentada para la obtención del título de doctor por la Universidad de Málaga, titulada: BIFUNCTIONAL ACTIVATED CARBON-BASED CATALYSTS FOR RAW BIO-OIL HYDRODEOXYGENATION

Realizada bajo la tutorización de D. JOSÉ RODRÍGUEZ MIRASOL y dirección de D. JAVIER BILBAO ELORRIAGA (si tuviera varios directores deberá hacer constar el nombre de todos)

DECLARO QUE:

La tesis presentada es una obra original que no infringe los derechos de propiedad intelectual ni los derechos de propiedad industrial u otros, conforme al ordenamiento jurídico vigente (Real Decreto Legislativo 1/1996, de 12 de abril, por el que se aprueba el texto refundido de la Ley de Propiedad Intelectual, regularizando, aclarando y armonizando las disposiciones legales vigentes sobre la materia), modificado por la Ley 2/2019, de 1 de marzo.

Igualmente asumo, ante a la Universidad de Málaga y ante cualquier otra instancia, la responsabilidad que pudiera derivarse en caso de plagio de contenidos en la tesis presentada, conforme al ordenamiento jurídico vigente.

En Málaga, a 10 de ENERO de 2021

Fdo.: TOMÁS CORDERO LANZAC

UNIVERSIDAD
DE MÁLAGA

UNIVERSIDAD
DE MÁLAGA

UNIVERSIDAD
DE MÁLAGA

D. JOSÉ RODRÍGUEZ MIRASOL, Catedrático de Ingeniería Química de la Universidad de Málaga,

D. JAVIER BILBAO ELORRIAGA, Catedrático de Ingeniería Química de la Universidad del País Vasco,

CERTIFICAN: Que el trabajo de investigación recogido en la presente Memoria ha sido realizado bajo su dirección en el Departamento de Ingeniería Química de la Universidad de Málaga por D. TOMÁS CORDERO LANZAC, y reúne, a su juicio, contenido científico suficiente y las condiciones necesarias para ser presentado y defendido ante el Tribunal correspondiente para optar al Grado de Doctor en la Universidad de Málaga.

Málaga, enero 2021

Fdo: JOSÉ RODRÍGUEZ MIRASOL

Fdo: JAVIER BILBAO ELORRIAGA

UNIVERSIDAD
DE MÁLAGA

UNIVERSIDAD
DE MÁLAGA

Abstract

This thesis is focused on the hydrodeoxygenation (HDO) of raw bio-oil, the liquid product of lignocellulosic biomass fast pyrolysis. HDO is a route for the valorization of this interesting renewable source, whose direct application is not allowed due to its high oxygen content. The aim of this work is to contribute to the development of a biorefinery process through the proposal of suitable catalysts, the understanding of reaction-deactivation mechanisms and the development of a kinetic model that considers the fast deactivation. The used bifunctional catalysts for HDO are based on activated carbon (AC) as a support, which derives from olive stone, also a lignocellulosic biomass waste, and was prepared by chemical activation of the olive stone with H_3PO_4. The resulting support (ACP) presents a well-developed micro- and mesoporous structure, suitable for achieving a good dispersion of the metallic function. Moreover, it presents stable acid sites, provided by the surface P-groups that are anchored to the carbon structure during the activation process. Three different bimetallic catalysts were prepared by incipient wetting impregnation of noble (PtPd) and transition metals (NiW and CoMo) over the ACP support. The activity, selectivity, and stability of these catalysts were tested and their performance were compared to that of a PtPd catalyst with a HY zeolite support.

The experimental HDO runs were carried out in a packed bed reactor using raw bio-oil as the feed and the following reaction conditions: 400−475 °C; 65 bar; space time, 0.15−0.6 g h $\mathrm{g}_{\mathrm{bio-oil}}^{-1}$; H_2/bio-oil ratio, 20000 $\mathrm{cm}_{\mathrm{H_2}}^{3}$ $\mathrm{cm}_{\mathrm{bio-oil}}^{-3}$ and time on stream, 0−10 h. A thorough characterization of the reaction products were performed using different chromatographic and spectroscopic techniques. The composition of the gaseous, liquid aqueous fraction, liquid organic fraction and solid products were analyzed. The operation in a continuous reactor allows for studying the different stages of non-steady trickled bed regime. At low temperature or space time values, the catalysts are quickly deactivated by the deposition of carbonaceous deposits. However, at most of the studied conditions, they undergo an initial deactivation and subsequently reach a pseudo-steady state, which is attributed to a pseudo-equilibrium in deactivation mechanisms.

The ACP support shows a surprisingly better performance than that of the HY zeolite in a reaction medium with the presence of water. The higher hydrothermal stability and better dispersion of the metallic function, offered by the ACP-supported catalysts lead to high hydrogenation and hydrodeoxygenation activity.

UNIVERSIDAD
DE MÁLAGA

Then, an aqueous liquid fraction with high concentrations of water and methanol as the main organic compound is attained. The organic fraction is mainly formed by aromatic compounds (1 and 2-ring) due to the condensation of light reactants on the acid sites of the catalyst. On the other hand, the transition metal-based catalysts exhibit a moderate hydrodeoxygenation activity, which enhances the production of high value-added chemicals as aromatics and phenols. The addition of HZSM-5 zeolite to the catalytic bed also improve the yields of these 1-ring aromatic compounds due to its shape selectivity.

After the reactions, analysis of the carbonaceous solid deposited during the raw bio-oil HDO were performed in order to specifically study the location, nature and origin of the deactivating species. Two main species are identified on the surface of the catalyst. On the one hand, a carbonaceous species with aliphatic structure and oxygen functionalities, which is deposited on the external surface. On the other hand, a polyaromatic species, located within the micropores of the catalyst, presumably near to the active sites. The formation mechanism of the former is thermal, and it is promoted at low temperatures and using transition metal catalysts. Due to its nature and structure, this carbonaceous species is named thermal lignin (TL). Otherwise, coke is formed from the condensation of hydrocarbons promoted by the acid sites of the catalyst and is named catalytic coke.

From the kinetic experimental results, an original lump-based kinetic model is proposed for the raw bio-oil HDO considering catalyst deactivation. The reaction network is described with seven lumps of compounds and eleven individual steps, accounting for reactions of different nature: (1) hydrodeoxygenation; (2) decarboxylation/decarbonylation; (3) thermal repolymerization of bio-oil towards TL; (4) condensation of aromatics towards coke structures, and; (5) aging of TL to coke. A first order concentration-independent and selective deactivation kinetic model fits the experimental evolution with time of the product distribution in the transient state, where the catalyst is partially deactivated. A simplification of the model predicts well the HDO performance during the pseudo-steady state, conditions more likely to be operated in a potential implementation of the process at a larger scale.

Overall, this thesis contributes to a better understanding of the raw bio-oil valorization through HDO. Our main proposals are: an original active, selective and stable catalyst; an in-depth study of deactivation phenomenon; establishing the required operation conditions for the production of aromatic and phenolic compounds, and; the development of a kinetic model that can be valuable for future simulation studies focused on establishing the optimal operation conditions, process strategy and scaling-up.

Acknowledgements

Me permito la licencia de comenzar los agradecimientos de esta segunda tesis de manera más informal, más familiar. Quiero agradecer a Pepe, mi padre y el *tio* Juan por haber sido fuente de inspiración y familia científica todos estos años. Muchas gracias al Prof. José Rodríguez-Mirasol por tutorizar y permitirme hacer esta tesis, así como por sus consejos tanto científicos como personales.

Al Prof. Javier Bilbao, mi mentor, y al que le debo gran parte de lo conseguido hasta ahora y de lo que pudiera llegar a conseguir. Nunca podré agradecerte la confianza y libertad de la que he dispuesto estos años.

Al Prof. Andrés T. Aguayo, el modelado cinético de esta tesis es solo una mínima parte de lo que has aportado a mi trabajo. Al Prof. José M. Arandes, Prof. Tomás Cordero y Dr. Pedro Castaño por lo que han aportado a cada uno de los capítulos de esta tesis. Y al personal de los servicios generales, Dra. María D. Marqués, Dra. María Del Valle Martínez de Yuso, Dr. Gregorio Martín, Dr. Adolfo Martínez (SCAI, UMA), Dra. Isabel Collado y Dr. Antonio Veloso (UPV/EHU).

A las tres personas sin las que esta tesis no hubiera sido posible. Al Dr. Roberto Palos, parte fundamental en el arranque y puesta a punto de este proyecto y a la Dra. Idoia Hita, apoyo muy importante para redondear los resultados que aquí se reflejan. Trabajar con vosotros ha sido realmente sencillo desde mi primer día en el laboratorio. Una mención especial merece el Dr. Francisco J. García-Mateos. Contigo di los primero pasos en un laboratorio, y desinteresadamente, me has ayudado durante estos años incluso en temas que no te correspondían. Este proyecto sería inviable sin tu colaboración y generosidad.

A los miembros del grupo Terma de la UMA por acogerme en mis visitas y considerarme uno más del grupo. Especialmente, a aquellos con los que más he compartido, Dr. José Palomo, Miguel A. Rodríguez-Cano y especialmente a la jefa, Dra. Juana M. Rosas. Igualmente, a los miembros, compañeros y amigos del grupo CPWV de la UPV/EHU, destacando a *la familia*: Dr. Aitor Atxutegi y Dr. Pablo Rodríguez-Vega.

Y finalmente, a mi familia. A mi hermana por recordarme que hay otra forma de ver la vida y a mi padre por todas sus enseñanzas. Sin embargo, si esto ha sido posible es gracias a la cultura del esfuerzo y del trabajo, que son herencia directa de mi madre. Gracias a los dos por la educación que me disteis e inculcarme los valores que me han permitido alcanzar mis objetivos hasta hoy.

Tomás Cordero-Lanzac

UNIVERSIDAD
DE MÁLAGA

La realización de esta tesis ha sido posible gracias a la financiación del Gobierno de España con los proyectos CTQ2015-68654-R, CTQ2015-67425-R y CTQ2016-79646-P y a la financiación del Gobierno Vasco con el proyecto IT1218-19.

UNIVERSIDAD
DE MÁLAGA

Al Prof. Javier Bilbao,
con motivo de su última tesis dirigida.

UNIVERSIDAD
DE MÁLAGA

UNIVERSIDAD
DE MÁLAGA

Contents

Abstract ix

Acknowledgements xi

1 Introduction 1
- 1.1 Routes for biomass valorization 2
  - 1.1.1 Bio-oil 5
  - 1.1.2 Processes for bio-oil valorization 6
- 1.2 Bio-oil hydrodeoxygenation (HDO) 14
  - 1.2.1 Catalysts 14
  - 1.2.2 HDO mechanisms 19
  - 1.2.3 Formation and deposition of carbonaceous deposits 23
  - 1.2.4 Two-stage HDO 25
- 1.3 Activated carbons 27
  - 1.3.1 Activation of lignocellulosic biomass with H_3PO_4 30
  - 1.3.2 Applications of activated carbons 34
  - 1.3.3 Carbon materials as catalyst support in HDO 37
- 1.4 Bio-oil HDO within a sustainable biorefinery 40
- 1.5 Aim and objectives 43

2 Experimental 45
- 2.1 Catalysts 46
  - 2.1.1 Preparation 46
  - 2.1.2 Characterization 47
- 2.2 Reaction unit 48
- 2.3 Analysis of bio-oil and reaction products 50

3 Evaluation of the activated carbon as acid support 53
- 3.1 Abstract 54
- 3.2 Experimental 55
  - 3.2.1 Catalysts preparation and characterization 55
  - 3.2.2 Bio-oil 57

3.2.3 Reaction equipment and procedures 57
3.3 Properties of the catalysts 59
3.4 Products yield and catalysts stability 64
3.5 Composition of the liquid fractions 69
3.6 Composition of the gas fraction 73
3.7 Composition of the solid fraction 75

4 Catalyst deactivation by coke deposition 79
4.1 Abstract 80
4.2 Experimental 81
4.2.1 Catalyst preparation 81
4.2.2 Bio-oil and liquid product characterization 81
4.2.3 HDO runs 84
4.2.4 Used catalyst characterization 85
4.3 Evolution of the conversion and composition 87
4.4 Location of deactivating species on the porous structure of the catalyst 96
4.5 Nature of deactivating species 98
4.6 Deactivation mechanism during the raw bio-oil HDO 104

5 Comparison of metallic functions and zeolite additives 107
5.1 Abstract 108
5.2 Experimental 109
5.2.1 Catalyst preparation 109
5.2.2 Catalyst characterization 109
5.2.3 Bio-oil 111
5.2.4 Hydroprocessing unit and product analysis 111
5.3 Properties of the fresh catalysts 113
5.4 Performance of the catalysts with time 117
5.5 Effect of the addition of a physically mixed zeolite 122
5.6 Catalyst deactivation 127

6 Kinetic model for the raw bio-oil HDO 135
6.1 Abstract 136
6.2 Experimental 137
6.2.1 Catalysts preparation 137
6.2.2 Catalyst characterization 137
6.2.3 Production and composition of raw bio-oil 138
6.2.4 HDO runs 139
6.3 Methodology 142
6.4 Catalyst properties 144

UNIVERSIDAD
DE MÁLAGA

6.5 Evolution with time on stream of bio-oil HDO 146
6.6 HDO reaction network 148
6.7 Kinetic model for the transient state 150
6.8 Adaptation of the kinetic model for the pseudo-steady state 157

7 General conclusions **161**

8 Resumen **167**

List of Figures **183**

List of Tables **189**

List of Schemes **191**

Nomenclature **193**

References **199**

A Related publications **217**

UNIVERSIDAD
DE MÁLAGA

UNIVERSIDAD
DE MÁLAGA

Chapter 1

Introduction

This Chapter gives a brief introduction to the technologies for the valorization of biomass through the liquid product of its pyrolysis, bio-oil. The main characteristics of this mixture of oxygenated organic compounds are discussed, as well as the different strategies for upgrading its physical properties and composition. Especially, a review of the current state of the art on bio-oil hydrodeoxygenation is discussed, including mechanistic considerations and used catalysts. In this regard, activated carbon materials are introduced as interesting porous materials for different applications, including hydrodeoxygenation. And the particular properties of those activated with H_3PO_4 are explained. The final part of this Section describes the concept of biorefinery and how this thesis can contribute to its development by using biomass-derived materials for upgrading a biomass-derived feedstock.

UNIVERSIDAD
DE MÁLAGA

1.1 Routes for biomass valorization

The valorization of lignocellulosic biomass plays a key role in the energy scenario because of the increasing energy demand and the stricter environmental restrictions, mainly related to the CO_2 emissions from fossil fuels utilization [1]. The energy consumption is expected to reach 16 000 million tons by 2040, with a share of renewable sources of approximately 40% [2]. In this scenario, biomass is an attractive renewable source of chemicals, energy, and fuels (Figure 1.1), which not only offers a more efficient alternative form a sustainability point of view, but also plays a role in the management of agricultural and forest waste. Biomass-derived feedstock is also attracting great research interest due to the foreseeable midterm depletion of fossil resources. According to the nature of the process, lignocellulosic biomass valorization strategies can be divided in three main routes: chemical, biochemical and thermochemical processes. These processes enable the development

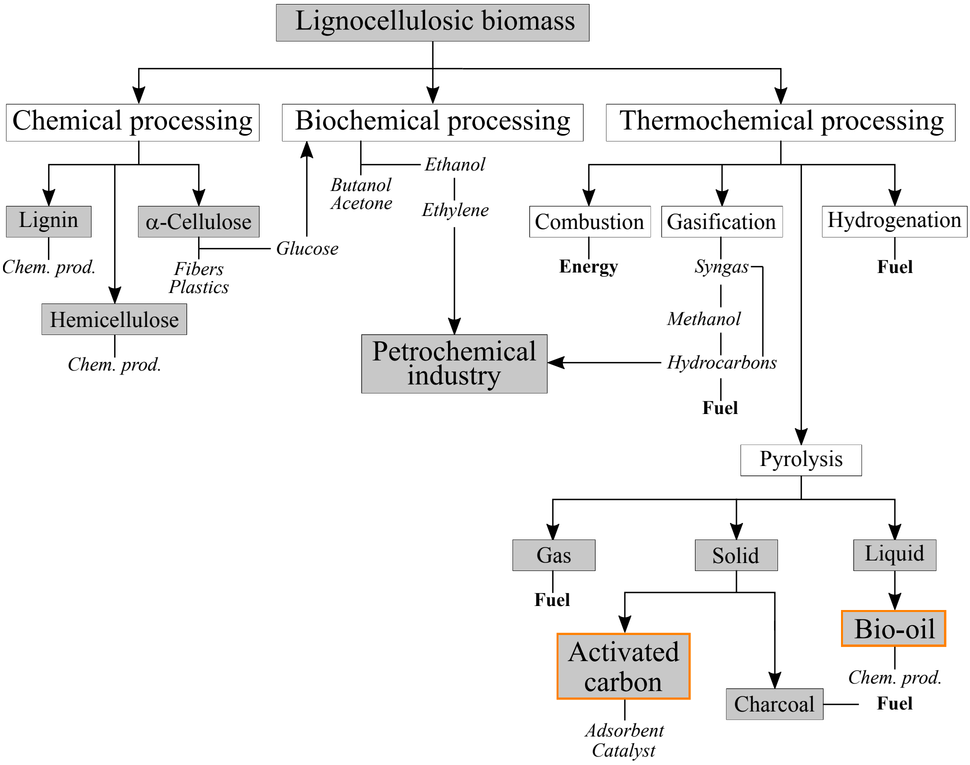
Lignocellulosic biomass
Chemical processing
Biochemical processing
Thermochemical processing
Lignin
α-Cellulose
Chem. prod.
Fibers
Plastics
Glucose
Hemicellulose
Chem. prod.
Ethanol
Butanol
Acetone
Ethylene
Petrochemical industry
Combustion
Energy
Gasification
Syngas
Methanol
Hydrocarbons
Fuel
Hydrogenation
Fuel
Pyrolysis
Gas
Fuel
Solid
Liquid
Bio-oil
Chem. prod.
Fuel
Activated carbon
Adsorbent
Catalyst
Charcoal

Fig. 1.1. Routes for the valorization of lignocellulosic biomass (adapted from [1]).

of a potential so-called biorefinery, where fossil fuels could be successfully substituted by biomass as the main resources source [3–5].

Chemical processing of lignocellulosic biomass mainly consists of hydrolysis reactions in which chemical value-added chemicals can be obtained through depolymerization of the three main biopolymers: cellulose, hemicellulose and lignin [6]. The production of bio-based monomers has caught great attention and several high-impact researches were published in the last decade, mainly focused on the possibilities of lignin as source of chemicals [7, 8]. While Jae et al. [7] and Long et al. [9] analyzed the effect of using solvents for stabilizing and increasing the yields of targeted products, Shuai et al. [8] combined chemical and thermochemical processes in order to maximize the carbon efficiency in the production of glucose, xylose and lignin.

Nonetheless, most of the researches on biomass valorization are focused on three key processes: fermentation (biochemical process), gasification and pyrolysis (both thermochemical processes) [10]. The main product of biomass fermentation is ethanol, which is a well-know fuel additive for gasoline or diesel [11, 12], and source of hydrocarbons in the fuel range, olefins (mainly ethylene) [13] and H_2 [14]. Ethanol was considered as the hypothetical key intermediate for the implementation of biorefineries because of this versatility (see the linkage with petrochemical industry in Figure 1.1). However, the feasibility of the industrial production of ethanol from biomass requires additional advances on several fronts [15], as: (i) increasing the efficiency of cellulose and hemicellulose depolymerization to fermentable sugars; (ii) developing more active and selective fermentation microorganisms; (iii) advancing in the fermentation of lignocellulosic biomass that does not interfere with human and animal feed chain [16], or; (iv) minimizing the energy requirements and improving its productivity by stage integration [17].

Biomass gasification has also received great attention in the literature because of the development of the gas-to-liquid (GTL) valorization routes [18]. The knowledge of *syngas* production from oil and coal allowed a fast and straightforward development of biomass gasification, which is mainly focused on the production of methanol, dimethyl ether (in one stage or derived from methanol) and hydrocarbons *via* methanol or *via* Fischer-Tropsh synthesis. The importance of gasification lies in the offered second linkage to the established petrochemical industry (Figure 1.1), which facilitates the use of biomass-derived chemicals. For this reason, new developments on the process have been proposed aiming for stage integration, energy optimization and cleaner operations [19]. Different reactor configurations have been used for biomass gasification, such as moving bed, bubbling fluidized bed or entrained-flow reactors [20]. One can also highlight the remarkable performance of spouted bed reactors for biomass gasification, offering optimal heat transfer between gas and solid particles and negligible bed segregation [21, 22]. Generally, the main byproduct obtained with the *syngas* is called tar, a mixture of aromatics and oxygenated heavy products, whose presence limits the valorization of *syngas*. The selectivity of the process is reported to be improved by using catalysts, which also implies studying thermodynamics, catalyst stability and deactivation kinetics for catalytic gasification [23].

The pyrolysis of lignocellulosic biomass is however reported as the most efficient route for its valorization, because of the potential of the liquid product (bio-oil) [24]. This thermochemical route consists of the decomposition of lignocellulosic biomass in the absence of oxygen, producing a liquid fraction (bio-oil), a solid waste (char), and non-condensable gases (Figure 1.1). The yield of each one depends on the pyrolysis conditions and process parameters [25]. The gaseous product does not offer other interesting application but its combustion as a fuel and the produced energy can be used to meet the energy requirements of the process [10]. Pyrolysis conditions can be tuned aiming for maximizing the yield of char. In this case, slow heating rates are used and the process is named carbonization [26]. Following this methodology, activated carbons, which are interesting materials for adsorption, catalytic and electrochemical applications, can be synthesized. The preparation methods and applications of these materials will be better detailed in Section 1.3. However, the economic viability of biomass pyrolysis mainly depends on the bio-oil utilization.

Fast pyrolysis of lignocellulosic biomass promotes high yields of bio-oil. Fast pyrolysis technology has been extensively developed and high productions of bio-oil are usually obtained using low temperatures (450−550 °C), high heating rates (10^3−10^4 °C s^{-1}) and short residence time of volatiles (<1 s). At these conditions, Sharifzadeh et al. [27] reported yields of bio-oil of 60−70% using different types of biomass. Generally, fast pyrolysis is carried out in relatively simple units and involving production costs lower than those required for competing technologies of other thermochemical routes [28, 29]. The most studied reactor configurations for biomass pyrolysis are bubbling fluidized bed reactors, circulating fluidized or dragging bed reactors, ablative reactors, conical spouted bed reactors, screw reactors and vacuum reactors [15]. Fast pyrolysis also offers promising possibilities given its limited environmental impact (limited emissions due to the low temperature), and great potential for the valorization of the resulting bio-oil [29]. The possible implementation of geographically delocalized pyrolysis units is also an advantage of this route with respect to others presented in Figure 1.1, with bio-oil being produced near to the biomass source collection and being valorized at large scale in already working refinery units [30].

1.1.1 Bio-oil

Bio-oil is a highly complex mixture of hundreds of organic oxygenated compounds with a significant concentration of water, which depends on the biomass source [31]. The concentration of water, normally ranged within 20 and 35 wt% but values up to 50 wt% has been reported for agricultural residues [10], derives from the water intrinsically contained in biomass and that released from cellulose and hemicellulose decomposition. On the other hand, oxygenates originate from the depolymerization of cellulose, hemicellulose and lignin, and include phenols, ketones, acids, esters, aldehydes, alcohols, furans, anhydrous-sugars, nitrogen-containing compounds, and carboxylic acids [32, 33]. In essence, bio-oil is a micro-emulsion of these compounds in water but also contains an oligomeric fraction of components comprising macromolecules. This aqueous and organic fraction mixture, mainly stabilized by hydrogen bonds [34], presents an average molecular weight of ca. 5000 g mol^{-1}. This factor makes difficult the quantification of bio-oil components by commonly used chromatography techniques.

Chromatography analyses coupled with mass spectrometry identification is usually combined with spectroscopic techniques, such as Fourier transformed infrared (FTIR) or nuclear magnetic resonance (NMR), thus providing more accurate information on the nature of bio-oil compounds [35, 36]. And in terms of quantification, bidimensional gas chromatography (GC×GC) coupled with mass spectrometry identification increases the identification range offered by single GC methods [37]. Nevertheless, Harman-Ware et al. [38] used gel permeation chromatography (GPC) in order to characterize bio-oils and detected a significantly important fraction of heavy oligomers, whose identification was not feasible with the aforementioned techniques. In this way, advanced characterization techniques are required. Ultrahigh resolution Fourier Transform ion cyclotron resonance mass spectrometry (FT-ICR/MS) combined with electrospray ionization (ESI) mode enables the elucidation of the composition of heavy complex mixtures as bio-oil [39]. By this method, heavy compounds can be grouped in classes accounting for the number of carbon and oxygen atoms, thus detecting most of the macromolecules in the oligomeric or organic fraction of bio-oil [40].

The main average properties, determined by Gollakota et al. [41], who collected data from numerous bio-oil samples, are summarized in Table 1.1. Bio-oil is a viscous (40−100 cP) and corrosive (pH, 2.1−4.0) liquid with low heating value (HHV, 16−19 MJ kg^{-1}), properties that ostensibly limit its transportation, storage and direct use as a fuel [42]. Furthermore, its high oxygen content makes it immiscible with O-free fuels derived from fossil fuels. The oxygen-containing heavy oligomers are also thermally and chemically unstable, which hinders bio-oil management [10, 15]. For this reason, some authors have studied the separation of the aqueous and

Table 1.1. Average properties of raw bio-oil and heavy fuel (adapted from [41]).

Property	Bio-oil	Heavy oil
Water content (wt%)	15–30	0.1
pH	2.1–4.0	–
Density (kg m^{-3})	1200	940
Elemental analysis		
C	48–65	83–86
H	5.5–7	11–14
O	30–45	<1.0
N	0–0.3	<0.3
S	<0.05	<3.0
Ash (wt%)	0–0.2	0.1
Higher Heating Value (MJ kg^{-1})	16–19	40
Viscosity (cP at 50 °C)	40–100	180
Solids (wt%)	0.2–1	1
Distillation residue (wt%)	<50	1
Turbine emissions (g MJ^{-1})		
NO_x	<0.7	1.4
SO_x	0	0.28

organic fractions by adding extra water to bio-oil feedstock [43]. This strategy allows an independent valorization of each fraction, obtaining a more stable aqueous fraction and an organic fraction with significantly higher calorific value [44].

1.1.2 Processes for bio-oil valorization

In summary, most of the drawbacks and poor properties that avoid the direct use of bio-oil are related to the high oxygen content, mainly present in form of macromolecules or oligomers. Thereby, the upgrading of bio-oil mainly consists of the removal of oxygen, which has been an important challenge and subject of abundant research over the past 30 years [45], mainly focused on bio-oil stabilization and adjusting its composition for different applications [46–48]. Among the studied processes for bio-oil upgrading or valorization, one can highlight: (i) the catalytic pyrolysis of biomass; (ii) the stabilization of bio-oil; (iii) the catalytic cracking of bio-oil; (iv) the steam reforming of bio-oil, or; (v) the hydrodeoxygenation of bio-oil.

Catalytic pyrolysis

As a first approach, bio-oil composition can be upgraded by directly modifying the pyrolysis process. The use of a catalyst is a straightforward strategy aiming for the minimization of oxygenated compounds in the product stream by promoting dehydration, decarbonilation and decarboxylation reactions that yield H_2O, CO and CO_2, respectively. The main goal of adding a catalyst is minimizing the presence of carboxyl and carbonyl functional groups, which are responsible for bio-oil acidity and viscosity. In this way, a more stable and easy-to-handle bio-oil is obtained [10].

Different catalysts have been evaluated for the catalytic pyrolysis of biomass. Chen et al. [47] compared the bio-oil yield and composition obtained by thermal pyrolysis using metal oxide-based catalysts as Al_2O_3, CaO, MgO, CuO, Fe_2O_3, NiO, ZnO, ZrO_2, TiO_2, the mesoporous alumosilicate MCM-41 and the microporous zeolite HZSM-5. According to their results, the yield of bio-oil, pH and water content can be balanced with the suitable catalyst and operation conditions. They also found that CaO primarily promotes the oxygen removal by decarboxylation, whereas most of the catalysts favor dehydration reactions. Due to the high activity and severe shape selectivity of HZSM-5 zeolite, the direct production of 1-ring aromatic chemicals have been analyzed through catalytic pyrolysis [49]. Indeed, Olazar et al. [50] studied the catalytic pyrolysis of sawdust in a conical spouted bed reactor at 400−500 °C, finding an increase in the hydrocarbon yield but interestingly reducing the produced CO_2 in favor of the arisen H_2O.

This strategy of adjusting bio-oil composition in the pyrolysis stage can be performed with the catalyst *in-situ* (in the pyrolysis reactor) or *ex-situ* (in a secondary inline reactor), in which the volatile products of the thermal pyrolysis are treated (Figure 1.2). Iisa et al. [51] reported a significant decrease in the organic oxygen concentration using catalytic pyrolysis instead of the thermochemical process. Moreover, they found slightly higher amounts of oxygen compounds using the *in-situ* configuration, which also promotes the catalyst deactivation. Regarding the reactor configuration, catalytic pyrolysis (both *in-situ* and *ex-situ*) is usually carried out using fluidized bed reactors for the pyrolysis stage. However, other non-conventional pyrolyzers have also been evaluated, such as spouted bed, plasma, free-fall, rotating cone, microwave and auger reactors [10].

Bio-oil stabilization

The unstable nature of bio-oil originates from the high reactivity of some of its oxygenated compounds and makes unfeasible its long time transportation and storage [46]. Bio-oil aging is a well-known transformation process undergone by the complex mixture. Bertero et al. [52] studied the thermal conditioning of bio-oil, inducing physico-chemical changes on its composition that stabilizes the feedstock. The addition of some reactants have also been reported for a chemical conditioning of bio-oil, involving estherification and condensation reactions of short-chained oxygenated, that increase bio-oil viscosity and water content [53]. Ultimately, a phase separation due to the micro-emulsion break can be observe. Therefore, prior

UNIVERSIDAD
DE MÁLAGA

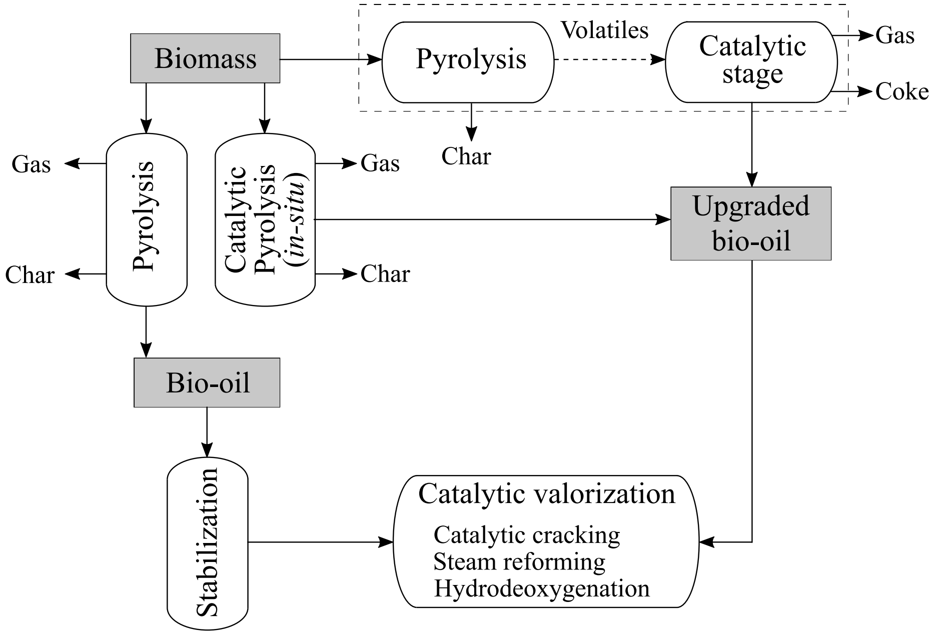
Biomass
Pyrolysis
Volatiles
Catalytic stage
Gas
Coke
Char
Gas
Char
Pyrolysis
Catalytic Pyrolysis (in-situ)
Gas
Char
Upgraded bio-oil
Bio-oil
Stabilization
Catalytic valorization
Catalytic cracking
Steam reforming
Hydrodeoxygenation

Fig. 1.2. Alternative strategies for the valorization and upgrading of bio-oil (adapted from [10]).

to the catalytic valorization of bio-oil, a stabilization stage is required in order to adequate its properties to the subsequent valorization stage.

Most of the applied pretreatments are based on physical methods, with biomass drying, ash and char removal, the addition of solvents, emulsification and antioxidants being the most common [54]. Due to the higher cost of emulsified oils and some antioxidants, the addition of solvents is specially attractive. Methanol has been reported as the most effective additive, observing a significant increase in bio-oil stability using 10 wt% of methanol in the storage tank. Li et al. [46] evaluated the techno-economic viability of bio-oil incorporation into an already implemented refinery, considering stabilization as a crucial stage. In this case, the proposed stabilization consists in a fractionation process followed by a mild cracking of the heavy fraction.

Catalytic cracking

Catalytic cracking is a well-known and widely studied acid-catalyzed reaction in which long-chained hydrocarbons are converted into shorter-chained ones. The reaction mechanism starts with the formation of a tricoordinated carbocation (carbenium ion) that initiates the different propagation pathways [55]. In this regard, β-scission, hydrogen transfer, oligomerization and cyclization-aromatization pathways are the main routes involved in the catalytic cracking of hydrocarbons. The mechanistic step that has driven most researches is the initial formation of this carbenium ion [56]. However, Boronat et al. [57] demonstrated the relatively easy formation of this crucial carbocation from olefins, which are much more reactive, *via* protonation and involving the formation of alkoxy species intermediates. In this way, the catalytic cracking of oxygenates is favored because of the easier production of olefins (by deoxygenation), which rapidly start the cracking mechanism.

Gayubo et al. [58, 59] evaluated the reactions and proposed mechanisms for most of the oxygenated compounds present in bio-oil: alcohols, phenols, aldehydes, ketones and carboxylic acids (Scheme 1.1). The deoxygenation of these compounds

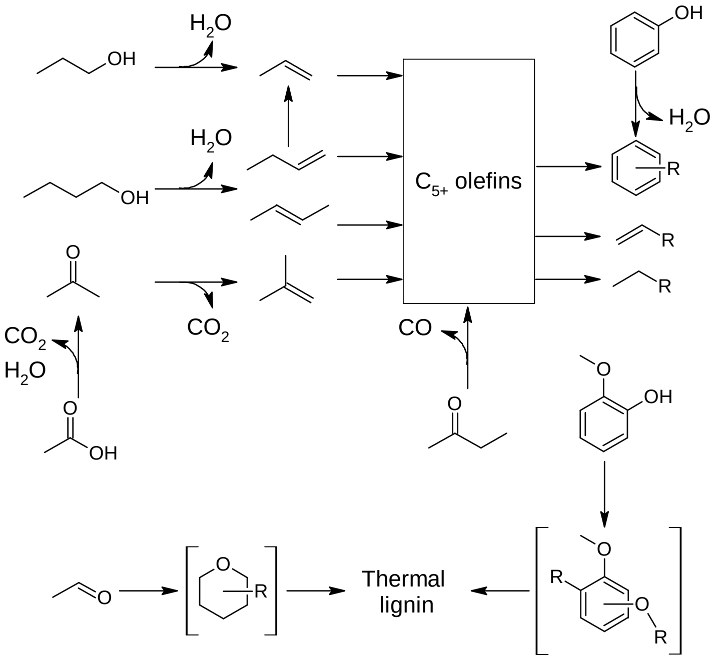

Scheme 1.1. Proposed pathways for the catalytic cracking of oxygenated compounds present in bio-oil (adapted from [58, 59]).

takes place through three main pathways, dehydration, decarbonylation and decarboxylation. According to the results of these authors, alcohols are the most reactive oxygenated species, directly yielding the corresponding alkene *via* dehydration. Nevertheless, phenol is almost unreactive at the tested moderate temperatures, indicating the high stability of the aromatic ring. Otherwise, methoxyphenols are the most reactive species, but the main product is of thermal origin and leads to a fast catalyst deactivation. This solid product is known as pyrolytic or thermal lignin.

Through a similar polymerization pathway, acetaldehyde catalytic cracking also causes a fast deactivation due to the deposition of thermal lignin. In this case, trimethyl tetrahydropiranes were identified as involved intermediates. An interesting result was reported by these authors regarding ketones transformation [59]. Butanone and compounds with longer chain forms long chained-olefins by a coupled mechanism involving decarbonylation and oligomerization pathways. Nonetheless, acetone, one of the main oxygenates in bio-oil, forms isobutene as the primary product, mainly releasing CO_2. This is the result of the complex mechanism of acetone self condensation that includes the decarboxylation route. And acetic acid is reported to easily release CO_2 by decarboxylation, evolving to acetone and thus initiating the catalytic cracking mechanism, of this latter.

Zeolites are commonly used in catalytic cracking reactions, and in the case of oxygenates transformation, both deoxygenation conversion and selectivity depend on the acidity and framework of the zeolite. HZSM-5 and HY zeolites were found to be the most active zeolites for bio-oil catalytic cracking in the temperature range of 290−410 °C [60]. Especially, HZSM-5 zeolite achieved a yield of hydrocarbons of 27.9 wt%. Nonetheless, the composition of both products were significantly different. Aromatics were the main compounds obtained with HZSM-5 zeolite, whereas the hydrocarbons obtained with HY zeolite mainly comprised aliphatic and naphthenic compounds (gasoline cut).

The main difference between the catalytic cracking of hydrocarbon and bio-oil feedstocks is the presence of water. Although water in the reaction medium can delay catalyst deactivation during the catalytic cracking, the operation conditions are restricted because of zeolite dealumination, which causes an irreversible deactivation. Gayubo et al. [13] studied the irreversible deactivation of an alkali-treated HZSM-5 zeolite during the conversion of ethanol into olefins. They reported a stable operation with negligible dealumination at 375 °C under 75 wt% of water in the feed. Nevertheless, increasing the temperature up to 400 °C limits the concentration of water in the feed to only 5 wt%.

Despite the better results obtained with HZSM-5, one of the most interesting applications of the catalytic cracking of bio-oil is its direct incorporation into the refinery catalytic cracking unit par excellence, the fluid catalytic cracking (FCC) reactor. A simplified diagram of bio-oil valorization by this strategy is depicted in Figure 1.3. Hita et al. [15] reviewed the possibilities of bio-oil as a feedstock for FCC units, highlighting: (i) a hydrogen transfer from hydrocarbons to oxygenates; (ii) a competitive adsorption on the acid sites of oxygenates and hydrocarbons (favored that of the latter); (iii) similar yields of gasoline co-feeding bio-oil; (iv) the presence of CO, CO_2, water and oxygenates in the product stream; (v) slightly higher concentration of aromatics in the gasoline cut, and; (vi) a significant increase in the coke content, with the presence of thermal lignin.

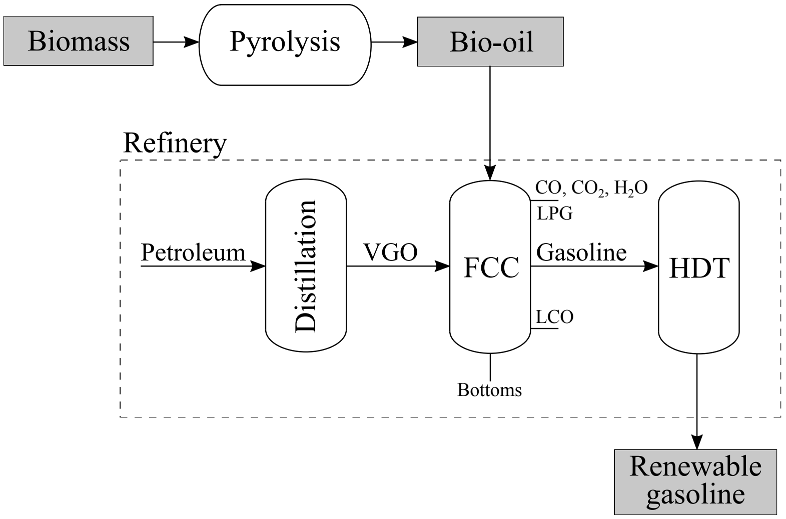

Fig. 1.3. Proposed valorization of bio-oil in FCC units (adapted from [61]).

Steam reforming

Steam reforming of bio-oil offers the possibility of producing hydrogen with remarkably high yields from a sustainable source as biomass. The main advantage of steam reforming is avoiding the water separation from oxygenates of bio-oil, which makes the process more feasible from an economic point of view [62]. Steam reforming can be summarized with a two-step reaction network as [63]

$$\begin{gathered} C_xH_yO_z + (x-z)H_2O \longrightarrow xCO + \frac{x+y}{2-z}H_2 \\ CO + H_2O \rightleftarrows CO_2 + H_2. \end{gathered}$$

These main reactions compete with those that lead to byproducts and coke formation as, methanation, cracking or Boudouard reactions.

Due to the difficult catalyst screening using raw bio-oil, most of the studies have been focused on model oxygenated compounds. Transition metals have been widely studied for the steam reforming of acetic acid. Especially, Hu and Lu [64] reported H_2 yields of 93% with a Ni catalyst supported on Al_2O_3, with negligible deactivation. Nonetheless, the best results regarding catalyst stability were reported for mixed oxides of Ce-Zr, which promotes the coke oxidation [65], and for La_2O_3, whose basic sites favors a reduction of coke deposition [66]. Supported noble metal catalysts have also exhibited great performances in this reaction, and especially, those of Rh achieved H_2 yields higher than 70% using not only acetic acid, but also heavier compounds as phenol [67].

In spite of the great potential of this technology, reforming of raw bio-oil is still challenging because of the fast formation of thermal lignin at the reaction temperatures (ca 700 °C). Some researches have been directed to the steam reforming of the aqueous fraction of bio-oil after a phase separation adding water [68]. Although the catalyst deactivation was improved, the catalyst stability is not acceptable for this reaction. Therefore, the steam reforming of complex oxygenated mixtures and raw bio-oil have been reported to be more efficient in a two-stage process [69].

Two-stage valorization processes

An efficient strategy in order to mitigate catalyst deactivation is a valorization process consisted of two stages inline (Figure 1.4). The first is a thermal process in which the thermal lignin is deposited at controlled conditions. Thereby, the unstable oxygenated compounds that easily repolymerize forming the solid product are retained in this stage. Most of the phenolic derivatives and other oxygenates

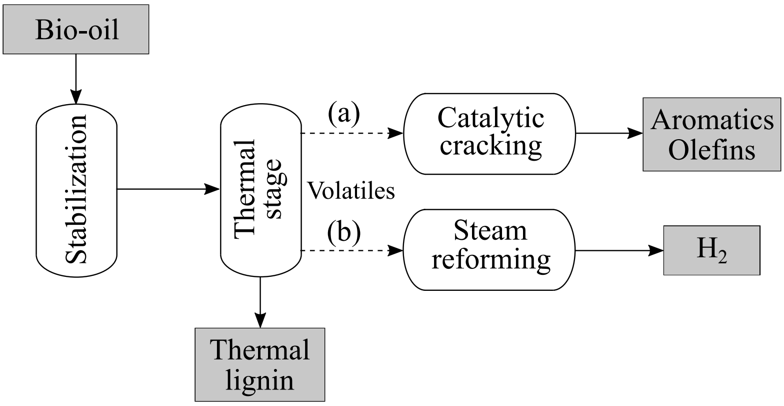

Fig. 1.4. Two-stage (a) catalytic cracking or (b) steam reforming of bio-oil for the removal of thermal lignin (adapted from [69] and [70]).

as acetaldehyde (Scheme 1.1) are removed from the volatile fraction, which is fed into the catalytic stage. Once overcome the main drawback of raw bio-oil processing, the deactivation of the catalyst in the catalytic stage (the second one) can be significantly attenuated.

Gayubo et al. [70] proposed this strategy for the production of aromatics and olefins, with the catalytic cracking of volatiles being the second stage. They used a modified HZSM-5 catalyst, which allowed the aromatic production to be maximized. They observed a significant reduction of the zeolite deactivation because of the thermal lignin removal. Moreover, Valle et al. [69] and Arandia et al. [63] also reported a similar configuration for the H_2 production through steam reforming and oxidative steam reforming (second stage). In both cases, they used Ni-based catalysts with different supports, and especially in the case of steam reforming, they observed a stable operation during more than 250 min without noteworthy deactivation by coking [69].

1.2 Bio-oil hydrodeoxygenation (HDO)

Among the strategies for bio-oil stabilization/valorization, hydrodeoxygenation (HDO) is one of the most effective technologies in terms of carbon economy [71]. As previously stated, a stabilization through oxygen removal is a required operation, and HDO makes the most of bio-oil great potential as a fuel [72, 73], feedstock in new or conventional refinery units [74, 75] or a source of high-quality products, as phenolics and aromatics [76, 77]. Essentially, all biomass-derived streams for producing fuels and chemicals show similar HDO requirements. The main drawbacks of this technique are the high H_2 consumption and the relatively harsh operation conditions, which are however widely-ranged depending on the targeted goal of hydroprocessing.

Bio-oil HDO is less limited than cracking, and can be tuned in order to obtain fuel or partially deoxygenated bio-oil [78, 79]. Hydrodeoxygenated bio-oil has been used in turbines [45] or for a subsequent valorization through cracking or hydrocracking (targeting the conversion of phenols and furans) [80]. The range of operating conditions studied for HDO bio-oil, in terms of pressure and temperature, is very wide [81], as well as the catalysts studied. Overall, the main reactions that take place in the HDO process are [82]: hydrogenolysis of the $\mathrm{C-O}$ bond (forming water as a byproduct), dehydration, decarboxylation, hydrogenation of unsaturated compounds and hydrocracking ($\mathrm{C-C}$ bond cleavage through a carbocation mechanism). Nevertheless, and due to bio-oil instability, HDO is commonly studied in discontinuous batch reactors and using model oxygenated compounds [83–85], whereas studies in continuous setups or either handling real feedstock are still scarce.

1.2.1 Catalysts

HDO has primarily been studied over conventional sulfided transition metals comprising Ni, Mo, Co, W and/or combinations of these. Nonetheless, the high tendency towards coke formation of these catalysts, as well as the necessity to add an external sulfur source to the reaction medium for their activation, direct catalyst preferences towards reduced metals. So far, noble (Pt, Pd, Ru, Rh) and transition metals (Ni, Mo, Co, W)-based catalysts have been tested, as well as bimetallic combinations within each group (Pt-Pd, Rh-Pd, Pt-Sn, Ni-Mo, Ni-W, Ni-Co, Co-Mo). Studies on a wide range of catalyst supports have shown the important role of their physico-chemical properties (porosity and acidity) in HDO reactions, especially on the conversion of bulkier and highly refractory components. Among the analyzed supports, one can highlight SiO_2, SiO_2–Al_2O_3, TiO_2, ZrO_2, zeolites and carbon [86, 87]. Saidi et al. [72] reviewed the state of the art on the HDO of bio-oil and

UNIVERSIDAD
DE MÁLAGA

gathered the most studied catalyst for the process. Table 1.2 summarizes some of this information, detailing the commonly used catalyst, reaction conditions and model compounds of bio-oil. Although many researches have been conducted in discontinuous or batch reactors, the information on Table 1.2 has been limited to those carried out in packed bed reactors.

Noble metals

Noble metal-based catalysts for hydrocarbon hydroprocessing show higher activity than those of transition metals, which allows lower operating severity to be used [88, 89]. Milder operation conditions usually lead to highly hydrogenated final products [90, 91]. The most studied noble metals in the HDO process are Pt, Pd, Ru, Rh and their bimetallic combinations [92–96]. Generally, Pd and Pt catalysts present the highest activity for decarboxylation and decarbonylation pathways, whereas Ru catalysts show better HDO activity. Snåre et al. [97] tested the effect of noble metals on oxygen removal from stearic acid as model compound. They used similar metal loading in all cases, and reported the following activity order

$$\mathrm{Pd} > \mathrm{Pt} > \mathrm{Ni} > \mathrm{Rh} > \mathrm{Ir} > \mathrm{Ru} > \mathrm{Os}.$$

Moreover, they confirmed that Pd promotes the decarboxylation pathway, whereas Pt favors decarbonylation. According to Newman et al. [98], who evaluated Ru supported on different materials, the high hydrogenation ability of noble metals allows two mechanisms to take place simultaneously: a direct hydrogenation on big metal particles and a H−H bond cleavage and spill over mechanism on small particles. Regarding the also promoted deactivation during HDO (as in other bio-oil processing technologies), Zhang et al. [73] were able to attenuate coke formation during the HDO of the organic fraction of bio-oil over a Ru catalyst by using super/sub-critical ethanol as a solvent.

Numerous researches have also been reported with bimetallic catalysts. Resende et al. [99] discussed that the addition of a second metal can avoid problems with sintering in Pd catalysts. And the combination of Rh with Pt and Pd catalysts was reported to enhance significantly the guaiacol HDO in comparison to the monometallic Pt and Pd catalysts [100]. Moreover, the higher hydrogenation activity and more stable performance of a PtPd bimetallic catalyst than those of its monometallic Pt and Pd counterparts was also observed [101].

Nonetheless, noble metals are expensive and their activity, in most cases, also depends on their content and the properties of the used support, which could compromise the economic viability. Furthermore, they are highly active for aromatic ring hydrogenation and C−C bond hydrocracking, which significantly increases the H_2 consumption of the process [72]. In this regard, Gutierrez et al. [100] studied

Table 1.2. Catalysts (including noble metal, transition metals, metal sufides and metal phosphides), conditions and representative model compounds proposed for bio-oil HDO in packed bed reactors (adapted from [72]).

Metal	Support	T (°C)	P (bar)	Model compound
Pt	Al_2O_3	200	40	Guaiacol
Pt	Al_2O_3	200	40	Cresol
Pt	γ-Al_2O_3	300	1.4	Methylanisole
Pt	HZSM-5	200	40	Guaiacol
Pt	HZSM-5	200	40	Cresol
Pt	SiO_2-Al_2O_3	300	1.4	Methylanisole
Pt	HY	200−250	40	Phenol
Rh	SiO_2	300	10	Anisole
RuMo	C	350−400	40	Guaiacol
Pd	C	80	5	Phenol
CoMo	Al_2O_3	340	70	Ethylphenol
CoMo	Al_2O_3	300	50	Anisole
Mo	Al_2O_3	340	70	Ethylphenol
NiMo	SiO_2-Al_2O_3	300	50	Phenol
Ni	SiO_2	300	50	Anisole
Ni	γ-Al_2O_3	300	50	Anisole
NiW	C	150−300	15	Phenol
NiCu	CeO_2	320	10	Anisole
NiCu	δ-Al_2O_3	300	10	Anisole
Fe	C	250−450	1	Guaiacol
CoMoS	–	300	40	Guaiacol
CoMoS	γ-Al_2O_3	300	40	Guaiacol
CoMoS	Al_2O_3	300	28.5	Phenol
CoMoS	TiO_2	300	40	Guaiacol
CoMoS	ZrO_2	300	40	Guaiacol
NiMoS	γ-Al_2O_3	250	15	Phenol
MoS_2	–	300	40	Guaiacol
MoS_2	–	300	50	Anisole
MoS_2	γ-Al_2O_3	300	40	Guaiacol
MoS_2	γ-Al_2O_3	300	50	Anisole
Ni_2P	SiO_2	300	15	Anisole
NiMoP	SiO_2	300	15	Anisole
MoP	SiO_2	300	15	Anisole
Co_2P	SiO_2	300	1	Guaiacol
Fe_2P	SiO_2	300	1	Guaiacol
WP	SiO_2	300	1	Guaiacol

the guaiacol HDO with three different noble metal-based catalysts and compared their activities with a suitable combination of transition metals and support. They concluded that a CoMo catalyst can achieve higher HDO activity than those obtained with Pt and Pd catalysts, despite a Rh-based catalyst resulted the most active one under their conditions.

Transition metals

The low abundance that increases the cost of noble metal catalysts hiders their application at large scale [102]. And for this reason, studies on transition metals has caught a lot of attention in recent years. The most commonly used transition metal catalysts are Ni, Co, Mo or W supported catalysts [103–106]. One of the main hindrances on the bio-oil upgrading by hydroprocessing is the competition of HDO and aromatic ring hydrogenation [72]. In this sense, the lower activity of transition metals as hydrogenation catalysts can lead to more deoxygenated molecules without an excesive H_2 consumption for the saturation of aromatic rings. Olcese et al. [76] reported significant selectivities to benzene, toluene and xylenes through the guiacol HDO using a Fe-based catalyst without much aromatic ring hydrogenation. The deoxygenation activity of phenolic compounds towards aromatics in Fe-based catalysts has been explained by the oxophilic character of Fe, which favors the scission of aromatic C–O bonds [107]. A good performance was also observed for a Co catalyst at the same conditions. However, this latter also catalyzed the undesired methanation pathway, which leads to a carbon loss without oxygen removal. Otherwise, Zhao et al. [108] found higher HDO conversion for propylphenol with a Ni catalyst than that obtained with a Pd catalyst using the same support. But in this case, the main obtained products were naphthenics, with minimum concentrations of benzene and alkylbenzenes.

In general, transition metals have also offered better HDO activity by combining different metals in bimetallic catalysts. Huynh et al. [109] investigated the effect of adding Cu and Co to a Ni catalyst. They reported a promoted phenol HDO and a decrease in the formation of coke with the NiCo catalyst. However, the addition of Cu in their catalytic system presented a negative synergistic effect. Other authors analyzed the influence of Co and Mo on Ni catalysts [110], finding a key role, especially of Mo, in the enhancement of guaiacol HDO. In a similar way, the CoMo combination has been reported to improve by 45% the selectivity of a Mo catalyst [111]. The low electron density and high electrophilicity of Mo have been reported as the cause of an enhanced C=O bond adsorption and activation [112].

Due to their use as hydrogenation catalysts, several studies have been conducted using sulfided transition metal catalysts (Table 1.2) [72]. In this way, their relatively high stability and low cost have driven these researches [113], mostly using bimetallic sulfided catalysts as CoMoS functions [114]. However, Whiffen and Smith [115] tested Mo sulfides, phosphides and oxides in the hydrodeoxygenation of methylphenol, and reported a better performance of the MoP catalyst, with the highest selectivity to hydrogenated compounds and the lowest yield of CO. High selectivity to aromatic compounds from aryl ethers and phenol using FeMoP catalysts was also observed by Rensel et al. [77], who correlated the lower activation energy required for the cleavage of the aromatic C–O bond with the Lewis acidity of these catalysts [116].

Supports

A major role of the catalyst activity and stability during HDO reactions is played by the support, which disperses the metal particles and allows less amount of metal to be used (specially important with noble metal catalysts). In the literature, both neutral and acid supports have been tested in different HDO reactions. Among the most used neutral supports, one can highlight α-Al_2O_3, SiO_2 or carbon, whereas bifunctional catalysts are usually prepared by depositing the metallic function on acid supports, such as γ-Al_2O_3, SiO_2, SiO_2-Al_2O_3, activated carbon or zeolites. The acid sites in the bifunctional catalysts are of vital importance to deoxygenate the most refractory compounds of bio-oil, especially phenols, due to a simultaneous methyl transfer and hydrodeoxygenation reactions [117, 118]. A major disadvantage of the acid support is the potential increase in the yields of coke associated with condensation reactions on the acid sites [72].

Lee et al. [119] analyzed the effect of γ-Al_2O_3, SiO_2-Al_2O_3 and activated carbon as support of noble metals for the guaiacol HDO. The main product was cyclohexane using SiO_2–Al_2O_3, but higher yields of cyclohexanol and methoxycyclohexanol were found when the support was γ-Al_2O_3 or the activated carbon. This was related to the promoted deoxygenation activity of the most acid SiO_2-Al_2O_3 support, which catalyzed alcohol dehydration. Furthermore, the application of γ-Al_2O_3 in bio-oil HDO is limited by its hydrophilic nature and acidity, which causes higher tendency to coke formation and declines catalyst stability. In this way, the use of non-alumina supports as modified mesoporous SiO_2, TiO_2, carbon materials or zeolites is a proposed methodology in order to achieve good deoxygenation degrees, while attenuating coke formation [10]. One example was given for the phenol HDO using Ni catalysts supported on SiO_2-ZrO_2 [120], which showed high selectivity to hydrocarbons, an anti-coking performance due to its amphoteric character and the suitable recyclability.

Regarding the attenuation of coke formation, supports based on hierarchical and mesoporous materials, such as SBA or SiO_2-Al_2O_3 (with moderate acidity) are suitable for promoting the diffusion of oxygenates with high-molecular weight, prone to repolymerize. The activity and product distribution obtained with Pt catalysts supported on a mesoporous SBA-15 and a microporous HZSM-5 were compared for the guiacol HDO [121]. And the highest yield to cyclohexane was obtained for the mesoporous support, ascribed to the severe shape selectivity of HZSM-5 zeolite that hinders the diffusion of guaiacol molecules. The HZSM-5 zeolite presents a high hydrothermal stability, and the limiting size of the MFI structure channels (5.1×5.5 and 5.3×5.6 Å) favors the production of phenolics and one-ring aromatics from bio-oil [122].

Also with the similar aim of avoiding deactivation, Echeandia et al. [123] compared NiW catalysts supported on mesoporous active carbons for phenol HDO, and concluded that much less coke was formed on the carbon catalyst than that observed on an Al_2O_3 support. Indeed, carbonaceous materials are one of the most studied alternatives as catalyst support for HDO due to their hydrothermal resistance, tunable porous properties, low cost and sustainable origin [124, 125]. A deeper introduction to activated carbon materials and their particular use in the HDO process will be detailed in Section 1.3.

1.2.2 HDO mechanisms

Hydrodeoxygenation is a complex process that involves a set of different individual reactions. The commonly used bifunctional catalysts even increase the possible pathways taking place. Some of these pathways are of different nature and will be promoting as a function of the reaction conditions, namely reaction temperature, pressure or H_2 partial pressure in the reaction medium. Mortensen et al. [82] summarized the main pathways involved at HDO conditions, which are illustrated in Scheme 1.2. Following the main pathway, oxygen is effectively removed in the form of water without further modification of the carbon chain. However, this reaction competes with the rest pathways, which makes decrease the overall carbon efficiency of the process. In the absence of hydrogen or with very low partial pressure, oxygen can be removed by dehydration, but the presence of olefins is quite disfavored at HDO conditions due to their easy hydrogenation to paraffins. Nonetheless, there are two pathways that usually coexist with HDO at any given conditions: decarbonylation and decarboxylation. As indicated in the previous Section, the metallic function can promote a preferential oxygen removal by decarbonylation or decarboxylation [97]. But at HDO conditions, oxygenated compounds are not the only reactive species, since reactions of the formed hydrocarbons can also take place. In this regard, hydrogenation (on metallic sites), cracking (on acid sites) and hydrocracking (on metallic/acid sites) reactions occur simultaneously to oxygen-removal pathways.

The nature of the oxygenated compounds also plays an important role in the

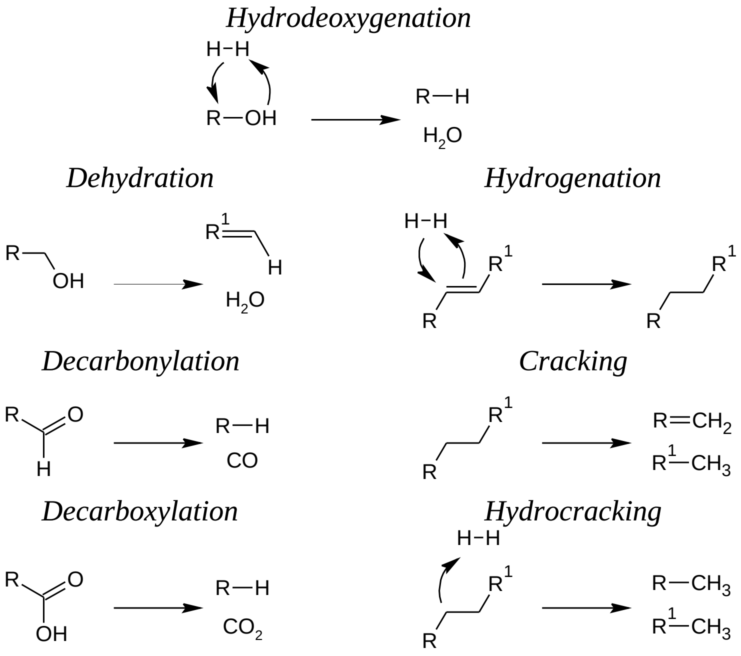
Hydrodeoxygenation
H-H
R—OH
R—H
H_2O
Dehydration
R
OH
R^1
H
H_2O
Hydrogenation
H-H
R^1
R
R^1
R
Decarbonylation
R
O
H
R—H
CO
Cracking
R^1
R
$R{=}CH_2$
R^1—CH_3
Decarboxylation
R
O
OH
R—H
CO_2
Hydrocracking
H-H
R^1
R
R—CH_3
R^1—CH_3

Scheme 1.2. Main pathways involved in bio-oil HDO (adapted from [82]).

mechanism. Furimsky [126] reviewed the most relevant aspects of HDO mechanisms and made a thermodynamic study of the C–O bond cleavage. He reported the bond dissociation energies displayed in Table 1.3. The bond strength of the O attached to an aromatic carbon (Ar) is 83 kJ mol^{-1} higher than that of the O attached to an aliphatic carbon in the case of ethers (RO–R and RO–Ar) and alcohols/phenols (R–OH and Ar–OH). This implies that O removal from phenols and aromatic ethers is more difficult than from alcohols and aliphatic ethers. Again, depending on the feed, the selected operation conditions will be crucial.

Table 1.3. Effect of C–O bond nature on the required dissociation energy (adapted from [126]).

Bond	Dissociation energy (kJ mol^{-1})
RO–R	339
RO–Ar	422
R–OH	385
Ar–OH	468

For example, the Ar−O bond can be converted into a R−O after the hydrogenation of the aromatic ring, which would facilitate the oxygen elimination. Then, H_2 pressure and the catalyst selection (selectively promoting hydrogenation) may be important factors influencing HDO.

Given the complexity of unraveling the catalytic conversion of raw bio-oil, because of the numerous compounds and reaction steps, model compouds have been primarily targeted in order to understand the fundamentals of HDO reactions [127]. Auersvald et al. [128] established the following bio-oil component reactivity order for the HDO of bio-oil over a NiMo catalyst. From higher to lower reactivity: aldehydes, syringols, guaiacols, benzenediols, esters/lactones, ketones, alcohols, furans, carboxylic acids and phenols. In this scenario, several pathways have been proposed for the HDO of the representative oxygenates of bio-oil: acetone [103, 129], acetic acid [130], phenol [131, 132], cresol [130, 133], anisole [72, 133, 134] or guaiacol [72, 119, 133, 134].

Because of their relevance, regarding both the concentration in bio-oil and amount of publications, the proposed mechanisms for certain oxygenates of bio-oil are summarized herein. Acetone is one of the most abundant light oxygenates in bio-oil, and according to Zhang et al. [103], its hydrodeoxygenation can follow the different pathways depicted in Scheme 1.3. Apart from the direct hydrogenation of the C=O bond with the subsequent hydrodeoxygenation to propane, these authors proposed two alternative routes explaining the presence of methane and long hydrocarbons at conditions of suppressed decarbonylation. The first route is based on the decomposition of acetone to methane, yielding acetaldehyde, which

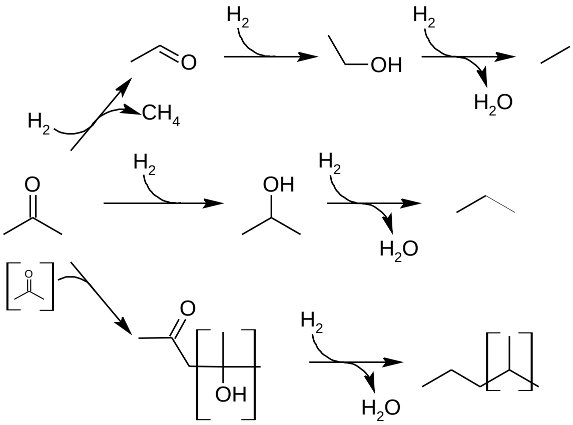

Scheme 1.3. Proposed pathway for acetone HDO (adapted from [103]).

forms ethane *via* ethanol. As previously explained (Scheme 1.1), acetaldehyde is a unstable intermediate that can lead to a fast formation of solid deposits. On the other hand, the production of long hydrocarbons from acetone is explained by a self-condensation mechanism, which leads to saturated compounds through hydrodeoxygenation/hydrogenation pathways.

As the simplest oxygenated aromatic molecule, phenol is also widely studied as a model compound of bio-oil. The mechanism proposed by Senol et al. [132] consists of two main routes (Scheme 1.4). The direct hydrodeoxygenation of the C−O bond yielding benzene, or the previous hydrogenation of the aromatic ring. In both cases, the final product expected is cyclohexane. As suggested by the thermodynamic studies of Furimsky [126] (Table 1.3), the operation conditions can affect the followed pathway and the selectivity to final products.

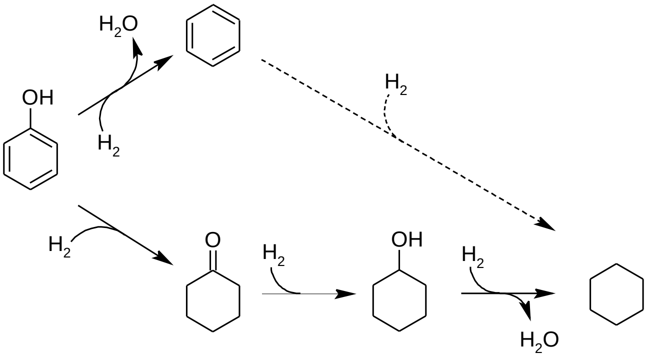

Scheme 1.4. Proposed pathway for phenol HDO (adapted from [132]).

The mechanism is much more complex when molecules have different oxygen functionalities. This is the case of guaiacol, whose HDO mechanism, along with that of anisole, is also widely reported. The reaction network proposed by Runnebaum et al. [134] is depicted in Scheme 1.5. A greater number of possibilities is proposed for this molecule. Among them, one can highlight the hydrodeoxygenation to form methoxyphenol (1 in Scheme 1.5), elimination of methoxy group as methanol (2 and 9), decomposition of methoxy group towards methane (3 and 10), methyl shift form methoxy group (4, 11 and 12) and methyl shift involving two molecules (5−8).

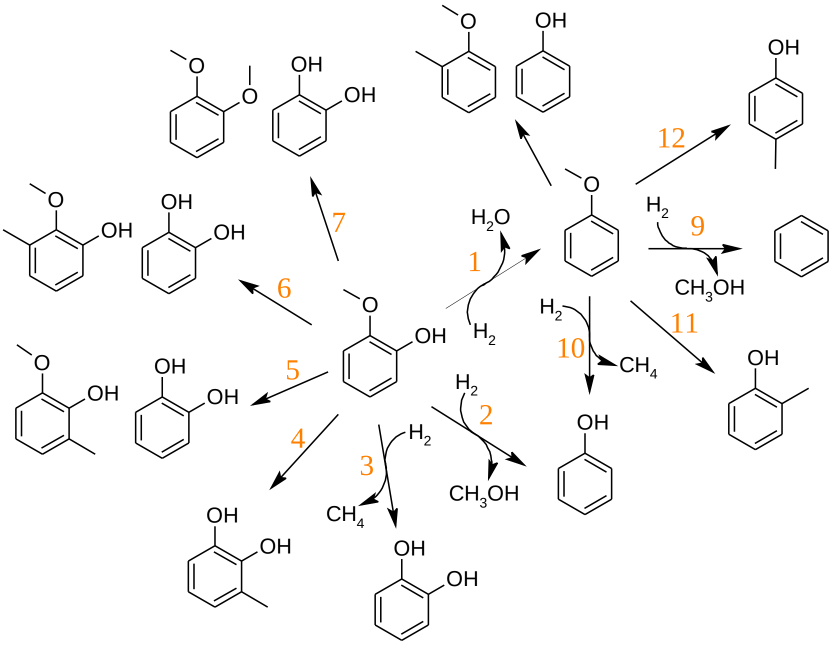

Scheme 1.5. Proposed pathway for guaiacol HDO (adapted from [134]).

1.2.3 Formation and deposition of carbonaceous deposits

Most of the studies on HDO mechanisms neglect deactivation pathways and more important, the role of the feedstock composition and catalyst properties in the carbonaceous deposit formation routes [82, 135, 136]. Several researches have pointed out the difficulties attained to the use raw bio-oil, which have driven modifications in the process configuration [70, 80]. For this reason, the pathways of carbonaceous deposit formation, the influence of bio-oil composition and the nature of these deposits require further investigation due to their relevance on the catalyst deactivation.

The massive formation of deposits is related to the thermal instability of some oxygenated components of bio-oil. The tendency of these compounds to repolymerize and form lignin-like structures is high, which also causes difficulties of bio-oil transportation and storage [42, 137]. This is aggravated at reaction conditions of high temperature and using packed bed reactors, where these thermal reactions ultimately lead to reactor clogging. In this regard, proposing an overall mechanism for catalyst deactivation that considers all the causes of deactivation from bio-oil requires conditions of stable operation [138], and taking the interaction between most of intermediates into account.

Valle et al. [139] proposed a parallel mechanism for catalyst deactivation during the catalytic cracking of bio-oil (Scheme 1.6). According to their results, dealing with bio-oil and acid sites leads to different mechanisms of carbonaceous deposits formation. The first route is associated with bio-oil instability, from oxygenated compounds and because of thermal repolymerization. This route occurs in parallel to that ascribed to the condensation of hydrocarbons on the acid sites towards catalytic coke. Ibarra et al. [140] also studied the catalytic cracking of bio-oil but at FCC conditions, aiming for a potential valorization of bio-oil co-fed with refinery streams (VGO). But interestingly, they found that operating with bio-oil at high temperature allows a stable operation because of a pseudo-equilibrium between the repolymerization/condensation of coke precursors and their cracking.

Nevertheless, the least expensive option for a stable operation at industrial scale is a thermal pretreatment (Figure 1.4), which decreases the carbon efficiency of the overall process or a two-stage HDO process. A mild HDO pretreatment is more efficient in terms of carbon atoms but also more expensive due to the hydrogen

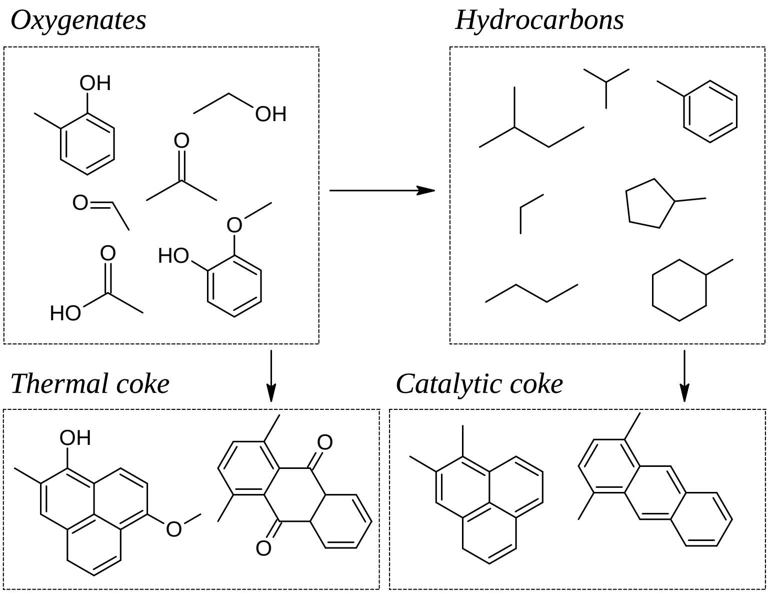

Scheme 1.6. Proposed parallel deactivation mechanism for bio-oil processing (adapted from [139]).

requirement.

1.2.4 Two-stage HDO

In raw bio-oil hydroprocessing, the HDO of the more refractory and polyaromatic oxygenated fraction requires harsh conditions. However, this can lead to a fast catalyst deactivation because of the promoted repolymerization of bio-oil unstable compounds and condensation of polyaromatic structures to coke (favored with acid supports). As an alternative, the group of Elliott [80, 141, 142] in the Pacific Northwest National Laboratory (PNNL) has proposed a configuration based on two HDO stages using different conditions for maximizing the hydrocarbon production in a continuous setup (yields of ca. 50 wt%). The PNNL configuration consisted of a two-stage sequenced HDO process, with a raw bio-oil mild HDO followed by a deep HDO of the products, in order to improve the quality of the heavy first-stage products [143].

With this configuration, Zacher et al. [80] proposed a potential biorefinery in which bio-oil could be incorporated into the established petroleum refinery industry (Figure 1.5). From this proposal, several researches have been conducted, mainly using packed bed reactors and testing different catalysts and conditions in each stage. Valle et al. [10] gathered the main proposals in the literature and sorted them out chronologically (Table 1.4). In general terms, most studies used noble metal catalysts in the mild HDO stage and transition metal catalysts for the second one. In fact, the key factor in this configuration is the possibility of subjecting noble metal catalysts to mild conditions. Thereby, the hydrogenation of aromatic

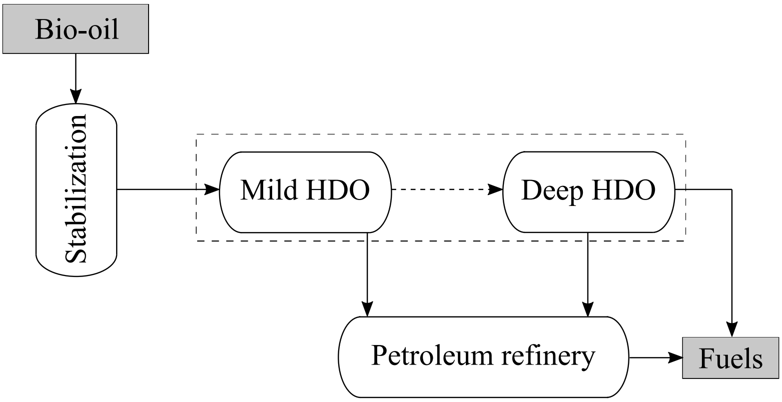

Fig. 1.5. Proposed integration of the two-stage HDO process into petroleum refinery (adapted from [80]).

Table 1.4. Proposed catalysts and conditions for the two-stage mild/deep HDO process (adapted from [10]).

	Mild HDO		Deep HDO	
Biomass	Catalyst	Conditions	Catalyst	Conditions
Red oak and switchgrass	Ru/C	220 °C 100 bar	$CoMo/Al_2O_3$	400 °C 100 bar
Pine wood	Ru/C	75–175 °C 52 bar	Ru/C, Pt/C	200–275 °C 52–100 bar
Spruce wood	Ni Raney	250°C 85 bar	Ni Raney	400 °C 170 bar
Red oak and corn stover	Ru/C	140 °C 121 bar	Pd/C	370 °C 121 bar
Pine wood	Ru/C	250 °C 190 bar	$NiMo/Al_2O_3$	375 °C 190 bar
Loblolly pine	Ni/SiO_2-Al_2O_3	340 °C 69 bar	Ni/SiO_2-Al_2O_3	400 °C 69 bar
Mallee wood	Pd/C	230 °C 70 bar	$NiMo/Al_2O_3$	375–450 °C 70 bar
White oak wood	Ru/C	130 °C 138 bar	Pt/ZrP	300–400 °C 138 bar

rings and the C–C bond cleavage reactions are avoided, also decreasing ostensibly the catalyst deactivation. The more expensive catalyst is then used in a stable operation with limited deactivation. This catalyst is able to hydrogenate the most reactive components in the phenolic oil, thereby stabilizing the feedstock for higher temperature hydroprocessing [142]. Subsequently, the stabilized product can be treated at harsher conditions in a process with lower necessity of oxygen removal and faster deactivation. For this reason, transition metal catalysts are normally used for this second deep HDO stage. According to recent results [80], more than 70 h of continuous bio-oil hydroprocessing can be achieved by stabilizing bio-oil in a first stage with a Ru/C catalyst at temperatures under 170 °C and pressures under 100 bar.

UNIVERSIDAD
DE MÁLAGA

1.3 Activated carbons

Activated carbons are solid materials, whose developed porosity and chemical surface properties have been responsible for their market success over many years. In essence, they are formed by a three-dimensional network of carbon atoms arranged in both hexagonal clusters (graphite-type structure) and individual atoms bonded in such a way as a stable porous structure is generated [144]. This chemical cross-linking of polycyclic aromatic molecules also provides carbon materials with high chemical [145, 146], hydrothermal [147] and electrochemical stability [148, 149]. And in this regard, they are classified as amorphous carbon materials although certain ordered atoms can be found in their structure.

Activated carbons (ACs) can be prepare in many different shapes, which also increases the possible applications of these materials. Their traditionally most used configuration is as granular material (Figure 1.6a), and the majority of their applications are reported for activated carbon powder. In many cases, their morphology

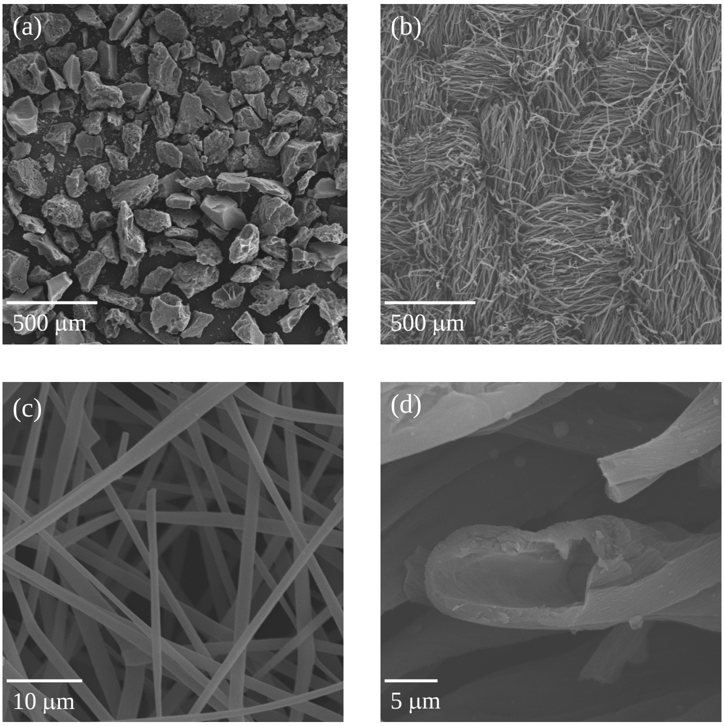

Fig. 1.6. Different activated carbon shapes: (a) granular, (b) fiber mesh, (c) individual fibers and (d) tubes.

is linked to that of the precursor. By way of example, activated carbon cloth is synthesized from textile waste [150], which possesses a mesh-type morphology with interconnected fibers. Despite the AC morphology will depend on the preparation conditions [151], a material with similar structure to that of the precursor can be obtained (Figure 1.6b). Nonetheless, advanced AC configurations have also been reported for specific applications as electrodes. Individual AC fibers (Figure 1.6c) and tubes (Figure 1.6d) were studied as cheaper and more sustainable alternatives to ordered structures as carbon nanotube [152].

As detailed in Figure 1.1, ACs are produced from the solid product of the pyrolysis of biomass. For this reason, they can be prepared from different sources as long as the carbon content is high enough. As examples of different precursors, one can highlight petroleum coke [153], tires [154], rice husk [155] or the aforementioned textile waste [150]. Nevertheless, the most interesting option form sustainability point of view is lignocellulosic biomass waste. Their relatively high carbon content and renewable source make them an attractive selection for activated carbon production. Table 1.5 lists the elemental and proximate analysis of different lignocellulosic biomass as potential precursors of activated carbon. In all cases, lignocellulosic biomass presents a carbon content around 50 wt% with negligible amounts of ashes and considerable values of fixed carbon [156]. Moreover, the interest of this biomass valorization due to its availability and low price is boosted when lignocellulosic waste is used, with the added value of the waste management [157]. In this scenario, one can include the case of olive stone. Especially in Spain, one of the greatest worldwide exporter of olive oil, olive stone is an important agricultural waste, which is already cleaned and separated in the own olive oil industry and requires for a suitable management [158].

Table 1.5. Elemental and proximate analysis of different lignocellulosic biomass (adapted from [156]).

Biomass	Elemental analysis (wt%)			Proximate analysis (wt%)		
	C	H	O	Ash	Volatile	Fixed carbon
Eucalyptus wood	47.1	5.9	46.6	0.3	85.7	14.0
Oak wood	51.8	6.6	41.3	0.6	86.9	12.5
Beech wood	49.6	6.1	44.1	0.4	88.2	11.5
Palm shell	50.0	6.9	41.0	1.2	78.5	20.3
Coconut shell	53.9	6.1	39.7	0.7	74.9	24.4
Macadamia shell	53.0	6.0	40.7	0.4	79.7	19.9
Peach stone	51.4	6.0	40.4	1.6	79.0	19.4
Apricot stone	52.4	6.6	38.8	1.0	80.4	18.6
Olive stone	48.1	6.0	45.7	0.4	80.2	19.4

The thermochemical conversion of these lignocellulosic precursors is a sustainable process for the production of carbon-rich materials [159]. When the maximization of the solid product is aimed, the pyrolysis of biomass (Figure 1.1) is conducted by slow heating [26]. And this particular case of pyrolysis is known as carbonization. Even though a solid product mainly formed by carbon can be obtained through the carbonization of biomass, an activation treatment must be performed in order to achieve the suitable porosity characteristic of ACs. Two routes for the preparation of activated carbons are used: chemical and physical activation (Figure 1.7). The latter is simpler, and it is based on two subsequent thermochemical process. Thereby, the carbonization of the precursor is followed by a partial gasification (in the presence of O_2, CO_2 or any other reactant), in which the material develops the porosity as a consequence of the oxidation of its surface [153, 155]. On the other hand, the chemical activation requires a previous stage before the carbonization of the precursor. First, the precursor is impregnated with the activating agent. Different reactants have been reported for the activation of biomass, such as KOH [161], $ZnCl_2$ [162] or H_3PO_4 [163, 164]. The objective of this impregnation is the reaction of the precursor carbon chains with the activating agent, then favoring the development of the porosity. The impreganted precursor is then carbonized and washed in order to remove the unreacted activating agent (Figure 1.7).

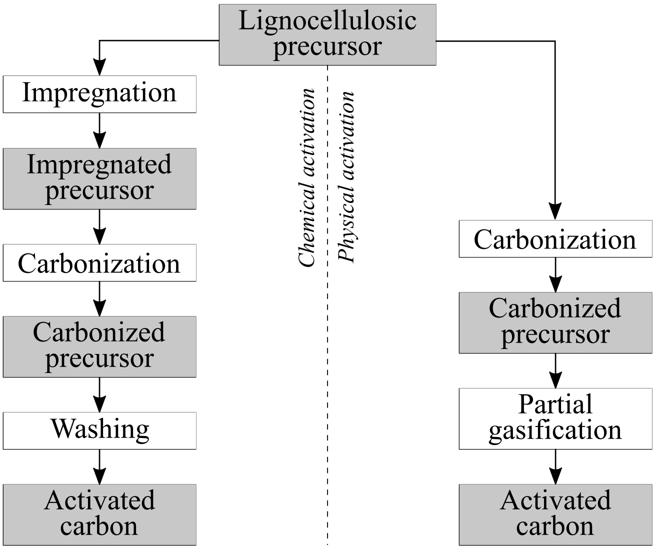
Lignocellulosic precursor
Impregnation
Impregnated precursor
Carbonization
Carbonized precursor
Washing
Activated carbon
Chemical activation
Physical activation
Carbonization
Carbonized precursor
Partial gasification
Activated carbon

Fig. 1.7. Routes for the preparation of activated carbons from lignocellulosic precursors (adapted from [160]).

Along with porosity, the surface AC chemical composition is also dependent on the preparation conditions. During the activation process, some oxygen functionalities are anchored to the carbon structure, and the aromatization of the carbon structure increases with the activation temperature. Lua et al. [165] reported the effect of temperature on the remaining functional groups after the chemical activation of a biomass with KOH. They concluded that the aromatization of the carbon structure goes hand in hand with the loss of oxygen functionalities on the carbon surface. And in several applications, these functionalities of heteroatoms are reported to be of paramount importance. With this aim, ACs are sometimes subjected to additional chemical treatments in order to incorporate new functional groups. One of the most used treatment is the AC surface oxidation with HNO_3. By this method, both oxygen and nitrogen functionalities are fixed in the AC structure, which was reported to be beneficial for adsorption [166], catalytic [167] and electrochemical applications [168]. However, the positive effect of other heteroatom functionalities as sulfur and phosphorus has also been reported in several applications [169–172].

1.3.1 Activation of lignocellulosic biomass with H_3PO_4

Among the chemical activating reactants, H_3PO_4 stands out as one of the most used and interesting, given the properties of the resulting AC. Phosphoric acid acts not only as a catalyst for bond-cleavage and cross-linking reactions but also forms phosphate and polyphosphate bridges that connect biopolymer fragments. Jagtoyen and Derbyshire [173] proposed the mechanism of lignocellulosic biomass chemical activation with H_3PO_4. It takes place in a sequenced two-stage process, respectively detailed in Schemes 1.7a and 1.7b. As 61−75 wt% of lignocellulosic biomass is formed by cellulose and hemicellulose (the rest is lignin) [174], the mechanism is proposed for a standard sugar-based chained polymer. Note that radicals R can be hydrogen atoms (cellulose) or an additional cellulose-like chain (hemicellulose).

During the first stage, promoted at temperatures lower than 450 °C, the insertion of phosphate groups within the biopolymer chains leads to the expansion of the carbonaceous structure (Scheme 1.7a). And after the removal of this phosphate ester groups by washing, a expanded porous structure is generated. As also observed, orto- and pyrophosphoric acid are in equilibrium at the activation temperatures. Cross-linking reactions of this later lead to the formation of polyphosphate ester groups within the carbon structure. On the other hand, the elimination of phosphate and polyphosphate groups is favored at temperatures higher than 450 °C (Scheme 1.7b). Because of this elimination, cross-linking reactions dramatically decrease, collapsing the porosity. This goes hand in hand with the aromatization

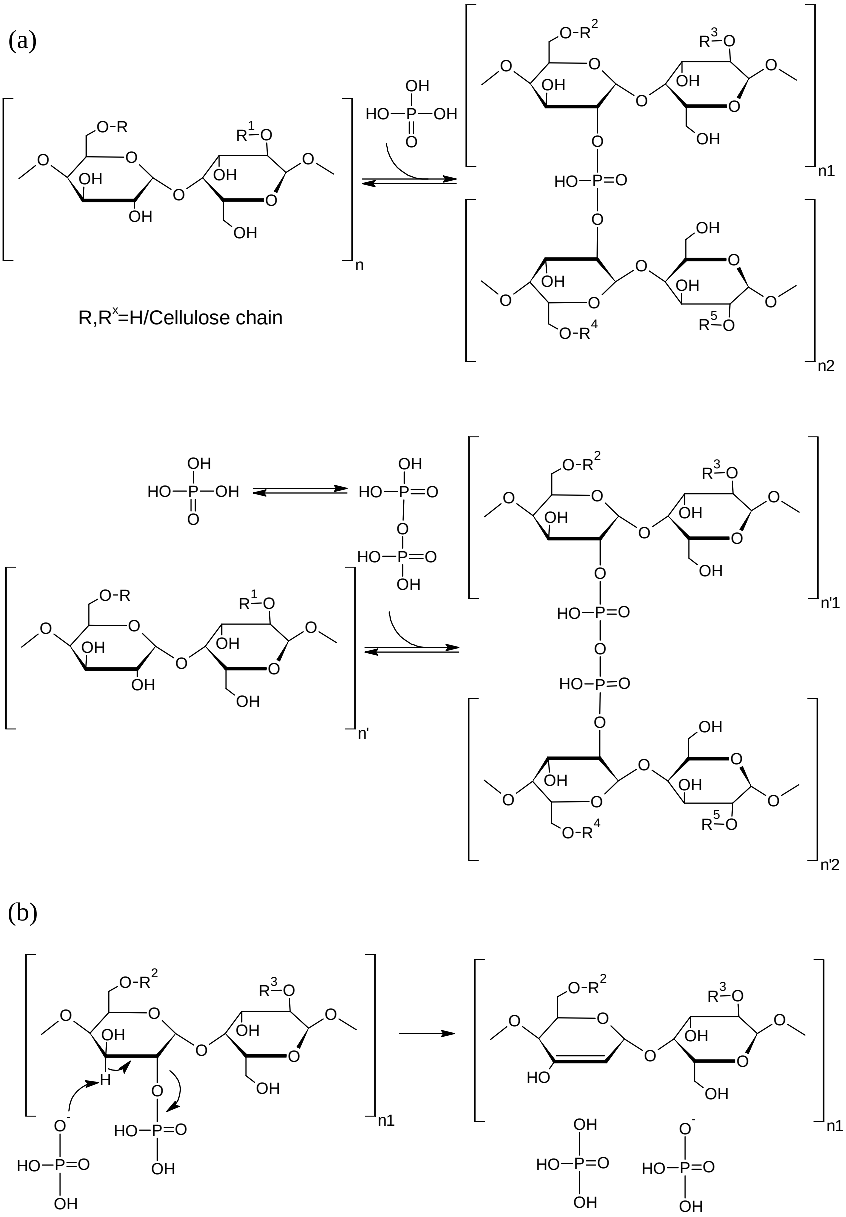
(a)
R,R^x=H/Cellulose chain
O-R
R^1-O
OH
HO—P—OH
O
n
n1
n2
O-R^2
R^3-O
O-R^4
R^5-O
HO—P=O
n'
n'1
n'2
(b)
H
O^-
HO

Scheme 1.7. (a) Formation of phosphate ester on side chains (cross-linking) and (b) elimination of H_3PO_4 during biomass activation (adapted from [173]).

of the carbon chains, with the unsaturations being generated through the aforementioned elimination and a hydrogen transfer reaction with bulky phosphate ions.

The main physico-chemical properties of the activated carbon will be determined by the used conditions, which direct the mechanism of biopolymers reaction with H_3PO_4. In particular, Bedia et al. [124] studied the effect of temperature and the amount of used H_3PO_4 on the porosity and surface composition of activated carbon prepared from olive stone. Table 1.6 lists selected data reported for two activation temperatures and three different H_3PO_4/Olive stone impregnation ratio ($R_{H_3PO_4}$) in each case. Their results were consistent with the mechanistic considerations of Jagtoyen and Derbyshire [173]. At both activation temperatures, a maximum specific surface area (S_{BET}) is observed for an optimal impregnation ratio. The more probable formation of polyphosphate using high amounts of H_3PO_4 is evidenced by the increase in the mesopore volume reported by these authors. And the tendency of the carbon structure to collapse at higher temperature is also observed in Table 1.6.

The second interesting feature of this chemical activation process with H_3PO_4 is the formation of P-functionalities on the carbon structure (Table 1.6). Puziy et al. [170] analyzed by several techniques the properties of these P-groups. They concluded that some P-groups provide the AC with an outstanding cation-exchange capability and the acidity of these functionalities is chemically and thermally more stable than that induced by oxidative treatments of ACs. Valero-Romero et al. [164] also studied these anchored functionalities and evaluated the effect of inert and oxidative heat treatments to P-containing activated carbons (ACP) on the P-group modifications. The most relevant functional groups proposed by these authors are summarized in the ACP structure of Figure 1.8. Phosphorus can be found directly bonded to the carbon structure or through oxygen bonds. Moreover, these lattice P-groups can be bonded to one, two or even three carbon atoms. After

Table 1.6. Porous properties and chemical surface composition (adapted from [124]).

T (°C)	$R_{H_3PO_4}$ (w/w)	S_{BET} ($m^2\ g^{-1}$)	V_{mes} ($cm^3\ g^{-1}$)	Concentration (wt%)		
				C	O	P
500	0.5	1104	0.03	85.6	10.0	2.3
500	1.0	1441	0.17	83.6	10.5	3.9
500	2.0	1331	0.60	80.5	14.7	4.3
800	0.5	875	0.02	86.2	8.3	4.7
800	1.0	1294	0.09	84.6	10.6	4.8
800	2.0	1073	0.69	82.0	10.6	6.0

activation treatment at high temperature, the aromatization of the carbon structure is promoted by the elimination of P-groups, and the remaining ones mainly present the reduced C_3PO form. The unpaired electron of the oxygen atom can enhance the performance of the AC in some applications, in a similar way to ketone functional groups [175]. Nevertheless, the thermal stability of the P-group is significantly higher, which enlarges the versatility of the material.

The activation of the precursor at lower temperature or subjecting ACP to an oxidation treatment leads to more oxidized P functional groups, such as $(CO)_3PO$, $CPO(OC)_2$, $(CO)_2PO_2$, CPO_3 or $COPO_3$. These three latter are specially interesting because of the acid character of the $-OH$ groups (Figure 1.8), which provides the ACP with acid character [164, 170]. Likewise, polyphosphate surface groups, whose presence is promoted when using high amounts of H_3PO_4, also exhibits this acid character. Although the acid features of these sites could be comparable to those attributed to oxygen functionalities (carboxylic, phenolic), the stability of each functional group differs ostensibly.

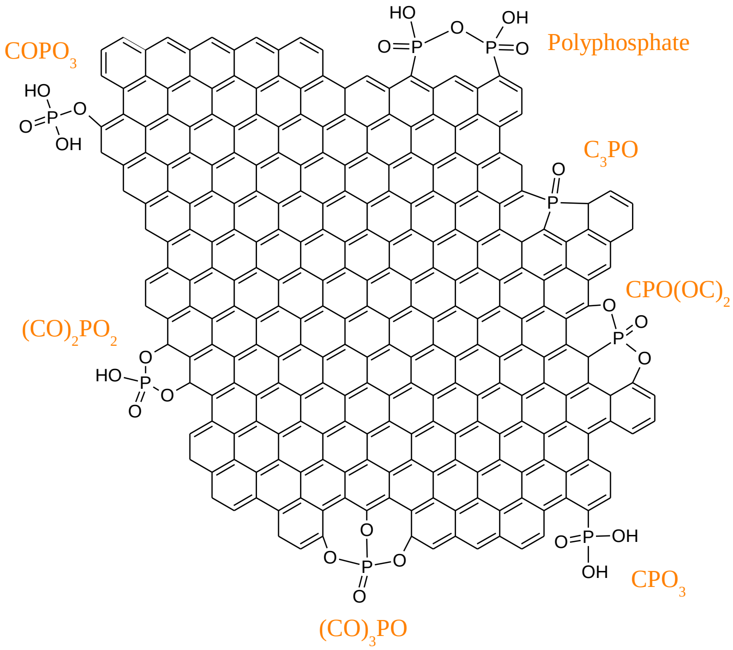

Fig. 1.8. Main P functionalities anchored on the carbon activated with H_3PO_4 (adapted from [164]).

Oxygen-based acid groups are known to decomposed at 250 °C [176], limiting the potential applications of acid ACs at higher temperature. This implies a reduced market in the field of acid catalysis, with most of processes taken place at significantly higher temperature. Otherwise, acid P-groups shows a remarkable stability at high temperature and oxidation conditions, which also enhances the oxidation resistance of the carbon structure. When ACP structure is subjected to air, P-groups ultimately form CPO_3 or $COPO_3$ acid species, which were reported to be stable up to 800 °C in inert atmosphere [177].

The oxidation mechanism and the high stability of the $C-P-O$ and $C-O-P$ bonds have been reported as the most plausible explanation of the stability of these sites and ACP materials. Phosphorus atoms have high affinity for oxygen, in such a way as the P-groups are preferentially oxidized, thus forming these CPO_3 or $COPO_3$ acid species and preventing carbon oxidation [178]. McKee et al. [179] attributed the oxidation inhibition to the transformation of $C-P-O$ bonds into $C-O-P$, suggesting this latter as the most stable bond of the structure. Nonetheless, Oh and Rodriguez [180] proposed an alternative configuration of the $C-P-O$ as the responsible for ACP stability. And Wu and Radovic [181] demonstrated the crucial role of both CPO_3 and $COPO_3$ species on the limitation of oxygen accessibility to the carbon structure. Although the discrepancies in the literature, ACP stability has been associated with the high stability of the acid P-groups, which allows the use of these acid materials at high temperatures under reductive and oxidative conditions.

1.3.2 Applications of activated carbons

Independently of the used route for the activation of the AC precursor, their main applications are directly related to the high-developed porosity. In terms of the field, they are mainly studied in environmental and energy applications, as pollutant removal, sustainable production of fuels and chemicals and energy devices. But their different applications can also be divided considering the role played by ACs. In this regard, adsorption, catalytic and electrochemical applications attract most of the attention (Figure 1.9) [182]. In all cases, the interest of ACs, apart from their sustainable nature, is the capability of retaining chemical compounds (Figure 1.9a), accumulating charges (Figure 1.9b) or dispersing the active sites of the catalyst within its pores (Figure 1.9c).

Adsorption applications

The most traditional application of ACs is the adsorption of chemical compounds for the removal of pollutants from gaseous or liquid streams [183]. Regarding a

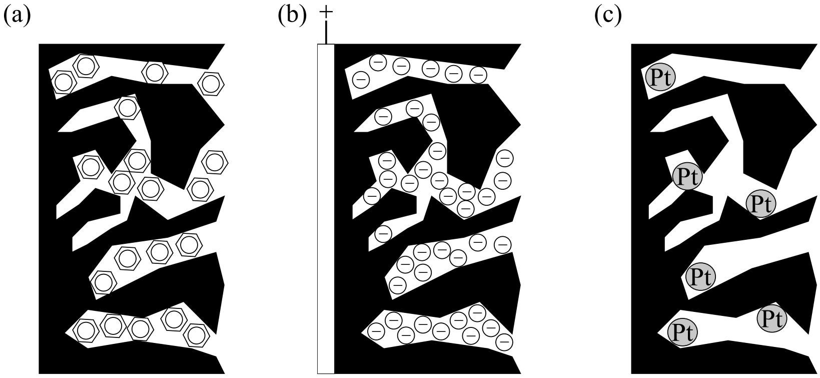

Fig. 1.9. Main applications of activated carbons in (a) adsorption, (b) electrochemical and (c) catalytic systems.

maximization of the adsorption capacity, adsorbents with small-size pores, high specific surface areas and micropore volume are required. In recent years, researches on gas phase adsorption are mainly focused on effluents from industries. Thereby, the combustion of fuels usually implies emissions of sulfur compounds as H_2S and mainly SO_2, which can be adsorbed using ACs [184]. Nonetheless, the major concern attached to the fuel combustion is the continuous emission of CO_2 to the atmosphere. For this reason, most of the case studies in gas phase adsorption using ACs are now focused on CO_2 capture [185, 186].

Among liquid phase adsorption processes, the waste water purification has been one of the greatest application of ACs. The adsorption of a wide variety of compounds found in industrially-used water has driven numerous studies in the literature. By way of example, one can highlight the removal of volatile organic compounds (VOCs), such as acetone, toluene, methanol or 2-propanol [187, 188]. Furthermore, the adsorption of heavy metals [189], and metal complexes [190, 191] has been analyzed using ACs prepared and modified using different procedures. Interestingly, Yin et al. [191] evaluated some precursors, activated with H_3PO_4, for the removal of Cd(II) and Ni(II) compounds. Other pollutants, whose removal from water effluents has been also investigated by adsorption, are those contained in cosmetic and pharmaceutical products [192]. In this way, the good adsorption performance of an olive stone-derived activated carbon with H_3PO_4 for the adsorption of pharmaceutical pollutants in waste water was demonstrated by García-Mateos et al. [193].

Electrochemical applications

In recent years, the use of activated carbon in electrochemical applications has been boosted, being mainly used as sensors [194], electrocatalysts [195, 196] and mostly in energy storage devices or supercapacitors [197, 198]. A capacitor is a electrical device able to accumulate charges that can be later used. An electrode with a positive charge (cathode) immersed in an aqueous electrolyte tends to attract (solvated) negatively charged ions (anions) to its surface, and *vice versa*, forming the well-known electric double layer [197, 199]. Charged species are therefore accumulated in this double layer, with the energy storage capability being a function of the layer surface, which directly depends on the electrode surface area (Figure 1.9b). In this sense, activated carbon electrodes offer a huge surface area for the accumulation of charges, making supercapacitors one of the most interesting applications of ACs in recent years [198, 200, 201]. There are also several factors that improve the supercapacitor performance, as the conductivity of the carbon material and the presence of Faradic reactions on heteroatom functionalities (pseudocapacitance). Again, both features have been reported to be enhanced by the presence of P-groups on the surface of ACs [202, 203].

Because of similar reasons, ACs have also been studied as support for electrocatalysts. Metallic active sites can be well dispersed on the carbon surface, which also facilitates the diffusion of reactants to the generated double layer. Hoang et al. [195] reported a AC-supported Ni electrocatalyst for the H_2 production by water splitting, one of the reactions that is catching significant scientific interest. Nevertheless, the production of energy in fuel cells is the most important electrocatalyst application of ACs. Especially, the electro-oxidation of methanol and ethanol are widely studied in the literature using noble metal catalysts supported on ACs due to the relevance of this anodic reaction in alcohol fuel cells [196, 204]. In this particular case, the use of carbon supports is limited by the electro-oxidation resistance of the materials, as certain potential cannot be exceeded due to the carbon degradation [205]. Berenguer et al. [149] found similarities between the oxidation and electro-oxidation mechanisms of P-containing ACs and reported an enhanced resistance when AC was activated using H_3PO_4.

Catalyst applications

For catalytic applications, ACs can be directly used in acid-catalyzed reactions. In this regard, ACPs are specially interesting because of the above introduced stable phosphate-type acid sites. Bedia et al. [206] reported the significant activity of ACPs for 2-propanol dehydration. But more interestingly, they studied the production of ethylene from ethanol dehydration using ACPs synthesized from olive stone [124]. They reported yields of ethylene near 100% at 350 °C, with a remarkable stability of the catalyst at temperatures above that of carboxylic group degradation and in a reaction medium with high concentration of water. This result highlights the remarkable hydrothermal resistance of these materials, a crucial property in the HDO reaction studied in this thesis.

Nonetheless, the use of ACs has been mainly studied as support for metallic or bifunctional catalysts because of their ability to incorporate well-dispersed sites within the developed porous structure (Figure 1.9c). Transition and noble metal catalysts supported on ACs have been evaluated in different processes, such as alcohol oxidation [207], H_2 production from hydrazine decomposition [208] or reforming processes [209], hydrodeclorination of waste water [210] or hydrogenation reactions [211, 212]. Hita et al. [125] proposed an ACP-supported PtPd catalyst as a more sustainable altternative for hydroprocessing a heavy oil derived from the pyrolysis of scrap tires. The feedstock was formed by a complex mixture of hydrocarbons and the operation conditions and H_2 concentrations were similar to those required for HDO process.

One of the main hindrances on the application of ACs to catalytic systems is the catalyst regenerability. In this sense, Shen et al. [159] pointed out the easy recovery of noble metals by the gasification or combustion of the AC and the deposited coke. And in the particular case of ACPs, the outstanding stability of the P-containing carbon structure has also allowed a partial regeneration by controlled combustion after the hydroprocessing of tire pyrolysis oil [213].

1.3.3 Carbon materials as catalyst support in HDO

Among the catalytic applications of ACs, especial attention must be paid to their use in HDO reactions. ACs have shown a promising performance in bio-oil HDO, which has been attributed to their chemical stability, high specific surface area and tailored pore size distribution [214]. In this regard, some functionalized ACs present a well-developed mesoporosity that favors an optimal dispersion of noble or transition metals, which has been reported to be important on HDO reactions [29, 92]. The importance of the carbon mesoporous structure not only on the activity, but also on the stability of the catalyst has also been reported [123], with a softened deposition of coke when using AC supports.

One of the most significant hurdles in raw bio-oil HDO is the high content of water in the reaction medium due to its presence in the feed [70] and its formation as a primary product of dehydration reactions that takes place during the HDO reaction (Scheme 1.2). ACs show a hydrophobic character and high hydrothermal resistance [215], which is even improved in those activated with H_3PO_4 due to the character of the anchored phosphate-like groups [124]. All in all, mesoporous carbon materials promote the swept of both water and coke precursors outside of the catalyst particle, and therefore their use has been broadly studied as one of the most attractive supports for the bio-oil HDO [92–95, 106, 119, 216].

As detailed in Section 1.2, most of the studies on HDO has been carried out using model compounds (see Table 1.2). As an example, Snåre et al. [97] tested a set of noble metals (Pd, Pt, Ir, Ru, Os) supported on AC, Al_2O_3, Cr_2O_3 and SiO_2 for the deoxygenation of stearic acid. Among all combinations, Pd/AC and Pt/AC showed the best activity and yields of targeted products. The best performance of ACs as support was attributed to the larger specific surface area, which attenuates the sintering of metallic particles and the formation of coke. Besides, they suggested a potential promotion of decarboxylation reactions associated with the oxygen-containing surface functional groups of the AC support.

Fewer works have been reported on HDO using raw bio-oil as a feedstock because of the previously discussed operational hurdles (Section 1.2). A selection of the most relevant results are listed in Table 1.7, where the used metallic function, the biomass and the HDO conditions are detailed. Elkasabi et al. [217] analyzed the effect of different noble metals and biomass used for the production of the bio-oil reactant, and concluded that the complex mixture of oxygenates derived from each biomass has as important influence as the used catalyst. This result highlights the importance of processing raw bio-oil, as model compounds cannot provide insights into the real synergistic effects between bio-oil components. The configuration of carbon materials has also been investigated [218], pointing out the relevance of the acidity and porosity on HDO, not only for ACs, but also for ordered structures as carbon nanotubes. On the other hand, the benefits of using transition metal phosphides or those attached to the two-stage HDO configuration were previously stated in Section 1.2. There are studies on the literature that also reported the positive effect of using activated carbon as support for Ni_2P and Co_2P catalysts [106], and as support in both stages of the sequenced mild/deep HDO technology [93].

Nonetheless, as previously discussed, the intrisic nature of carbon-based catalysts hinders the characterization of the carbonaceous deposits and their regeneration through combustion. This could be considered as a potential problem in a reaction with such a high tendency of forming coke. Studies using appropriate techniques for characterizing the coke will be required, thus favoring its selective

Table 1.7. Proposed catalysts and conditions for bio-oil HDO using carbon supports (adapted from [10]).

Metal	Biomass	T (°C)	P (bar)	Reference
Zn-Pd	Pine sawdust	150−250	14−41	[94]
Ni, Co	Hardwood	300	50	[106]
Pt, Ru, Pd	Switchgrass, eucalyptus	320	145	[217]
Ru	Oak chips	300	50	[218]
Pd, Pt, Ru, Ni	Pine sawdust	300−350	100	[219]

combustion, which was demonstrated possible using ACP supports [213]. In any case, the recovery of noble metals was proposed as the most attractive strategy in order to manage spent hydroprocessing catalysts [220], either through combustion or gasification of the carbon support [125, 221].

1.4 Bio-oil HDO within a sustainable biorefinery

The concept of biorefinery appeared in order to describe a biomass-based industry. Strictly, it was defined as *the sustainable processing of biomass into a spectrum of marketable products and energy* [3]. In essence, a biorefinery should integrate processes for biomass conversion and equipment to produce biofuels, power and chemicals, which would be the biomass-based equivalent to petroleum refinery. One of the core part of most biorefinery proposal is the sustainable production of bio-fuels form bio-oil. The important role within a biorefinery played by biomass pyrolysis and the catalytic alternatives of bio-oil for producing fuels were reviewed by Stocker [222]. On the other hand, Tschulkow et al. [223] recently analyzed a *lignin-first* biorefinery for the production of chemicals, and highlighted the techno-economic benefits of using different feedstocks, accounting for virgin and waste biomass of different nature.

Other biorefinery works have been focused on the evaluation of activated carbon production for their application in a sustainable refinery. A techno-economic analysis of a biorefinery in which waste was used for activated carbon preparation suggested the recommendation of producing these materials within the biorefinery framework [224]. And their use as adsorbent or catalyst was also proposed in order to enhance the environmental impact of a refinery [225]. In this regard, Istan et al. [226] reported an optimized biorefinery proposal focused on biomass pyrolysis, and evaluated the economic viability of integrating the production of bio-oil and activated carbons from pistachio nutshell. Although the valuable integration of using both liquid and solid products from biomass, Kaur et al. [227] recently concluded that very little work has been reported on the simultaneous use or production of biofuels and biochar. Therefore, further work must be conducted in this topic, aiming for increasing the interest of a potential future biorefinery.

In this scenario, this thesis proposes a suitable strategy for the biorefinery concept according to the previous statements. An overall diagram of the process is depicted in Figure 1.10. Two different biomass are used and from them, bio-oil and activated carbon are produced *via* pyrolysis (fast pyrolysis for bio-oil and carbonization for actvated carbons). Different catalysts are prepared using the carbonaceous support and are used for the hydrodeoxygenation of the bio-oil.

Requirements for biorefinery development

The feasibility of biomass and bio-oil valorization at large scale nowadays is assumed to be dependent on the revamping of already implemented technologies, thus limiting the required investment for the sustainable transition. In this way, using the existing refinery infrastructure as FCC or hydroprocessing units will be imperative. Hita et al. [15] reviewed the possibilities of valorizing bio-oil in FCC

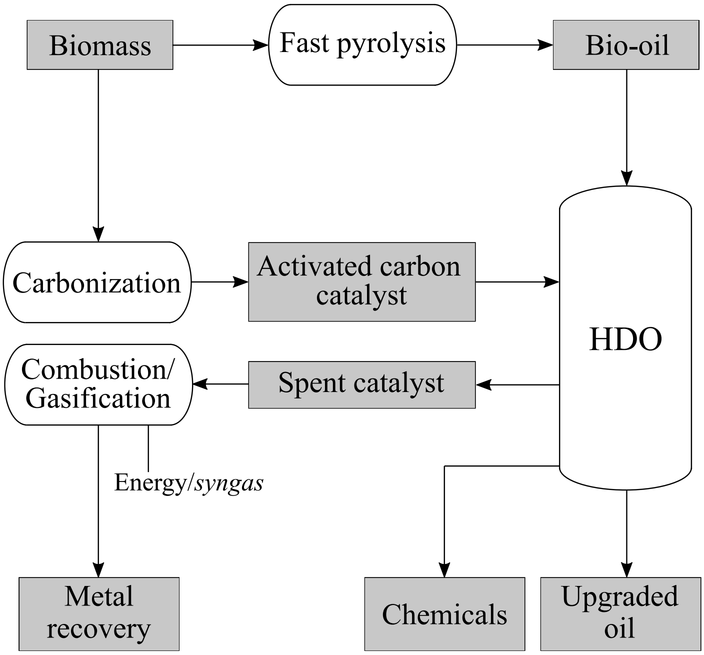
Biomass
Fast pyrolysis
Bio-oil
Carbonization
Activated carbon catalyst
HDO
Combustion/ Gasification
Spent catalyst
Energy/*syngas*
Metal recovery
Chemicals
Upgraded oil

Fig. 1.10. Overall diagram of the HDO process.

units, mainly by co-feeding it with VGO. Unlike hydropocessing units, the versatility of the FCC unit and its presence in most refineries have made this route the most extensively studied for bio-oil valorization, especially for model compounds or pretreated fractions [140, 228–231]. The results obtained from the cracking of VGO and raw bio-oil mixture (20 wt%) under FCC conditions showed the advantages of co-feeding bio-oil due to the existence of mechanistical synergies between oxygenates and hydrocarbons [232]. Ibarra et al. [233] also found feasible the valorization of pure bio-oil under FCC conditions. Nonetheless, this route offers some disadvantages, as the low gasoline selectivity and carbon efficiency because of the promoted decarboxylation and decarbonylation pathways. Furthermore, feeding high proportions of bio-oil into the FCC unit leads to a gasoline with high concentration of oxygenates that require further treatments [232].

These drawbacks could potentially be overcome through HDO. Again, revamping current hydroprocessing units is required, which could also make additional bio-oil pretreatments mandatory [92, 93]. In any case, the process should be performed with raw bio-oil and in continuous reactors, which include the fewest amount of HDO works in the literature as discussed in Section 1.2. Therefore, the development, design and revamping of hydroprocessing units for bio-oil HDO (and therefore advancing towards a biorefinery scenario) will be subjected to an increase in studies at real operating conditions that enable the development of realistic kinetic models of the process.

Kinetic models for HDO

Although some authors have directed their goal to the development of kinetic models for the bio-oil HDO, most of them have been developed from experimental data with model compounds. Encouraging results have been reported at a mechanistic level, and important advances have been made with models based on density functional theory (DFT). Lu et al. [234] theoretically proved the pathways of C−O bond cleavage and the limiting steps of aromatic formation from guaiacol. Zhou et al. [235] studied the HDO of phenol, applying DFT calculations on a microkinetic model of the process over a NiMo catalyst. At a macroscopic level, He et al. [236] reported a simple kinetic model for the HDO of guaiacol in a batch reactor that faithfully reproduces the effect of temperature on the oxygen removal capability of a Rh-based catalyst. Arora et al. [237] also proposed a model for the HDO in a batch reactor but using stearic acid as model compound and a Langmuir-Hinshelwood-type kinetic equation. And Iino et al. [238] modeled the performance of a fixed bed continuous reactor for the HDO of methyltetrahydrofuran.

The modifications of the pathways due to the synergistic effects arising from the great amount of simultaneous reactions and different oxygen functionalities in bio-oil are not taken into account in these works. Moreover, the high reactivity of the feedstock components that provokes a deposition of a solid product should be considered for a reliable kinetic model of raw bio-oil processing. According to these premises, lump-based kinetic models offer the possibility of reproducing the kinetics of a complex catalytic process by grouping a wide spectrum of compounds with similar kinetic behavior based on macroscopic measurements [239]. From the results of Till et al. [240], the uncertainty of processes involving such a high amount of compounds and reactions can be significantly reduced with these lumped models. Indeed, they were reported for modeling the hydroconversion of crude oil-derived compounds [241, 242], and the HDO of lignin [243].

An optimized computation methodology for lump-based kinetic models has been previously proposed [244], considering rigorously the relationship between reaction and deactivation kinetics. The results obtained for the catalytic cracking of *n*-pentane confirmed the effectiveness of the methodology, which could be applied to bio-oil HDO in order to predict, not only the individual reactions that take place (Scheme 1.2) but also the influence of the reaction medium on deactivation pathways when raw bio-oil is used (Scheme 1.6).

1.5 Aim and objectives

This work aims to widen the current state of the art on raw bio-oil processing in order to advance to a potential scenario in which biorefineries get more and more significance. The main objective of this thesis is to contribute to the understanding and development of a process based on raw bio-oil hydrodeoxygenation (HDO). The requirements of an efficient transition towards a more sustainable fuel and chemical productions have encouraged the work to be done at the most realistic possible conditions. For this reason, the thesis deal with HDO from the collection of experimental data in a continuous reactor. This allows evaluating the feasibility, difficulties and possibilities of raw bio-oil HDO, analyzing with special attention the formation of solid deposits. The following specific objectives were set in order to achieve the main goal:

- To develop the required experimental setup and set the suitable conditions in order to obtain products of interest from raw bio-oil HDO, collecting the required data from the gaseous, liquid and solid products for a rigorous evaluation of the reaction.
- To evaluate the performance of activated carbons with H_3PO_4 (ACP) as the support of a bifunctional catalyst, comparing it with that of an acid inorganic support in terms of activity, stability and selectivity.
- To compare the behavior of noble and transition metal bifuctional catalysts supported on ACP.
- To establish a relationship between the reaction medium composition and the properties of the deposited carbonaceous solids in order to elucidate the nature and origin of the deactivating species, as well as the influence of the support, metallic function and reaction conditions.
- To enhance the selectivity to value-added products as aromatics and phenolics by the addition of HZSM-5 zeolites to the catalytic bed, evaluating its influence on the process evolution and deposition of carbonaceous deposits.
- To develop a kinetic model for the raw bio-oil HDO that accounts for the main pathways involved in bio-oil processing and catalyst deactivation, defining solid product lumps that allow for a reliable prediction of the packed bed reactor performance.

These individual objectives are addressed in an orderly manner in each of the Chapters of the thesis.

UNIVERSIDAD
DE MÁLAGA

Chapter 2

Experimental

This Chapter describes general experimental procedures common in all Chapters of the thesis. Each of the following Chapters includes a detailed Experimental Section of the specific methods used in order to obtain the presented results. Here, schematic diagrams of the main equipment to prepare the catalyst and perform the hydrodeoxygenation runs are illustrated. A more complete description of these experimental setups is also provided. The main methods for the characterization of the fresh and used catalysts are also listed herein.

2.1 Catalysts

2.1.1 Preparation

The synthesis of the bifunctional catalysts consists in two different stages: (i) the preparation of the carbon support by chemical activation of olive stone precursor, and; (ii) the incorporation of the metallic function. The activated carbon support was prepared from olive stone (OS) provided by *Sociedad Coperativa Andaluza Olivera y Frutera San Isidro* (Málaga, Spain). The precursor was chemically activated with H_3PO_4 at different conditions, respectively indicated in the Experimental section of each Chapter. The activation treatment was carried out in a horizontal tube furnace (Carbolite GHA, Figure 2.1) under a continuous flow of N_2 of 150 cm^3 min^{-1}. The P-containing activated carbon supports (ACP) were washed, dried and sieved.

Afterwards, different pairs of metals were incorporated to the ACP support in order to obtain the bifunctional catalyst. Representative bimetallic functions of noble and transition metals were used, and in all cases, they were incorporated to the support by simultaneous incipient wetting impregnation. Aqueous solutions of the precursor salts were prepared, for which slightly acid conditions were required (pH = 3−4). Three bimetallic catalysts were synthesized, whose nominal concentrations in the catalyst and precursor salts are detailed in Table 2.1. The impregnated activated carbon supports with the metallic salt solutions were heat-treated using the same horizontal tube furnace previously shown for the olive stone

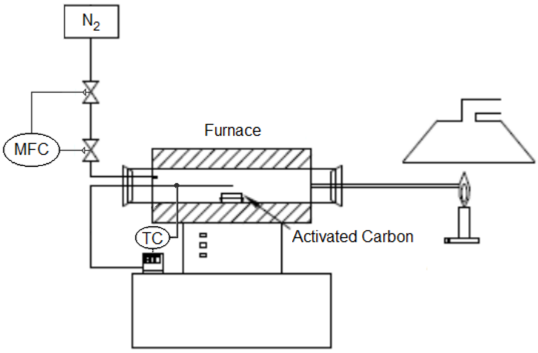

Fig. 2.1. Schematic diagram of the horizontal tube furnace setup (adapted from [160]).

Table 2.1. Nominal concentrations and salt precursors of the metallic function in the bifunctional catalysts.

Catalyst	Nominal concentration	Salt precursor
PtPd/ACP	1.0 wt% Pt	$HPtCl_6\ 6\,HCl$
	0.5 wt% Pd	$PdCl_2$
NiW/ACP	5.0 wt% Ni	$Ni(NO_3)\ 6\,H_2O$
	2.0 wt% W	$(NH_4)_6W_7O_{24}\ 6\,H_2O$
CoMo/ACP	3.0 wt% Co	$Co(NO_3)_2\ 6\,H_2O$
	12.0 wt% Mo	$(NH_4)_6Mo_7O_{24}\ 4\,H_2O$

activation (Figure 2.1). In all cases, the treatment was carried out at 400 °C for 2 h under a continuous flow of N_2 (150 cm^3 min^{-1}).

2.1.2 Characterization

The catalysts were characterized by several techniques in order to gather information about their physico-chemical properties. The used methods are summarized in Table 2.2, and the used procedures and conditions are detailed in the Experimental section of each Chapter.

Table 2.2. Techniques used for catalyst characterization.

Property	Characterization method
Porous structure	N_2 adsorption-desorption (*ASAP2020, Micromeritics*) CO_2 adsorption (*ASAP2010, Micromeritics*)
Morphology	Transmission electron micorscopy (*CM200, Philips*)
Acidity	NH_3 and *tert*-butylamine adsorption-TPD (*DSC-111, Setaram and Thermostar MS, Balzers*) Pyridine adsorption (*Nicolet 6700, ThermoFischer*)
Composition	X-ray photoelectron spectroscopy (*5700C, Physical Electronics*) Inductively coupled plasma high resolution mass spectrometry (*Element XR, ThermoFisher*) Energy-dispersive X-ray (*Talos F200X, FEI*)
Metal surface	CO chemisorption (*ASAP2010, Micromeritics*)

2.2 Reaction unit

The hydrodeoxygenation (HDO) runs were carried out in an automated reaction equipment (Microactivity Reference, PID Eng&Tech), in detail schematized in Figure 2.2, where the different sections are clearly identified: a reactant feeding section, a reaction section and a product collection section.

Feeding section

The system is provided with three inputs for gases and one for liquids. Gases are directly fed into the reaction section through individual lines, each one with mass flow controllers (Bronkhorst High-Tech) that allow feeding a maximum of 200 cm^3 min^{-1}. The available gases are N_2 (inert gas for conditioning and cooling down the system), Air (oxidant gas for regenerating the catalyst) and H_2 (reactive and pretreatment gas for hydroprocessing and reducing the catalyst). Bio-oil is fed using a HPLC 307 pump (Gilson), provided with a pressure restrictor of 20 bar (overpressure) that feeds liquid from 0.01 to 5 mL min^{-1} at pressures up to 600 bar.

Reaction section

The core part of this section is the down-flow packed bed reactor (9 mm of internal diameter and 30 cm length), which is heated by a cylindrical ceramic oven (max. temperature 600 °C). The reactor is located in an oven chamber, in which

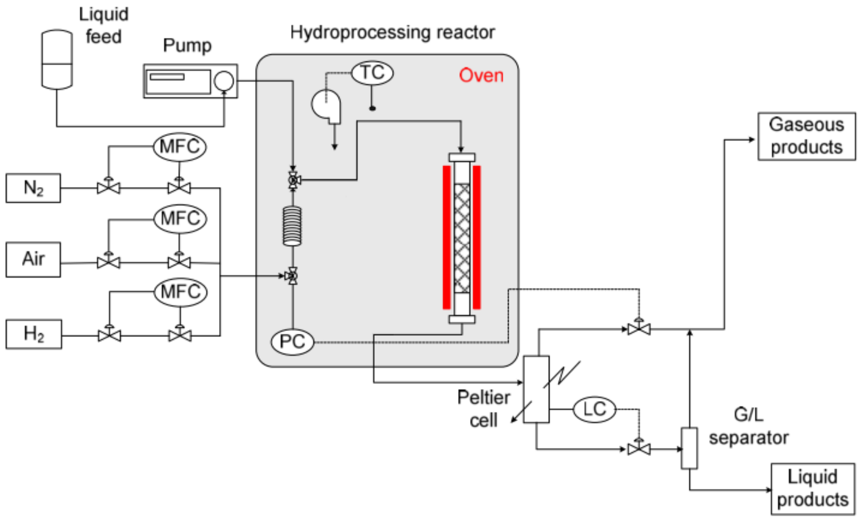

Fig. 2.2. Schematic diagram of the reaction unit (adapted from [245]).

the gas and liquid reactants are mixed before entering the reactor. The temperature is measured in the oven chamber and in the reactor by K-type thermocouples, and a pressure valve regulates the reaction pressure. Both features are controlled by TOHO TTM-005 controllers, which enable monitoring the different operation temperature and pressure. The catalyst pretreatments and reaction conditions are specifically detailed in the Experimental Section of each Chapter.

Product collection section

At the outlet of the reactor, products are directed to a Peltier cell at 0 °C, where the liquid products are condensed and retained in the cell. Gaseous products are depressurized, after going through the aforementioned pressure valve, and cooled down to room temperature. Samples of liquid and gaseous products are manually collected each hour of reaction from the condenser and the cooled gas line, respectively.

2.3 Analysis of bio-oil and reaction products

Bio-oil was provided by Ikerlan IK4 (Miñano, Spain), and was obtained through the fast pyrolysis of black poplar sawdust in a pilot plant, whose core is a conical spouted bed. The pilot plant has a capacity of 25 kg h^{-1} and is provided with two hoppers for storing the biomass, which is fed into the reactor through two screws and rotary valves. Pyrolysis experiments were carried out at 450 °C and, after the char collection in two cyclones, the bio-oil was retained in a condensation tower [246]. Due to the instability of bio-oil compounds, it was stored in a fridge at 4 °C.

After the HDO of raw bio-oil, gaseous, liquid and solid products were obtained as detailed in Section 2.2. A diagram of the product collection is shown in Figure 2.3. The gas product was sampled for their analysis, and the solid product deposited on the catalyst surface during the reaction was analyzed after each HDO run. As observed, the liquid product presented two fractions, aqueous and organic (AF and OF, respectively). An emulsion of both is obtained as collected because of the depressurization. After 1−2 hours standing, a clear phase separation was observed. Then, both fractions were easily separated by decantation. In order to close the mass balance, each fraction was weighed for quantifying the carbon products.

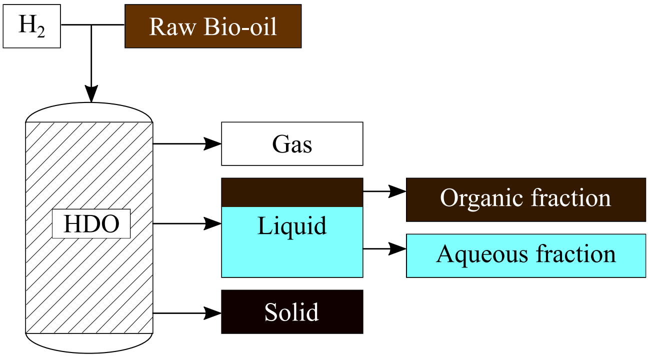

Fig. 2.3. Diagram of products collection.

Each phase of products was characterized by several techniques, which are listed in Table 2.3, and detailed in the Experimental Section of the corresponding Chapter.

Table 2.3. Techniques used for bio-oil and reaction product characterization.

	Characterization method
Bio-oil and liquid product	Ultimate Analysis (*TruSpec, LECO*)
	Gas chromatography/Mass spectrometry (*GC/MS QP2010, Shimadzu*)
	Bidimensional gas chromatography/Mass spectrometry (*7890A GC/5975C MS, Agilent*)
	Karl-Fisher titration (*830 KF Titrino plus, Metrohm*)
	Fourier-transformed infrared spectroscopy (*Nicolet 6700, ThermoFischer*)
	^{1}H nuclear magnetic resonance spectroscopy (*AV500, Bruker*)
Gas	Micro gas chromatography (*3000A, Agilent*)
Solid	Thermogravimetric-Temperature-programmed oxidation (*TGA Q5000 IR, TA Instrument*)
	Fourier-transform infrared spectroscopy (*Nicolet 6700, ThermoFischer*)
	Laser desorption-ionization/Mass spectroscopy (*Autoflex Speed, Bruker*)

UNIVERSIDAD
DE MÁLAGA

Chapter 3

Evaluation of the activated carbon as acid support

Results published in *Appl. Catal. B Environ.* **2017**, *203*, 389-399:

Stability of an acid activated carbon based bifunctional catalyst for the raw bio-oil hydrodeoxygenation.

Tomás Cordero-Lanzac[a], Roberto Palos[a], José M. Arandes[a], Pedro Castaño[a], José Rodríguez-Mirasol[b], Tomás Cordero[b], Javier Bilbao[a]
[a] *Department of Chemical Engineering, University of the Basque Country (UPV/EHU), PO Box 644-48080, Bilbao, Spain.*
[b] *Universidad de Málaga, Department of Chemical Engineering, Campus de Teatinos s/n 29010, Malaga, Spain.*

3.1 Abstract

The performance (activity, selectivity and stability) of a Pt-Pd catalyst supported on a phosphorus-containing activated carbon (ACP) has been studied in the hydrodeoxygenation (HDO) of raw bio-oil, and compared with another bifunctional catalyst prepared with a FCC (Fluid Catalytic Cracking) catalyst as acid support. Experiments have been carried out in a packed bed reactor (trickle bed) under the following conditions: 400−450 °C; 65 bar; space time, 0.18 g h $g_{bio-oil}^{-1}$; H_2/bio-oil ratio, 20000 $cm^3_{H_2}$ $cm^{-3}_{bio-oil}$; time on stream, 0−10 h. The catalyst reaches a pseudo-steady state at 450 °C after 6 h on stream, preserving a constant activity as a consequence of the simultaneous hydrogenation and cracking of the deposited coke. At these conditions, the yield of C_{5+} hydrocarbons is 20 wt%. This organic liquid fraction mainly contains aromatics, and thus, it may require an additional mild hydrocracking treatment for its valorization as fuel. On the other hand, the gas fraction obtained can be used directly as fuel, and the aqueous liquid fraction (with high concentration of methanol, 58 wt%) is interesting as co-feedstock with methanol in a methanol-to-olefins (MTO) unit.

Chapter 4

Catalyst deactivation by coke deposition

Results published in *Appl. Catal. B Environ.* **2018**, *239*, 513-524:

Revealing the pathways of catalyst deactivation by coke during the hydrodeoxygenation of raw bio-oil.

Tomás Cordero-Lanzac[a], Roberto Palos[a], Idoia Hita[a,b], José M. Arandes[a], José Rodríguez-Mirasol[c], Tomás Cordero[c], Javier Bilbao[a], Pedro Castaño[a]

[a] *Department of Chemical Engineering, University of the Basque Country (UPV/EHU), PO Box 644-48080, Bilbao, Spain.*

[b] *Chemical Engineering Department, University of Groningen, Nijenborgh 4, 9747 AG, Groningen, The Netherlands.*

[c] *Universidad de Málaga, Department of Chemical Engineering, Campus de Teatinos s/n 29010, Malaga, Spain.*

4.1 Abstract

Virtually all processes aiming fuels and chemicals from biomass entail no less than one step for removing oxygen by hydrodeoxygenation (HDO). The bottleneck of bio-oil HDO is the formation of deactivating-carbonaceous species on the catalyst surface. In this work, we have studied the deactivation pathways of catalysts based on noble metal nanoparticles (Pt-Pd) supported on mildly acid supports during the HDO of raw bio-oil. At conditions of accelerated deactivation, monitoring the evolution with time on stream of hydrocarbon and oxygenated compounds in the reaction medium, the intermediates on the catalyst surface and the nature-location of deactivating species, two parallel deactivation routes have been revealed: the deposition of (i) thermal or pyrolytic lignin from alkyl(methoxy) phenols, on the catalyst mesopores and favored at low temperature, and; of (ii) aromatic coke from polycyclic aromatic hydrocarbons, starting on the catalyst micropores through condensation reactions and promoted by acid sites and high temperature. Nevertheless, catalyst deactivation can be controlled within limits at harsh temperature conditions (450 °C) due to the preferential HDO of alkyl(methoxy) phenols into aromatics and the steady formation-hydrocracking of the aromatic precursors of coke.

Chapter 5

Comparison of metallic functions and zeolite additives

Results published in *Appl. Catal. B Environ.* **2019**, *259*, 118112:

Enhanced production of phenolics and aromatics from raw bio-oil using HZSM-5 zeolite additives for PtPd/C and NiW/C catalysts.

Idoia Hita[a], Tomás Cordero-Lanzac[a], Francisco J. García-Mateos[b], M. Josune Azkoiti[a], José Rodríguez-Mirasol[c], Tomás Cordero[c], Javier Bilbao[a]

[a] *Department of Chemical Engineering, University of the Basque Country (UPV/EHU), PO Box 644-48080, Bilbao, Spain.*

[b] *Universidad de Málaga, Department of Chemical Engineering, Campus de Teatinos s/n 29010, Malaga, Spain.*

5.1 Abstract

This study delves into the performance of a PtPd and a NiW catalysts supported on a phosphorus-containing activated carbon (ACP) in the hydrodeoxygenation (HDO) of raw bio-oil. The phenolic and aromatic product yield enhancement produced by incorporating physically mixed HZSM-5 zeolites (20 wt%) of different Si/Al ratio (15 and 140 in zeolites Z15 and Z140, respectively) in the catalytic bed is also investigated. The HDO runs have been conducted in a packed bed reactor at: 450 °C; 65 bar; space time, 0.15 g h $g_{bio-oil}^{-1}$; 90 cm^3 min^{-1} H_2; and time on stream up to 6 h. After a fast initial deactivation due to coke deposition the catalysts reach a pseudo-steady state at which the carbon product yields are higher than in fresh catalyst conditions. The catalyst of NiW provides yields of 42.3 wt% liquid carbon products (in a dry bio-oil basis), containing 5.3 wt% phenolic and 12.3 wt% aromatic components in the liquid. Its combination with Z140 zeolite is the most efficient catalyst with a yields of carbon products of 47.3 wt%, including 6.8 wt% phenolics and 15.5 wt% aromatics. This low-acidity zeolite promotes the synergy with the dehydrogenation activity of metallic sites by favoring the acid-catalyzed cracking reactions of the bio-oil oxygenates, while simultaneously limiting gas product and coke formation. Two types of coke have been detected, of thermal origin and catalytic coke, with the formation of the latter being dependent on the acidity of the zeolite.

Chapter 6

Kinetic model for the raw bio-oil HDO

Results published in *Chem. Eng. J.* **2020**, *400*, 124679:

Adaptable kinetic model for the transient and pseudo-steady states in the hydrodeoxygenation of raw bio-oil.

Tomás Cordero-Lanzac[a,b], Idoia Hita[a,c], Francisco J. García-Mateos[b], Pedro Castaño[a,c], José Rodríguez-Mirasol[c], Tomás Cordero[c], Javier Bilbao[a]
[a] *Department of Chemical Engineering, University of the Basque Country (UPV/EHU), PO Box 644-48080, Bilbao, Spain.*
[b] *Universidad de Málaga, Department of Chemical Engineering, Campus de Teatinos s/n 29010, Malaga, Spain.*
[c] *Multiscale Reaction Engineering, KAUST Catalysis Center (KCC), King Abdullah University of Science and Technology (KAUST), Thuwal, 23955-6900, Saudi Arabia*

6.1 Abstract

The hydrodeoxygenation (HDO) of raw bio-oil is an attractive route for the production of fuels and chemicals from biomass. For the sake of advancing towards the implantation of HDO at larger scale, an adaptable kinetic model is presented for this process. A CoMo bifunctional catalyst supported on an activated carbon has been used. The P-functionalities of the activated carbon support provide the catalyst with enhanced acid features. The HDO runs have been carried out in a continuous packed bed reactor at 425−475 °C. Two subsequent reaction stages have been observed during the experimental runs: a transient and a pseudo-steady state. In the former stage, the catalyst is partially deactivated whereas in the latter, an apparent constant activity is reached. The model decodes the complex reaction network of HDO with seven lumps and eleven reaction steps. The proposed model accounts for the evolution with time of the reaction medium composition in the transient state, considering the reactions involved in the gas phase and the ones of solid product deposition and catalyst deactivation. Important contributions of decarboxylation/decarbonylation/decomposition and repolymerization pathways towards $CO/CO_2/CH_4$ and thermal lignin are observed. The model also estimates the product distribution in the pseudo-steady state, in which the net deposition of solid products and the catalyst deactivation are negligible. In this state, the catalyst shows a partially inhibited conversion of phenolic compounds and the maximum yield of aromatics, which are the most interesting value-added chemicals. The proposed kinetic model could play a key role in the design of reactors for the HDO process at higher scale.

Chapter 7

General conclusions

UNIVERSIDAD
DE MÁLAGA

On the relevance of the results

The results obtained in this work fulfill the objectives of advancing towards the implementation of raw bio-oil hydrodeoxigenation (HDO). The large-scale valorization of biomass contributes to the strategies for decreasing CO_2 emissions and climate change mitigation. With this goal, the potential of biomass fast pyrolysis can be combined with already-established hydroprocessing units, aiming at the production of fuels and chemicals from this sustainable source.

Raw bio-oil HDO is a complex process, involving a lot of individual reactions and a fast deactivation by coking. Different stages of the process development have been studied herein, and the main achievements are related to: i) the development of active, stable and selective catalysts, also derived from biomass; ii) the screening of noble and transition metals for the bifunctional catalyst and the addition of HZSM-5 as an additive; iii) the selection of optimal operation conditions for the production of 1-ring aromatic and phenolic compounds; iv) the understanding of catalyst deactivation and the connection between the reaction network and the formation of carbonaceous deposits, and; v) the development of a lump-based kinetic model, considering the reaction medium composition and the deactivation kinetics.

On the use of activated carbons as a catalyst support

Activated carbons prepared by chemical activation with H_3PO_4 (ACP) show a remarkable performance as support for raw bio-oil HDO. ACP shows better results in this reaction than a catalyst supported on fluid catalytic cracking discarded catalyst at 400−450 °C, 65 bar, space time, 0.18 g h $g_{\mathrm{bio-oil}}^{-1}$ and H_2/bio-oil ratio, 20000 $cm^3_{H_2}$ $cm^{-3}_{\mathrm{bio-oil}}$. Especially, higher HDO conversion and selectivity to hydrocarbon products are achieved with the ACP support, which also leads to a stable operation after 6 h on stream. At the early stages of the reaction, the catalyst undergoes an initial deactivation, after which a pseudo-steady state of operation is observed. This is attributed to the achievement of similar rates of coke precursor condensation and hydrocracking.

Reaching the pseudo-steady state is proven to be highly dependent on the support properties and reaction conditions using the same metallic function (PtPd). The hydrothermal stability of the acid sites generated on the ACP surface favors the operation in a reaction medium with high concentration of water (the main product of bio-oil HDO). Moreover, high temperatures promote the cracking mechanism of coke precursors. Although hydrogenation is hindered increasing temperature, at least 450 °C are required in order to reach the conditions of steady operation and catalyst stability. The attenuation of deactivation by reaching stable operation conditions is important to advance towards the implementation of raw bio-oil HDO.

On the activated carbon catalyst deactivation

Deactivation by the deposition of carbon matter on the catalyst surface is significant during the raw bio-oil HDO. At conditions of accelerated deactivation, two main deactivation pathways are described, which respectively lead to the formation of thermal lignin and catalytic coke. The contribution of each deactivation pathway is influenced by several factors and conditions, as temperature, acid properties of the support or the metallic function. Thermal lignin originates from the repolymerization of the oxygenates in bio-oil following a thermal mechanism. The formation of this solid product on the external surface of the catalyst is fast. It presents an aliphatic nature and high content of oxygen. This mechanism is promoted at low temperature, and the massive formation of thermal lignin leads to the reactor clogging at 400 °C.

Catalytic coke is formed through the condensation of aromatic products on the acid sites of the catalyst support. In this regard, catalytic coke presents an aromatic nature, with low oxygen content and is located within the micropores of the support near to the acid sites. This deactivation mechanism is slower and therefore, more difficult to control. Despite the inevitable formation of carbon deposits, the continuous processing of bio-oil requires the operation conditions (acidity and high temperature) at which the formation of catalytic coke is favored and that of thermal lignin mostly suppressed. The understanding of these deactivation mechanisms is required for relating them to the global reaction network and their consideration in a kinetic model of the process.

On the performance of different metallic functions

Noble and transition metal functions supported on the ACP are evaluated in the raw bio-oil HDO. In all cases, aqueous and organic liquid fractions are observed, whose compositions vary as a function of the used metals. Noble metals (PtPd) show much higher HDO activity, producing high yields of water, as the main product of hydrodeoxygenation, and methanol, as the shortest-chained oxygenate identified. These are the two main compounds in the aqueous fraction, making it suitable for an alternative feed in a methanol-to-olefins unit. The organic fraction is formed by branched aromatics and polyaromatics, thus requiring a second hydroprocessing conditioning in order to be used as a fuel.

Transition metals (NiW and CoMo) have a moderate HDO activity, which allows higher yields of organic products to be obtained. The selectivity to methanol in the aqueous fraction is ostensibly decreased but the total yields of hydrocarbons, and especially of value-added chemicals as aromatics and phenolics, are promoted in the organic fraction.

The modification of the reaction medium composition also varies the contribution of each deactivation pathway. The higher presence of oxygenates in the reaction medium using the transition metals favors the formation of O-containing thermal lignin due to the instability of these compounds. Otherwise, the high concentration of aromatics using the noble metal catalyst leads to a favored formation of catalytic coke within the micropores of the activated carbon support. Therefore, the product distribution can be tuned by selecting each of the metallic functions, with the use of cheap transition metals being of a great interest for the production of value-added chemicals.

On the addition of HZSM-5 zeolites to the catalytic bed

Following the strategy of increasing the production of these value-added aromatic and phenolic compounds, the use of physical mixtures of the ACP-based catalysts with HZSM-5 zeolites is attractive. The effect of zeolite acidity is evaluated, and two HZSM-5 zeolites with Si/Al ratios of 15 and 140 are used. The most acid zeolite (Si/Al = 15) excessively promotes dehydration, decarboxylation and condensation reactions, leading to high yields of water and gaseous products. Especially its combination with the noble metal catalyst prompts a fast formation of catalytic coke due to the presence of polyaromatic structures in the reaction medium. Nevertheless, the addition of the least acid HZSM-5 zeolite (Si/Al = 140) enhances the yields of carbon products. Interestingly, the shape selectivity of the zeolite enables increasing the selectivity to 1-ring aromatic and phenolics, obtaining the best results with the combination of this zeolite with the transition metal catalyst (NiW). The moderate acidity of this zeolite and the low density of acid sites also avoid a faster deactivation using its physical mixture with ACP-based catalysts.

On the reaction network and kinetic model

Three operation stages are observed during the raw bio-oil HDO using all catalysts and physical mixtures with HZSM-5 zeolites: a first stabilization stage, a transient-state stage and a pseudo-steady-state stage. A kinetic model for the transient and pseudo-steady states of operation is proposed for a selected transition metal (CoMo) catalyst supported on ACP, from HDO experiments collected at 425−475 °C, 65 bar, space time of 0.15−0.6 g h $g^{-1}_{\text{bio-oil}}$, 20000 $cm^{3}_{H_2}$ $cm^{-3}_{\text{bio-oil}}$ and time on stream up to 6 h.

The HDO of raw bio-oil is modeled using a lump-based reaction network of 7 lumps comprising short-chained oxygenates, hydrocarbons, alkylphenolics, alkylaromatics, gases (CO, CO_2 and CH_4) and solid thermal lignin and catalytic coke. The system consists of 11 reaction steps of five different natures: catalytic, thermal, decarboxylation/decarbonylation/decomposition, condensation to coke and coke aging. The consideration of solid products is required due to the high amount of carbon deposits, and entails an improvement from previous models of catalytic processes. A first order concentration-independent and selective deactivation kinetic model fits the evolution with time of the product distribution in the transient state, where the formation of solid and gas products are estimated to be promoted. The kinetic model for the transient state and its adaptation for the pseudo-steady state predict the enhancement of alkylphenolic and alkylaromatic compounds in the steady operation, mainly observed for the transition metal-based catalysts.

The development of this kinetic model requires for all the previous results, including optimal reaction conditions, catalyst screening, catalyst stability and deactivation pathways. This tool is then useful in order to design and simulate reactors at larger scale according to the special characteristics of this complex process and therefore, it can help laying the foundation for a HDO-based biorrefinery.

UNIVERSIDAD
DE MÁLAGA

Chapter 8

Resumen

UNIVERSIDAD
DE MÁLAGA

Contextualización y fases del estudio

En el actual escenario de transición energética, y para reducir las emisiones de gases de efecto invernadero, la biomasa (en particular la lignocelulósica, no válida para la alimentación) recibe una gran atención como fuente renovable de energía y de materias primas hidrocarbonadas que actualmente son obtenidas desde fuentes fósiles. Entre las rutas de valorización de la biomasa, las termoquímicas (pirólisis, gasificación) tienen buenas perspectivas para su implantación a gran escala, y conducen a la producción de combustibles líquidos y productos químicos mediante un amplio abanico de rutas catalíticas alternativas. La pirólisis rápida de biomasa (en atmósfera inerte, con elevada velocidad de calentamiento y reducido tiempo de residencia de los volátiles), permite una valorización integral de los productos (gas, líquido y char). La combustión del gas aporta la energía requerida en el proceso, el char puede ser valorizado como adsorbente, catalizador o soporte de éste. El líquido (bio-oil), obtenido con un rendimiento del orden del 65% en masa, es una emulsión inestable de diferentes familias de oxigenados y tiene una propiedades (acidez, corrosividad, contenido de agua) inadecuadas para su uso directo como combustible. Sin embargo, ofrece atractivas posibilidades de valorización, mediante la extracción de componentes de interés comercial (levoglucosano, ácido acético, fenoles,. . . . .), por conversión mediante procesos catalíticos en corrientes de uso como combustibles líquidos y materias primas de síntesis (olefinas, aromáticos), o bien para la producción de H2, mediante reformado con vapor. Además, la pirólisis rápida de biomasa tiene ventajas energéticas respecto a la gasificación (baja temperatura) y medioambientales (reducidas emisiones de subproductos) y puede realizarse de forma deslocalizada geográficamente, en equipos con tecnologías relativamente sencillas y de reducido inmovilizado.

Esta tesis está centrada en el proceso de hidrodeoxigenación (HDO) del bio-oil. Este proceso (a elevada presión y con catalizadores bifuncionales) es clave para adecuar la composición y propiedades del bio-oil para su uso como combustible, para facilitar su posterior conversión en otro proceso catalítico (como puede ser su co-alimentación a una unidad de craqueo catalítico, FCC) y para la obtención finalista de combustibles y productos químicos. Estos objetivos de adecuación o conversión del bio-oil mediante HDO requieren la selección del catalizador y de las condiciones de operación idóneas. La contribución de esta tesis se extiende en las diferentes facetas del desarrollo de un proceso catalítico: (i) discriminación y propuesta de un catalizador adecuado; (ii) comprensión del mecanismo y definición de un esquema de reacción que considere las etapas individuales, y; (iii) desarrollo de un modelo cinético útil para cuantificar la distribución de productos y su evolución con el tiempo. La consideración de la desactivación del catalizador, es una constante en la tesis, porque condiciona los resultados en las diferentes facetas del estudio.

Los **catalizadores** bifuncionales estudiados, de base carbonosa, han sido preparados a partir de un residuo lignocelulósico, como es el hueso de aceituna. Estos catalizadores se enfrentan a un reto de estabilidad, debido a las condiciones de la reacción, con un elevado contenido de agua en el medio, alta temperatura (400-475 °C) y presión (65 bar). La estabilidad del catalizador es conseguida con la preparación de un soporte de carbón activo (denominado ACP) mediante activación del hueso de aceituna con ácido fosfórico. El método de activación química genera centros ácidos térmicamente estables en el ACP, cuya sinergia con la actividad de hidrogenación de los centros metálicos soportados es fundamental para el buen comportamiento de los catalizadores bifuncionales preparados.

La actividad, selectividad y estabilidad de los catalizadores con ACP como soporte se ha comparado con las de un catalizador preparado con un material de zeolita HY (catalizador de FCC equilibrado). De esta forma se pone en valor la aplicación original en la HDO del bio-oil de un catalizador con un soporte de esta naturaleza, cuando lo habitual es la utilización de un soporte inorgánico, tanto para metales nobles como de transición.

La alimentación de bio-oil completo en lugar de la utilización de oxigenados modelo o la fracción acuosa del bio-oil y además, la **operación en un reactor de lecho fijo** con alimentación de un flujo continuo del bio-oil, son características de esta tesis que han permitido analizar aspectos "reales" de esta reacción multifásica, como la desactivación del catalizador, y obtener unos resultados con un razonable acercamiento a la realidad de cómo será este proceso multifásico a mayor escala.

Esto no es posible en los reactores discontinuos habitualmente utilizados en las reacciones de valorización del bio-oil. Así, en el intervalo de temperatura adecuado para una reacción de larga duración, se han observado sucesivamente tres etapas de reacción: (i) la estabilización del flujo en el lecho catalítico, hasta alcanzar un régimen de contacto gas-liquido-sólido característico del *trickle bed*; (ii) un estado transitorio, en el que la reacción de HDO avanza con una notable desactivación del catalizador, que incide en el rendimiento y distribución de productos, y; (iii) un estado pseudo-estable del catalizador (interesante para una implantación del proceso) en el que los resultados son constantes con el tiempo. Siendo necesario pasar por la primera etapa, el interés se ha centrado en las dos siguientes, porque la segunda etapa condiciona los resultados y condiciones adecuadas de la tercera. Esta operación en el estado pseudo-estable centra el interés con la perspectiva de realizar el proceso a mayor escala.

Debido a su importancia en los resultados, se ha prestado una gran atención en el desarrollo de la tesis a la **desactivación del catalizador**. Este es un problema común a los procesos de valorización del bio-oil, y en particular del bio-oil completo. Se ha abordado aquí el estudio de la desactivación, evaluando: (i) la evolución con el tiempo de las prestaciones del catalizador (conversión, rendimientos y selectividades de productos), y; (ii) las causas de la desactivación (deterioro de las propiedades del catalizador por la deposición de material carbonoso). La relación entre ambos fenómenos (efectos y causas de la desactivación) ha llevado a establecer un mecanismo, para una comprensión racional del problema, identificando los precursores de los materiales carbonosos depositados, la diferente naturaleza de estos, las rutas de su formación y su incidencia en la desactivación.

La HDO del bio-oil transcurre mediante un sistema complejo de reacciones de hidrogenación, deshidratación, craqueo, ciclación, aromatización y condensación a poliaromáticos, como las más relevantes. La representación cuantitativa de estas reacciones con un modelo cinético requiere establecer un **esquema de reacción de lumps**, que contemple estas etapas de reacción y entre ellas la formación del material carbonoso que desactiva el catalizador.

Es destacable que el progreso de la HDO del bio-oil hacia su implantación industrial está limitado por la falta de un modelo cinético, herramienta necesaria para el diseño del reactor y la optimización de las condiciones de operación. En este sentido, la tesis ha adaptado un carácter más finalista que los estudios de la bibliografía en el tema. Así se ha establecido un **modelo cinético** válido en un amplio intervalo de condiciones. Para el modelado se han aplicado criterios avanzados para procesos catalíticos, resolviendo los problemas inherentes a un sistema de reacción que es complejo y además, considerando cuantitativamente la formación de productos sólidos y la existencia de dos etapas sucesivas en el tiempo, de estado transitorio (desactivación) y de pseudo-estabilidad del catalizador. Así, el modelo cuantifica la formación de los dos productos sólidos (lignina térmica y coque catalítico. La velocidad de formación de la primera es máxima al inicio del periodo transitorio, con deposición preferente a la entrada del reactor, por la repolimerización de oxigenados del bio-oil. El comportamiento del catalizador en este periodo es cuantificado adecuadamente con un modelo de desactivación selectiva. Sin considerar las inexistentes reacciones secundarias de formación de material carbonoso en el estado pseudo-estable, el modelo cinético es adecuado para predecir el comportamiento del reactor en este estado, de actividad de HDO casi constante, con un notable rendimiento de productos de interés comercial (aromáticos y fenoles).

Descripción de los capítulos de la tesis

La memoria se ha estructurado en siete capítulos, en los que se justifica el interés de la tesis en base al estado actual de conocimiento del tema, y se explican las herramientas experimentales y de cálculo utilizadas, y los resultados correspondientes a las diferentes facetas estudiadas del proceso de HDO del bio-oil. Así, la memoria consta de un capitulo introductorio justificando la tesis, y mostrando el enfoque original de sus objetivos. A continuación, en un capitulo experimental se describen brevemente las técnicas y metodologías usadas, comunes en general en los cuatro capítulos centrales de resultados. El contenido de cada uno de estos cuatro capítulos corresponde al de cada una de las publicaciones emanadas de los resultados de esta tesis. Finalmente, en el último capítulo se presentan las conclusiones generales de la tesis, poniendo en valor los resultados más significativos de cada capítulo, y por tanto de las publicaciones emanadas que permiten la defensa de esta tesis por compendio de artículos.

Los capítulos de resultados tienen la misma configuración: Un breve resumen inicial; una sección experimental específica y constituyendo el grueso de cada capítulo, la explicación y discusión de los resultados correspondientes. A continuación se describen los contenidos de los diferentes capítulos.

Capítulo 1. Introducción

Se pasa revista a la actualidad de las diferentes rutas de valorización de biomasa para la producción de combustibles y materias primas. Entre ellas, se centra la atención en la hidrodeoxigenación (HDO) del bio-oil. La revisión del conocimiento y la tecnología de esta materia comprende un repaso a los catalizadores empleados y a su composición (función metálica y soporte ácido), condiciones de reacción y esquemas de reacción. Se analiza el progreso en la preparación y aplicación de materiales carbonosos como catalizadores y soportes de catalizadores metálicos y bifuncionales, prestando particular atención a la iniciativa de activación química de precursores lignocelulósicos para la obtención de carbones activos con propiedades idóneas como catalizadores ácidos, justificando su uso en esta tesis. Finalmente, se ha enmarcado el proceso de HDO de bio-oil en el contexto de desarrollo de una biorefinería (refinería sostenible basada en la biomasa). Los puntos de interés prioritario y las lagunas de conocimiento que condicionan el desarrollo tecnológico del proceso de HDO del bio-oil han permitido identificar los objetivos de esta tesis.

En el marco de contextualizar la tesis, se proponen sus objetivos. El objetivo principal es contribuir al desarrollo de un proceso catalítico de hidrodeoxigenación del bio-oil completo. Para ello, se proponen los siguientes **objetivos individuales**:

- Desarrollar un sistema experimental para procesar esta corriente compleja de forma continua.
- Evaluar los catalizadores de carbón activo como alternativa a soportes inorgánicos.
- Comparar el comportamiento de metales nobles y metales de transición.
- Establecer la relación entre la composición del medio y los mecanismos de desactivación.
- Determinar las condiciones adecuadas para la operación estable con un notable rendimiento de aromáticos y fenoles.
- Mejorar la selectividad a aromáticos y fenoles mediante la adición de zeolitas HZSM-5
- Desarrollar un modelo cinético para la HDO de bio-oil completo que cuantifique la evolución con el tiempo y la deposición de productos sólidos

Capítulo 2. Experimental

Se describen las etapas y metodología de preparación y caracterización de los catalizadores (frescos y usados) y los equipos de reacción y análisis de los productos. Como los equipos específicos de análisis se describen en cada capítulo, en este apartado general, se presentan los diagramas del horno tubular donde se han preparado los catalizadores de carbón activo, así como se resumen todos los catalizadores y precursores empleados. Igualmente, se muestra un diagrama del sistema de reacción, donde se detallan los sistemas de alimentación y las líneas de gases empleadas. Por último, se detallan esquemáticamente los productos obtenidos, en cuatro fases: gaseosa, líquida orgánica y acuosa, y sólida. Se enumeran todas las técnicas empleadas para la caracterización del bio-oil y de estas cuatro fases de productos.

Capítulo 3. Evaluación del carbón activo como soporte ácido

En este capítulo, correspondiente a la publicación: Appl. Catal. B. Environ. **2017**, *203*, 389−399, se muestran los resultados de actividad, selectividad y estabilidad de los catalizadores bifuncionales PtPd/ACP y PtPd/FCC, preparados por impregnación de la función metálica PtPd sobre carbón activo activado con H3PO4 (ACP) y sobre un catalizador utilizado en la unidad de FCC (basado en zeolita HY). Al ser el primer trabajo en el tema también se hizo un análisis primario del efecto de las condiciones de reacción sobre la conversión, rendimientos y selectividades de las fracciones de productos, estableciendo la ventana de operación para los trabajos posteriores.

Las propiedades fisico-químicas de los soportes estudiados son significativamente diferentes, lo que condiciona las propiedades de los catalizadores correspondientes. El catalizador PtPd/ACP tiene una superficie específica de 1305 m^2 g^{-1}, con una estructura de micro y mesoporos muy desarrollada. Por el contrario, el catalizador PtPd/FCC, tiene una pequeña superficie específica, de 53 m^2 g^{-1}, y una baja porosidad, correspondiente a una estructura predominantemente macroporosa (correspondiente a la matriz del catalizador de FCC). Además, el ACP aporta al catalizador una mayor acidez que el catalizador de FCC (equilibrado), debido a la generación de grupos superficiales de P durante el proceso de carbonización/activación de la biomasa (huesos de aceituna). Entre estos grupos activos, destacan las especies fosfato $-C-O-PO_3$ y $-C-PO_3$, con propiedades de ácido Brønsted y que tienen una elevada estabilidad hidrotérmica. La presencia generalizada de estos grupos ácidos en la superficie se ha demostrado mediante espectroscopía XPS. El procedimiento de activación y la estabilidad alcanzada son un progreso importante para la utilización del ACP en los catalizadores, dado que los grupos carboxilo también generados por la presencia de oxígeno en el precursor, se degradan y no son activos en las severas condiciones de reacción del proceso. Además, la estructura porosa del ACP soporte es idónea para facilitar la dispersión del metal impregnado. Así, mediante análisis TEM y adsorción de CO se ha determinado un menor tamaño de partículas metálicas, una mayor dispersión y una mayor superficie metálica en el catalizador soportado sobre ACP.

Los productos volátiles de la HDO de bio-oil son mayoritariamente líquidos y gases. Sin embargo, también tiene lugar la deposición de productos sólidos sobre el catalizador, con responsabilidad en su desactivación. El producto líquido, en la que se centra la atención por el interés de sus componentes, se compone de dos fracciones, acuosa y orgánica, separables por decantación. La fase acuosa está constituida por agua (como componente mayoritario) y diferentes oxigenados, con metanol, acetona, ácido acético y fenoles, como los más representativos. En la fase orgánica están presentes hidrocarburos, y entre ellos parafinas lineales, cicloparafinas y aromáticos.

Los rendimientos de las fracciones gaseosa y líquida orgánica aumentan al aumentar la temperatura de reacción, debido a que se favorecen los mecanismos de craqueo de los oxigenados del bio-oil. El máximo rendimiento de fracción orgánica (20.5% en masa) es obtenido con el catalizador PtPd/ACP a 450 °C, condición en la que es nítida la separación de fases en el producto líquido, lo cual no sucede a 400 °C debido a la insuficiente relación (fracción orgánica)/(fracción acuosa). La importancia del soporte se pone de manifiesto con el menor rendimiento de fase orgánica (14%) con el catalizador PtPd/FCC en las condiciones óptimas (450 °C), en las que es mayor el rendimiento de la fracción acuosa (27%).

Igualmente, las propiedades de los catalizadores tienen una gran incidencia en la selectividad y composición de las fracciones de productos. La concentración de oxigenados disminuye drásticamente al aumentar la temperatura con el catalizador PtPd/ACP. Con este catalizador, a 450 °C las concentraciones máximas de metanol y fenol en la fase acuosa son 55 y 10%, respectivamente, mientras que esta fase es el 21% del líquido usando el catalizador PtPd/FCC. En la fase orgánica, los compuestos mayoritarios son los aromáticos, alcanzándose una concentración de aromáticos de 1 anillo en la fase orgánica del 50% con el catalizador PtPd/ACP. La concentración no deseada de poliaromáticos es mayor con el catalizador PtPd/FCC (35%).

Un aspecto fundamental en la comparación de los catalizadores es su estabilidad, puesta a prueba en la HDO del bio-oil por las condiciones de elevada presión y temperatura, y la elevada concentración de agua en el medio de reacción. Además, los oxigenados en el bio-oil repolimerizan, bloqueando centros activos y progresivamente también los poros del soporte. Siguiendo la evolución con el tiempo de la generación de agua como una medida básica de la actividad, se observa una notable atenuación de la desactivación por encima de 450 °C, que es atribuida a la menor deposición de productos sólidos en el catalizador al aumentar la temperatura. Este efecto de la temperatura es tal, que a 450 °C y transcurrido un periodo de desactivación, los dos catalizadores alcanzan un estado pseudo-estable, en el que se mantiene constante la conversión y distribución de productos. La actividad del catalizador PtPd/ACP en este estado es mayor que la del catalizador PtPd/FCC, debido que sus propiedades metálicas y acidas son mejores en este estado.

Capítulo 4. Desactivación del catalizador por coque

Este capítulo recoge los resultados del estudio de los mecanismos de formación y deposición del coque en los dos catalizadores a diferentes temperaturas. Estos resultados corresponden a la publicación: Appl. Catal. B. Environ. **2018**, *239*, 513-524. El estudio ha requerido identificar los precursores de los depósitos carbonosos, mediante la relación entre la velocidad de deposición de cada uno de sus componentes (lignina térmica y coque) y la composición del medio de reacción, la cual es dependiente del catalizador y de la temperatura, y evoluciona con el tiempo.

Los catalizadores usados se han caracterizado mediante diferentes técnicas, para estudiar además de su contenido en el catalizador, la localización, naturaleza y composición del material carbonoso depositado. El análisis por adsorción-desorción de N_2 del deterioro de la estructura porosa de los catalizadores, permite relacionar la localización del coque con la composición del medio de reacción. Así, en condiciones de elevada concentración de oxigenados (baja temperatura) quedan bloqueados todos los poros del catalizador PtPd/ACP. Sin embargo, a 450 °C, con una elevada velocidad de HDO y en las condiciones en las que el catalizador mantiene una actividad remanente de HDO constante, el material carbonoso está depositado preferentemente en los microporos del catalizador.

El análisis termogravimétrico de oxidación a temperatura programada (TPO) ha permitido diferenciar las especies carbonosas en los catalizadores desactivados. Los perfiles TPO muestran tres picos, atribuidos a la combustión de tres fracciones carbonosas diferentes, de diferente composición y ubicación, y por tanto con diferentes temperaturas de combustión. La primera fracción (combustión en torno a 400 °C) corresponde a la lignina térmica, producto la repolimerización de los compuestos oxigenados del bio-oil. Se ha comprobado que este fenómeno es de origen térmico, porque se produce con la misma magnitud sobre un soporte poroso inerte para la HDO y transcurre mayoritariamente sobre la superficie externa del catalizador. La similitud de los perfiles TPO sin y con catalizador, lleva a identificar este primer pico con la lignina térmica. Analizando el efecto de las condiciones de reacción en esta deposición de lignina térmica, se observa que es favorecida en las condiciones de reducida velocidad de HDO (baja temperatura, y catalizador desactivado), en las que es elevada la concentración de oxigenados en el medio de reacción.

El análisis TPO del catalizador fresco ha permitido identificar el pico a mayor temperatura (550 °C) con la combustión del ACP soporte. Obviamente este pico no está presente en el catalizador PtPd/FCC desactivado. El pico a una temperatura intermedia (475 °C), es atribuido al coque de origen catalítico. Es la fracción carbonosa mayoritaria a elevada temperatura de reacción, y la velocidad de su deposición es mayor con una baja concentración de oxigenados en el medio de reacción y una elevada concentración de hidrocarburos productos de la HDO. En estas condiciones está desfavorecido el mecanismo de formación de lignina térmica desde los oxigenados, mientras que se favorece la condensación de los hidrocarburos aromáticos, formando estructuras poli-aromáticas condensadas de coque que bloquean los centros ácidos del catalizador.

El conocimiento de la composición del material carbonoso depositado se ha completado mediante análisis por espectroscopía de desorción/ionización por láser (LDI) y espectrofotmetría de transformada de Fourier (FTIR) de los catalizadores desactivados. Los resultados ratifican la relación antes descrita entre la causa (composición del medio de reacción y temperatura), el efecto directo (velocidad de deposición, localización y naturaleza del material carbonoso depositado) y el efecto indirecto y más importante (la disminución de la actividad de HDO con el tiempo). Así, se ha comprobado el carácter más alifático y ligero del sólido depositado a bajas temperaturas, mientras que el sólido depositado a 450 °C tiene una estructura más condensada. En cuanto a grupos funcionales presentes, el sólido en el catalizador PtPd/ACP usado a 400 °C presenta una elevada concentración de funcionalidades oxigenadas, destacando la presencia de grupos $-$OH y fenólicos, asociados a las cadenas poliméricas de la lignina. Resulta también interesante la composición del solido depositado sobre el catalizador PtPd/FCC a 450 °C, más alifático y oxigenado que el depositado en el PtPd/ACP a esta temperatura, y similar al depositado en el catalizador PtPd/ACP a 400 °C. Este resultado es consecuencia de la mayor actividad del catalizador PtPd/ACP para la HDO de bio-oil y del efecto de esta diferencia en la composición del medio de reacción.

Avanzando en la compresión de los resultados descritos y además, relacionando la evolución con el tiempo de la composición del medio de reacción y de las características de los materiales carbonosos depositados, se ha propuesto un mecanismo de desactivación. Este mecanismo considera la existencia de dos rutas de formación de los depósitos y que transcurren mediante reacciones coexistentes con las etapas de reacción implicadas en la HDO del bio-oil. En estas, los oxigenados del bio-oil (en particular los compuestos fenólicos, productos de la descomposición de la lignina en la biomasa), repolimerizan para formar lignina térmica. Este material se deposita rápidamente en la superficie externa del catalizador, tiene grupos oxigenados y provoca una rápida desactivación del catalizador. Este mecanismo, está favorecido a bajas temperaturas y con soportes poco ácidos, porque, el aumento de la temperatura y la acidez del soporte favorecen la HDO y el hidrocraqueo de los compuestos oxigenados, disminuyendo su concentración y en consecuencia la velocidad de repolimerización. Así, a 400 °C se observó el bloqueo del flujo en el reactor.

En paralelo, los compuestos oxigenados del bio-oil son convertidos en hidrocarburos y aromáticos (desde los fenoles) mediante reacciones de HDO. El aumento de la temperatura favore el avance de la HDO y de la condensación de los hidrocarburos hacia estructuras poliaromáticas (coque), mecanismo activado por los centros ácidos, y que conduce a la deposición de coque en los microporos del catalizador. En unas condiciones de limitada deposición de lignina térmica y de suficiente velocidad de hidrocraqueo de los intermedios precursores del coque (450 °C con el catalizador PtPd/ACP) la formación y eliminación de estos intermedios es equilibrada y el catalizador alcanza un estado pseudo-estable, en el que la actividad remanente de HDO se mantiene constante con el tiempo.

Capítulo 5. Comparación de las funciones metálicas y efecto de la adición de zeolita

Este capítulo corresponde a la publicación: Appl. Catal. B. Environ. **2019**, *259*, 118112. El primer objetivo es la propuesta de un catalizador de metales de transición (NiW/ACP) con el mismo soporte (ACP), y de menor coste que el anteriormente estudiado de metales nobles (PtPd/ACP). El segundo objetivo es evaluar la mejora de la HDO del bio-oil utilizando una mezcla de estos catalizadores bifuncionales con un catalizador ácido de zeolita HZSM-5, para potenciar las reacciones de craqueo e hidrocraqueo. La utilización de zeolitas con diferente acidez permite evaluar la capacidad de esta estrategia para orientar la distribución de productos.

El catalizador NiW/ACP se preparó con un mayor contenido metálico (5.0% Ni y 2.0% W) que el de PtPd/ACP (1.0% Pt y 0.5% Pd), diferencia que tiene como consecuencia un mayor bloqueo parcial de los microporos del soporte en la etapa de impregnación. Así, la superficie específica del PtPd/ACP es de 1380 m^2 g^{-1} y la del NiW/ACP de 886 m^2 g^{-1}, si bien esto no tiene apenas incidencia en el diámetro medio de poro (5.8 nm y 5.6 nm para los catalizadores PtPd/ACP y NiW/ACP, respectivamente). Además, la dispersión de la función metálica es similar y el tamaño de partícula metálica está en el intervalo 10−12 nm en ambos casos.

Las reacciones se llevaron a cabo usando un menor tiempo espacial que en los capítulos anteriores, lo cual permite la comparación de los catalizadores en condiciones de desactivación aún más rápida (al ser mayor la concentración de los oxigenados de bio-oil). También resulta más sencilla la evaluación de la cinética de la reacción. El catalizador PtPd/ACP es más activo en las reacciones de HDO y craqueo, y esto tiene como consecuencia diferencias en la corriente de productos. La primera es la inexistencia de la separación de fases usando el catalizador PtPd/ACP a 450 °C tras 6 h de reacción. Este comportamiento se debe a que los oxigenados pesados del bio-oil son transformados en oxigenados de cadena corta (con metanol como oxigenado mayoritario), gases ($CO/CO_2/CH_4$) y agua. La baja concentración de hidrocarburos pesados apolares provoca la formación de una fase (acuosa), con más de un 95% de agua.

Por el contrario, el producto líquido de la reacción con el catalizador NiW/ACP muestra dos fases, una orgánica y una acuosa, después de 3 h de reacción. El rendimiento total de productos carbonosos es el doble con este catalizador, debido a su menor actividad para las reacciones de HDO y craqueo, con un menor rendimiento de productos gaseosos y también de agua, pero también con una mayor variedad de compuestos en las fases acuosa y orgánica del líquido. Así, a diferencia del catalizador PtPd/ACP, la fase acuosa presenta acetona y ácido acético, además de metanol. En la fase orgánica están presentes fenoles y aromáticos de uno y dos anillos, cuya separación es sencilla mediante decantación.

Los resultados de la acelerada desactivación de los catalizadores corroboran las conclusiones del capítulo anterior (para catalizadores de PtPd), referentes a la relación de la deposición de los materiales carbonosos con la concentración de sus precursores en el medio de reacción. La menor actividad del catalizador NiW/ACP respecto al PtPd/ACP favorece la formación de lignina térmica, debido a la mayor concentración de oxigenados, y la mayor deposición de coque corresponde a situaciones de elevada concentración de aromáticos.

Dado el interés de la producción de aromáticos y fenoles, la utilización de catalizadores de zeolita HZSM-5, cuya capacidad de formación de monoaromáticos está bien establecida, ha perseguido este objetivo. Para evaluar el potencial de esta estrategia, se utilizaron mezclas de los catalizadores PtPd/ACP y NiW/ACP (con un 80%) con catalizadores de zeolitas HZSM-5 con diferente acidez (relación Si/Al de 15 y 140, denominadas Z15 y Z140, respectivamente). Con los dos catalizadores bifuncionales de referencia, el uso de la zeolita con menor acidez (Z140) mejora el rendimiento de productos carbonosos en el líquido, mientras que el uso de la zeolita Z15 lo disminuye, debido a que su elevada acidez favorece las reacciones de decarbonilación, decarboxilación y sobrecraqueo (con formación de gases $CO/CO_2/CH_4$), y también favorece las reacciones de condensación a poliaromáticos con la consiguiente disminución del rendimiento de aromáticos. En el líquido producto están presentes oxigenados de cadena corta (metanol, acetona y acido acético). Por tanto, para la producción de los compuestos de mayor valor añadido (fenoles, alquil fenóles, aromáticos BTX y otros alquil bencenos) resulta adecuada la combinación NiW/ACP+Z140, con rendimientos de compuestos fenólicos y aromáticos del 11 y 15%, respectivamente.

La utilización de zeolitas HZSM-5 como aditivos también modifica el contenido, naturaleza y composición del coque depositado, con resultados dependientes de la acidez de la zeolita. La presencia de la zeolita de baja acidez (Z140) apenas incide en la formación de lignina térmica, especialmente en el caso de la combinación NiW/ACP+Z140 y aumenta ligeramente la deposición de coque. Sin embargo, la zeolita Z15 resulta activa para el craqueo de las cadenas de lignina, evitando casi por completo su crecimiento y deposición. Sin embargo, la acidez de esta zeolita también favorece la condensación de los aromáticos, con la consiguiente disminución de su rendimiento y el aumento de la deposición de coque catalítico. Así, la combinación PtPd/ACP+Z15 presenta una rápida desactivación por coque, con un bloqueo prácticamente total de los centros metálicos (determinada mediante XPS) y de los poros del catalizador (mediante adsorción-desorción de N_2).

Capítulo 6. Modelado cinético de la HDO de bio-oil

El conocimiento del proceso adquirido en los capítulos anteriores se ha plasmado aquí en el modelado cinético de la HDO de bio-oil. Los resultados se recogen en la publicación: Chem. Eng. J. **2020**, *400*, 124679. El catalizador utilizado, de CoMo/ACP, tiene un comportamiento similar al del de NiW/ACP estudiado en el capítulo anterior. La primera etapa del estudio consistió en la experimentación con la temperatura y tiempo espacial como variables, analizando la evolución con el tiempo (hasta 6 h) de la concentración de los componentes del medio de reacción a la salida del reactor.

A partir de los resultados se puede concluir que en los experimentos se repite una pauta, con tres etapas claramente identificadas en el tiempo, características de las reacciones gas-líquido-sólido, las cuales requieren un periodo de tiempo para alcanzar un régimen de flujo estable. En primer lugar, la reacción tiene un periodo de estabilización del flujo, hasta alcanzar el régimen de *trickle bed*, con el mojado completo de la superficie del sólido y un eficiente contacto multifásico. Durante esta etapa se producen mayoritariamente gases $CO/CO_2/CH_4$, por descomposición térmica de los oxigenados ligeros del bio-oil,. Posteriormente, la reacción tiene un periodo transitorio en el que el catalizador se desactiva parcialmente por la deposición de material carbonoso, y en el que cambia significativamente con el tiempo la distribución de productos, aumentando los rendimientos de componentes líquidos (tanto reactantes como productos), y disminuyendo los de productos gaseosos. Trascurrido un tiempo, en torno a 5 h, la reacción alcanza un estado estacionario en el que el catalizador es pseudo-estable, y posteriormente los rendimientos y concentraciones a la salida del reactor son prácticamente constantes.

En cuanto a los productos sólidos, en el estado transitorio se observa una secuencia diferente en la formación con el tiempo de la lignina térmica y del coque. La formación de la lignina ocurre rápidamente, con el primer contacto de la alimentación con el catalizador, y su velocidad de deposición disminuye progresivamente. La tendencia de formación de coque es creciente con el tiempo, tendiendo a un contenido de coque constante. Esta situación se produce sin problemas operacionales en el intervalo 425-475 °C, adecuado para este proceso a mayor escala, y por tanto también para el modelado cinético.

El esquema de reacción para la HDO de bio-oil se ha definido con 7 lumps y 11 reacciones individuales. Así, se han considerado: (i) como reactantes, los reactivos oxigenados del bio-oil (oxigenados de cadena corta y fenoles); (ii) los productos de la HDO (hidrocarburos y aromáticos); (iii) los productos gaseosos, y; (iv) los productos sólidos (distinguiendo entre lignina térmica y coque).

El cálculo de los parámetros cinéticos (constantes cinéticas a la temperatura de referencia y energías de activación) se realiza por resolución de la ecuación de convección-dispersión-reacción en un elemento diferencial de volumen del reactor de lecho fijo, y considerando flujo ideal. Para ello, las ecuaciones para cada lump (expresadas en función de las fracciones molares) se resuelven simultáneamente con las cinéticas de desactivación, considerando para ello el término de acumulación en las ecuaciones de conservación. Los parámetros cinéticos de mejor ajuste corresponden a la minimización de una función objetivo error entre los valores calculados y experimentales de la evolución con el tiempo de las fracciones molares de los diferentes lumps.

En el planteamiento de los balances de materia del modelo se ha considerado la formación significativa de productos sólidos, utilizando una variable adicional que hace referencia a la fracción de carbono en los volátiles (gases+líquido), para cuantificar la cantidad de material carbonoso que se deposita o que forma eficientemente productos en fase líquida en función del tiempo espacial y del tiempo. Una peculiaridad en las ecuaciones de conservación de los productos sólidos es la no existencia del término de transporte, ya que una vez formados se depositan en el lecho catalítico.

La complejidad del mecanismo de desactivación y la diferente incidencia en las etapas del esquema de reacción, ha requerido la utilización de un modelo de desactivación selectiva, con diferentes actividades para cada etapa de reacción y con expresiones cinéticas en cada caso independientes de la concentración del medio de reacción. Este modelo de desactivación selectiva representa la realidad de la rápida desactivación de algunas reacciones como la formación de productos gaseosos o sólido y la lenta desactivación de otras como la formación de aromáticos e hidrocarburos.

El modelo cinético propuesto predice razonablemente bien los resultados experimentales en los diferentes periodos. En la primera hora del estado transitorio la elevada concentración de productos gaseosos, así como su incremento con el tiempo espacial y la temperatura (máximo rendimiento de 75%). Igualmente, la diferente evolución de cada lump con el tiempo es predicha correctamente. Por un lado, la desactivación no afecta a las reacciones de HDO durante el estado transitorio, mientras que la condensación de aromáticos a coque y la formación de productos gaseosos sufren la desactivación parcial del catalizado,r y la formación de lignina térmica es suprimida completamente después de 2 h de estado transitorio. Cabe señalar que el modelo es capaz de predecir la cantidad máxima de lignina térmica que se depositaria en ausencia de catalizador (7 g g^{-1}), valor muy elevado que haría imposible mantener un flujo continuo para el procesado de bio-oil. Un resultado acorde con el comentado es de la evolución de la fracción de carbono en la fase de volátiles. Esta variable toma valores menores al 20% durante las primeras 2 h de estado transitorio, para después mantenerse constante en un valor del 100%.

Las evoluciones de estas actividades justifican el aumento de compuestos fenólicos (reactantes) y aromáticos (intermedios del esquema de reacción) hasta los valores máximos en el estado estacionario, que es el de interés para un aumento de escala.

El modelo cinético se ha adaptado para facilitar la predicción de las distribuciones de productos en el estado estacionario. En esta situación, el término de acumulación no es requerido, y se consideran constantes los valores de las actividades calculados para este estado. Los parámetros cinéticos no sufren cambios sustanciales respecto a los calculados con el modelo para el estado transitorio y la composición a la salida del reactor es igualmente estimada correctamente con este modelo (12% fenoles y 25% de aromáticos). Con esta simplificación, se evitan las complejidades del modelo para el estado transitorio y disminuye significativamente el tiempo de cálculo.

Capitulo 7. Conclusiones generales

La tesis culmina con la presentación de unas conclusiones o consideraciones finales extraídas de los principales resultados en cada uno de los capítulos que ha dado lugar a la publicación de los diferentes artículos que componen esta tesis. Estas conclusiones ponen de manifiesto el cumplimiento de los objetivos previstos, con resultados relevantes sobre la HDO del bio-oil. Los resultados científicos corresponden a la propuesta de catalizadores originales con carbones activos como soportes, al conocimiento de las etapas del mecanismo de la HDO, la comprensión de la deposición de lignina térmica y coque, y la obtención de un modelo cinético basado en el mecanismo de HDO del bio-oil y de formación de depósitos, que permite cuantificar la evolución con el tiempo de la distribución de productos. Por su interés aplicado, el control de la desactivación del catalizador y la obtención de una ventana de condiciones de operación para la producción estable de aromáticos y fenoles, junto con un modelo cinético para cuantificar esta producción, son herramientas de interés para progresar hacia la implantación del proceso a mayor escala.

UNIVERSIDAD
DE MÁLAGA

List of Figures

1.1 Routes for the valorization of lignocellulosic biomass (adapted from [1]). 2
1.2 Alternative strategies for the valorization and upgrading of bio-oil (adapted from [10]). 8
1.3 Proposed valorization of bio-oil in FCC units (adapted from [61]). . . 11
1.4 Two-stage (a) catalytic cracking or (b) steam reforming of bio-oil for the removal of thermal lignin (adapted from [69] and [70]). 12
1.5 Proposed integration of the two-stage HDO process into petroleum refinery (adapted from [80]). 25
1.6 Different activated carbon shapes: (a) granular, (b) fiber mesh, (c) individual fibers and (d) tubes. 27
1.7 Routes for the preparation of activated carbons from lignocellulosic precursors (adapted from [160]). 29
1.8 Main P functionalities anchored on the carbon activated with H_3PO_4 (adapted from [164]). 33
1.9 Main applications of activated carbons in (a) adsorption, (b) electrochemical and (c) catalytic systems. 35
1.10 Overall diagram of the HDO process. 41

2.1 Schematic diagram of the horizontal tube furnace setup (adapted from [160]). 46
2.2 Schematic diagram of the reaction unit (adapted from [245]). 48
2.3 Diagram of products collection. 50

3.1 (a) N_2 adsorption-desorption isotherms and (b) pore size distribution for PtPd/ACP and PtPd/FCC catalysts. 60
3.2 TEM micrographs for (a) PtPd/ACP and (b) PtPd/FCC catalysts and Pt-Pd particle size distributions histograms for (c) PtPd/ACP and (d) PtPd/FCC catalysts. 61
3.3 P2p spectrum for PtPd/ACP obtained by XPS. 62

3.4 Evolution with time of the water content in the aqueous fraction for the PtPd/ACP catalyst at three different temperatures and for the PtPd/FCC catalyst at 450 °C. 66
3.5 Product yields obtained for PtPd/ACP catalyst at three temperatures and for PtPd/FCC catalyst at 450 °C. 67
3.6 Product distribution of the (a) aqueous and (b) organic fractions for PtPd/ACP catalyst at three temperatures and for PtPd/FCC catalyst at 450 °C. 69
3.7 (a) FTIR spectra of bio-oil and liquid products obtained at 450 °C for the PtPd/ACP catalyst (in blue the aqueous fraction and in black the organic one). (b) Relative evolution with time of alkane, aliphatic and aromatic relative concentrations obtained from ^{1}H-NMR measures (each fraction is normalized to one). 71
3.8 Gas fraction composition for PtPd/ACP catalyst at three temperatures and for PtPd/FCC catalyst at 450 °C. 73
3.9 TPO profiles of used PtPd/ACP catalysts at three reaction temperatures and used PtPd/FCC catalyst at 450 °C. 75

4.1 (a) Contour map of double bond equivalent (DBE) values versus the number of carbons for the raw bio-oil (color intensity referred to the relative abundance of each lump of compounds), and (b) DBE and (c) number of carbons versus their relative abundance (RA). . . 83
4.2 GC/MS chromatographs of raw bio-oil. 83
4.3 (a) Evolution with time of the HDO conversion and (b) product fraction distribution for the different catalysts and conditions. 87
4.4 FTIR spectra of the raw bio-oil, liquid product after 1 h on stream and liquid aqueous (AF) and organic fractions (OF) after 8 h on stream, using the (a) PtPd/ACP and (b) PtPd/FCC catalysts at 450 °C. 89
4.5 Intensity of the FTIR bands obtained from the integration of the spectra of the (a) aqueous and (b) organic fractions of liquid product with time using the PtPd/ACP and PtPd/FCC catalysts. 90
4.6 (a) GC/MS chromatograms of the aqueous fraction liquid product obtained with the PtPd/ACP and PtPd/FCC catalysts at 450 °C and (b) GC×GC/MS chromatogram of the organic fraction liquid product obtained with the PtPd/ACP catalyst at 450 °C (8 h on stream). 91

4.7 Contour map of DBE versus the number of carbons, and DBE and number of carbons versus their relative abundance (RA), for the aqueous fraction of the liquid product obtained with the PtPd/ACP catalyst at (a) 400 °C, (b) 425 °C and (c) 450 °C, and (d) with the PtPd/FCC catalyst at 450 °C. (Color intensity referred to the relative abundance of each lump of compounds). 92
4.8 Contour map of DBE versus the number of carbons, and DBE and number of carbons versus their relative abundance (RA), for the organic fraction of the liquid product obtained with the PtPd/ACP catalyst at (a) 400 °C, (b) 425 °C and (c) 450 °C, and (d) with the PtPd/FCC catalyst at 450 °C. (Color intensity referred to the relative abundance of each lump of compounds). 93
4.9 Distribution of representative products in the aqueous and organic fractions using PtPd/ACP and PtPd/FCC catalysts at 400−450 °C. 94
4.10 Deterioration of the main structural properties for the used (a) PtPd/ACP catalyst at 400−450 °C and (b) PtPd/FCC catalyst at 450 °C. 96
4.11 TPO profiles of (a) the used PtPd/ACP and PtPd/FCC catalysts, (b) the fresh ACP catalyst and the bare thermal lignin (TL). 98
4.12 (a) LDI/MS spectra of the fresh and used PtPd/ACP catalyst at 450 °C, and (b) normalized distribution of the LDI/MS profiles of the used catalysts. 100
4.13 Intensity of the FTIR bands obtained from the integration of the spectra for (a) the used PtPd/ACP catalysts at 400−450 °C and (b) the used PtPd/FCC catalyst at 450 °C. 101
4.14 FTIR spectra of the (a) fresh PtPd/ACP catalyst, (b) used PtPd/ACP catalyst and (c) used PtPd/FCC catalyst at 450 °C. 102

5.1 N_2 adsorption-desorption isotherms of the bare ACP support, Z140 zeolite, PtPd/ACP and NiW/ACP catalysts and the physical mixture of NiW/ACP+Z140. 113
5.2 TEM images and metal particle size distribution for the fresh (a, c) PtPd/ACP and (b, d) NiW/ACP catalysts. 115
5.3 Evolution with time of the main yields of products (in a wet bio-oil basis) obtained using the (a) PtPd/ACP and (b) NiW/ACP catalysts.117
5.4 Evolution with time of the yields of the main liquid carbon lumps using the (a) PtPd/ACP and (b) NiW/ACP catalysts. 118
5.5 Relative water content in the aqueous product phases formed with the PtPd/ACP and NiW/ACP catalysts. 119

5.6 Evolution with time of the relative composition of the oxygenate product lump formed using the (a) PtPd/ACP and (b) NiW/ACP catalysts. 120
5.7 Concentration of the main components in the gas products formed using the PtPd/ACP and NiW/ACP catalysts. 121
5.8 Evolution with time of the main yields of products (in a wet basis) obtained using the mixed (a) PtPd+Z140, (b) PtPd+Z15 (c) NiW+Z140 and (d) NiW+Z15 catalysts. 123
5.9 Evolution with time of the yield of total carbon products (on a dry basis) for the PtPd/ACP and NiW/ACP catalysts and their mixtures with Z140 and Z15 zeolites. 124
5.10 Effect of zeolite addition to (a) PtPd/ACP and (b) NiW/ACP catalysts on the evolution with time of TON in terms of obtained total carbon products. 125
5.11 Comparison of the main yields of products after 6 h on stream for the (a) PtPd/ACP and (b) NiW/ACP catalysts and their mixtures with Z140 and Z15 zeolites. 125
5.12 TPO profiles for the combustion of the fresh and used (a) PtPd/ACP and (b) NiW/ACP catalysts and their mixtures with Z140 and Z15 zeolites. 127
5.13 Deconvolution of the TPO profiles for the used mixed (a) PtPd+Z140 and (b) NiW+Z140 catalysts. 128
5.14 XPS spectra of (a, b) C1s and (c, d) O1s moieties for the fresh and used catalysts. 132
5.15 XPS spectra of (a, b) P2p, (c) Pt4f, (d) Pd3d, (e) Ni2p and (f) W4f moieties for the fresh and used catalysts. 133

6.1 Deconvolution of the TPO profiles for the used catalysts at (a) 425 °C, 0.3 g h $g_{\mathrm{bio-oil}}^{-1}$ and (b) 475 °C, 0.15 g h $g_{\mathrm{bio-oil}}^{-1}$. 139
6.2 (a) TEM micrograph of the CoMo/ACP catalyst and atomic distribution of (b) C, (c) O, (d) P, (e) Co and (f) Mo by EDX analysis. . 145
6.3 Evolution with time on stream of (a) the molar fractions of liquid (OX, HC, aPh, aA) and gaseous products (G), and (b) the content of solid products (TL and CK) in the catalyst at 450 °C. Space time, 0.3 g h $g_{\mathrm{bio-oil}}^{-1}$ (Error bars show the confidence interval from the C balance closure of experimental data). 146
6.4 Parity plot for the transient model fit at (a) 425 °C, (b) 450 °C and (c) 475 °C. 152

6.5 Comparison of the experimental data (symbols) to those predicted by the kinetic model (lines) for the evolution with space time of (a, b, c) the molar fractions of liquid and gaseous products and (d, e, f) the content of solid products in the catalyst at (a, d) 425 °C, (b, e) 450 °C and (c, f) 475 °C. $t = 0$. 153

6.6 Comparison of the experimental data (symbols) to those predicted by the kinetic model (lines) for the evolution with time of (a, b, c) the molar fractions of liquid and gaseous products and (d, e, f) the content of solid products in the catalyst at (a, d) 425 °C, (b, e) 450 °C and (c, f) 475 °C. Space time, 0.3 g h $\mathrm{g_{bio-oil}^{-1}}$. 155

6.7 Calculated evolution with space time and time of the carbon fraction in the gas+volatile phase at (a) 425 °C, (b) 450 °C and (c) 475 °C. . 156

6.8 Calculated evolution with time of the activity parameters at (a) 425 °C, (b) 450 °C and (c) 475 °C. 156

6.9 Comparison of the experimental data (symbols) to those predicted by the model (lines) for the evolution with space time of the molar fractions of liquid and gaseous products at (a) 425 °C, (b) 450 °C and (c) 475 °C. Time on stream, > 5 h. 158

6.10 Comparison of the apparent (a) kinetic constants (in $\mathrm{mol_C\ g^{-1}\ h^{-1}\ bar^{-1}}$) and (b) activation energy values (in $\mathrm{kJ\ mol^{-1}}$) for the kinetic model considering all reaction steps (transient state, Y axis) and the adaptation for the pseudo-steady state (X axis). 159

UNIVERSIDAD
DE MÁLAGA

List of Tables

1.1 Average properties of raw bio-oil and heavy fuel (adapted from [41]). 6
1.2 Catalysts (including noble metal, transition metals, metal sufides and metal phosphides), conditions and representative model compounds proposed for bio-oil HDO in packed bed reactors (adapted from [72]). 16
1.3 Effect of C−O bond nature on the required dissociation energy (adapted from [126]). 20
1.4 Proposed catalysts and conditions for the two-stage mild/deep HDO process (adapted from [10]). 26
1.5 Elemental and proximate analysis of different lignocellulosic biomass (adapted from [156]). 28
1.6 Porous properties and chemical surface composition (adapted from [124]). 32
1.7 Proposed catalysts and conditions for bio-oil HDO using carbon supports (adapted from [10]). 38

2.1 Nominal concentrations and salt precursors of the metallic function in the bifunctional catalysts. 47
2.2 Techniques used for catalyst characterization. 47
2.3 Techniques used for bio-oil and reaction product characterization. . . 51

3.1 Bio-oil composition. 57
3.2 Physico-chemical properties of the catalysts. 59
3.3 Main P groups identified in the activated carbon surface. 63
3.4 Product fraction yields for different reaction temperatures. Time on stream, 6 h. 64

4.1 Most representative compounds of bio-oil from black poplar sawdust. 84

5.1 Physico-chemical properties of the fresh catalyst. 114

5.2 Total coke content, relative content of each coke fractions (from TPO profile deconvolution) and C/O ratio (from XPS analysis) of the used catalysts. 128
5.3 Porous structural parameters of the used catalysts. 130
5.4 XPS surface composition of the used catalysts. 131

6.1 Most significant component detected in the raw bio-oil and liquid product analyses. 140
6.2 Physico-chemical properties of the fresh catalyst. 144
6.3 Kinetic parameters for the transient state model of raw bio-oil HDO. 151
6.4 Kinetic parameters for the pseudo-steady state model of raw bio-oil HDO. 158

List of Schemes

1.1 Proposed pathways for the catalytic cracking of oxygenated compounds present in bio-oil (adapted from [58, 59]). 9
1.2 Main pathways involved in bio-oil HDO (adapted from [82]). 20
1.3 Proposed pathway for acetone HDO (adapted from [103]). 21
1.4 Proposed pathway for phenol HDO (adapted from [132]). 22
1.5 Proposed pathway for guaiacol HDO (adapted from [134]). 23
1.6 Proposed parallel deactivation mechanism for bio-oil processing (adapted from [139]). 24
1.7 (a) Formation of phosphate ester on side chains (cross-linking) and (b) elimination of H_3PO_4 during biomass activation (adapted from [173]). 31

4.1 Proposed mechanism for raw bio-oil HDO including coke formation over the catalysts. 104

6.1 Reaction network for raw bio-oil HDO. 148
6.2 Detailed lump-based reaction network for raw bio-oil HDO. 149

UNIVERSIDAD
DE MÁLAGA

Nomenclature

a_k	Activity parameter k
a_{kf}	Final value of a_k after the transient-state stage
C_i	Content of the i solid product normalized per catalyst weight, $\mathrm{mol_C\ g^{-1}}$
C_{TL}^{max}	Maximum content of TL in the catalyst, $\mathrm{mol_C\ g^{-1}}$
c	Number of carbon atoms in the molecule
DBE	Double bond equivalent
E	Apparent activation energy, $\mathrm{kJ\ mol^{-1}}$
$E_{j/j}$	Ratio between the activation energy of each j step of the reaction in the transient and pseudo-steady state models
$F_{\mathrm{bio-oil}}$	Total mass flow rate of bio-oil, $\mathrm{g\ h^{-1}}$
F_{C}	Mass flow rate of the oxygenates in bio-oil, $\mathrm{g\ h^{-1}}$
F_i	Flow rates of each i product, $\mathrm{g\ h^{-1}}$ or $\mathrm{mol\ h^{-1}}$
F_{W}	Mass flow rate of water at the outlet of the reactor, $\mathrm{g\ h^{-1}}$
F_{W}^0	Mass flow rate of water at the entrance of the reactor, $\mathrm{g\ h^{-1}}$
F_{W}^t	Theoretical maximum mass flow rate of water at the outlet of the reactor with full HDO conversion, $\mathrm{g\ h^{-1}}$
G_C	Carbon fraction in the gas+volatile phase, $\mathrm{mol_C\ mol_C^{-1}}$
h	Number of hydrogen atoms in the molecule
k	Kinetic constant
k^*	Kinetic constant at the reference temperature

k_{dk}	Deactivation kinetic constant for each k activity, h^{-1}
k_j	Apparent kinetic constant for each j step of the reaction network
$k_{j/j}$	Ratio between the kinetic constant of each j step of the reaction in the transient and pseudo-steady state models
L	Catalytic bed length, m
N_C	(Carbon molar flow rate)/(total molar flow rate) ratio, $\mathrm{mol_C\ mol^{-1}}$
$n_{e,0}$	Total number of initial experimental data
$n_{e,d}$	Total number of experimental data at $t > 0$
n_l	Number of lumps
P	Pressure, bar
P_R	Partial pressure of the reactant R, bar
R	Universal gas constant
R_i	Formation rate of each i solid product, $\mathrm{mol_C\ g^{-1}\ h^{-1}}$
r_i	Formation rate of each i lump, $\mathrm{mol_C\ g^{-1}\ h^{-1}}$
r_j	Reaction rate of each j step of the reaction network, $\mathrm{mol_C\ g^{-1}\ h^{-1}}$
SSE	Sum of square errors
T	Temperature, K
T^*	Reference temperature, K
t	Time, h
v	Linear velocity of the gas, $\mathrm{m\ h^{-1}}$
X_{HDO}	HDO conversion
Y_i	Yield of each i product lump in dry basis
$\overline{Y_i}$	Yield of each i product in wet basis
y_i	Molar fraction in terms of contained C units, $\mathrm{mol_C\ mol_C^{-1}}$
y_i^e	Experimental molar fraction of each i lump in terms of contained C units, $\mathrm{mol_C\ mol_C^{-1}}$

$y_{i,0}$	Initial molar fraction of each i lump in terms of contained C units, $\mathrm{mol_C\ mol_C^{-1}}$
$y_{i,0}^{e}$	Initial experimental molar fraction of each i lump in terms of contained C units, $\mathrm{mol_C\ mol_C^{-1}}$
z	Longitudinal position of the reactor, m

Abbreviations

*t*BA	*tert*-Butylamine
AC	Activated carbon
ACP	P-containing activated carbon support
FCC	Discarded FCC catalyst used as support
HDO	Hydrodeoxygenation
OS	Olive stone
PSD	Pore size distribution, $\mathrm{cm^3\ g^{-1}\ Å^{-1}}$
$\mathrm{S_{DR}}$	Narrow micropore surface area, $\mathrm{m^2\ g^{-1}}$
$\mathrm{S_{ext}}$	External surface area, $\mathrm{m^2\ g^{-1}}$
$\mathrm{S_{BET}}$	BET specific surface area, $\mathrm{m^2\ g^{-1}}$
$\mathrm{S_{metal}}$	Metallic surface, $\mathrm{m^2\ g^{-1}}$
TON	Turnover number, $\mathrm{g_C\ mmol_{H+}^{-1}\ mg_M^{-1}}$
$\mathrm{V_{DR}}$	Narrow micropore volume, $\mathrm{cm^3\ g^{-1}}$
$\mathrm{V_{mes}}$	Mesopore volume, $\mathrm{cm^3\ g^{-1}}$
$\mathrm{V_{micr}}$	Micropore volume, $\mathrm{cm^3\ g^{-1}}$
$\mathrm{V_{pore}}$	Total pore volume, $\mathrm{cm^3\ g^{-1}}$

Greek Symbols

ε	Effective bed-particle porosity
ρ	Catalytic bed density, $\mathrm{kg\ m^{-3}}$

Lumps

AC	Acids, mainly acetic acid
AL	Alcohols, mainly 2-propanol
AT	Acetates, mainly methylacetate
aA	Alkylaromatics
aA1	1-ring alkylaromatics
aA2	2-ring alkylaromatics
aMP	Alkylmethoxyphenols
aNP	Alkylnaphthalenes
aPh	Alkylphenolics
CK	Catalytic coke
ET	Esters
G	Gaseous products
HC	Hydrocarbons
KT	Ketones, mainly acetone
LO	Light olefins
O	Olefins
OX	Oxygenates
PF	Paraffins
TL	Thermal lignin

Subscripts

d	Deactivation
i	Lump i
j	Step j of the reaction network
k	Activity k
R	Reactant

Superscripts

$*$	At the reference temperature
e	Experimental data

UNIVERSIDAD
DE MÁLAGA

References

[1] T. Cordero, PhD thesis, University of Malaga, **1987**.

[2] D. Guban, I. K. Muritala, M. Roeb, C. Sattler, *International Journal of Hydrogen Energy* **2020**, *45*, 26156–26165.

[3] F. Cherubini, *Energy Conversion and Management* **2010**, *51*, 1412–1421.

[4] C. Wang, X. Zhang, Q. Liu, Q. Zhang, L. Chen, L. Ma, *Fuel Processing Technology* **2020**, *208*, 106485.

[5] G. Dragone, A. A. Kerssemakers, J. L. Driessen, C. K. Yamakawa, L. P. Brumano, S. I. Mussatto, *Bioresource Technology* **2020**, *302*, 122847.

[6] V. L. Pachapur, S. Kaur Brar, Y. Le Bihan, *Bioresource Technology* **2020**, *299*, 122632.

[7] J. Jae, G. A. Tompsett, Y.-C. Lin, T. R. Carlson, J. Shen, T. Zhang, B. Yang, C. E. Wyman, W. C. Conner, G. W. Huber, *Energy and Environmental Science* **2010**, *3*, 358–365.

[8] L. Shuai, M. T. Amiri, Y. M. Questell-Santiago, F. Heroguel, Y. Li, H. Kim, R. Meilan, C. Chapple, J. Ralph, J. S. Luterbacher, *Science* **2016**, *354*, 329–334.

[9] J. Long, Q. Zhang, T. Wang, X. Zhang, Y. Xu, L. Ma, *Bioresource Technology* **2014**, *154*, 10–17.

[10] B. Valle, A. Remiro, N. García-Gómez, A. G. Gayubo, J. Bilbao, *Journal of Chemical Technology & Biotechnology* **2019**, *94*, 670–689.

[11] J. Badra, A. S. AlRamadan, S. M. Sarathy, *Applied Energy* **2017**, *203*, 778–793.

[12] J. E. Anderson, T. J. Wallington, *Energy and Fuels* **2020**, *34*, 4632–4642.

[13] A. G. Gayubo, A. Alonso, B. Valle, A. T. Aguayo, J. Bilbao, *Applied Catalysis B: Environmental* **2010**, *97*, 299–306.

[14] Y. C. Sharma, A. Kumar, R. Prasad, S. N. Upadhyay, *Renewable and Sustainable Energy Reviews* **2017**, *74*, 89–103.

[15] I. Hita, J. M. Arandes, J. Bilbao in *Chemical Catalysts for Biomass Upgrading*, Wiley-VCH Verlag GmbH & Co. KGaA, **2019**, Chapter 3.

[16] H. B. Aditiya, T. M. Mahlia, W. T. Chong, H. Nur, A. H. Sebayang, *Renewable and Sustainable Energy Reviews* **2016**, *66*, 631–653.

[17] W. van Zyl, L. Lynd, R. den Haan, J. Mcbride in *Advances in biochemical engineering/biotechnilogy*, **2007**, pp. 205–236.

[18] S. K. Sansaniwal, K. Pal, M. A. Rosen, S. K. Tyagi, *Renewable and Sustainable Energy Reviews* **2017**, *72*, 363–384.

[19] S. Heidenreich, P. U. Foscolo, *Progress in Energy and Combustion Science* **2015**, *46*, 72–95.

[20] A. Molino, S. Chianese, D. Musmarra, *Journal of Energy Chemistry* **2016**, *25*, 10–25.

[21] J. Alvarez, G. Lopez, M. Amutio, J. Bilbao, M. Olazar, *Energy Conversion and Management* **2019**, *181*, 214–222.

[22] M. Cortazar, G. Lopez, J. Alvarez, M. Amutio, J. Bilbao, M. Olazar, *Fuel* **2019**, *253*, 1446–1456.

[23] H. De Lasa, E. Salaices, J. Mazumder, R. Lucky, *Chemical Reviews* **2011**, *111*, 5404–5433.

[24] A. Sanna, *Bioenergy Research* **2014**, *7*, 36–47.

[25] R. E. Guedes, A. S. Luna, A. R. Torres, *Journal of Analytical and Applied Pyrolysis* **2018**, *129*, 134–149.

[26] V. Strezov, M. Patterson, V. Zymla, K. Fisher, T. J. Evans, P. F. Nelson, *Journal of Analytical and Applied Pyrolysis* **2007**, *79*, 91–100.

[27] M. Sharifzadeh, M. Sadeqzadeh, M. Guo, T. N. Borhani, N. V. Murthy Konda, M. C. Garcia, L. Wang, J. Hallett, N. Shah, *Progress in Energy and Combustion Science* **2019**, *71*, 1–80.

[28] D. Meier, B. Van De Beld, A. V. Bridgwater, D. C. Elliott, A. Oasmaa, F. Preto, *Renewable and Sustainable Energy Reviews* **2013**, *20*, 619–641.

[29] M. Patel, X. Zhang, A. Kumar, *Renewable and Sustainable Energy Reviews* **2016**, *53*, 1486–1489.

[30] G. W. Huber, S. Iborra, A. Corma, *Chemical Reviews* **2006**, *106*, 4044–4098.

[31] A Oasmaa, S Czernik, *Energy and Fuels* **1999**, *13*, 914–921.

[32] D. Carpenter, T. L. Westover, S. Czernik, W. Jablonski, *Green Chemistry* **2014**, *16*, 384–406.

[33] E. Lazzari, T. Schena, M. C. A. Marcelo, C. T. Primaz, A. N. Silva, M. F. Ferrão, T. Bjerk, E. B. Caramão, *Industrial Crops and Products* **2018**, *111*, 856–864.

[34] E. Fratini, M. Bonini, A. Oasmaa, Y. Solantausta, J. Teixeira, P. Baglioni, *Langmuir* **2006**, *22*, 306–312.

[35] C. M. Michailof, K. G. Kalogiannis, T. Sfetsas, D. T. Patiaka, A. A. Lappas, *Wiley Interdisciplinary Reviews: Energy and Environment* **2016**, *5*, 614–639.

[36] M. Staš, M. Auersvald, L. Kejla, D. Vrtiška, J. Kroufek, D. Kubička, *Trends in Analytical Chemistry* **2020**, *126*, 115857.

[37] Y. Wang, Y. Han, W. Hu, D. Fu, G. Wang, *Journal of Separation Science* **2020**, *43*, 360–371.

[38] A. E. Harman-Ware, J. R. Ferrell, *Energy and Fuels* **2018**, *32*, 8905–8920.

[39] M. Benés, R. Bilbao, J. M. Santos, J. Alves Melo, A. Wisniewski, I. Fonts, *Energy and Fuels* **2019**, *33*, 4272–4286.

[40] T. Kekäläinen, T. Venäläinen, J. Jänis, *Energy and Fuels* **2014**, *28*, 4596–4602.

[41] A. R. Gollakota, M. Reddy, M. D. Subramanyam, N. Kishore, *Renewable and Sustainable Energy Reviews* **2016**, *58*, 1543–1568.

[42] S. Oh, H. S. Choi, U. J. Kim, I. G. Choi, J. W. Choi, *Fuel* **2016**, *182*, 154–160.

[43] A. Oasmaa, T. Sundqvist, E. Kuoppala, M. Garcia-Perez, Y. Solantausta, C. Lindfors, V. Paasikallio, *Energy and Fuels* **2015**, *29*, 4373–4381.

[44] Y. Wang, S. Wang, F. Leng, J. Chen, L. Zhu, Z. Luo, *Separation and Purification Technology* **2015**, *152*, 123–132.

[45] D. C. Elliott, *Energy and Fuels* **2007**, *21*, 1792–1815.

[46] W. Li, Q. Dang, R. Smith, R. C. Brown, M. M. Wright, *ACS Sustainable Chemistry and Engineering* **2017**, *5*, 1528–1537.

[47] X. Chen, Y. Chen, H. Yang, X. Wang, Q. Che, W. Chen, H. Chen, *Bioresource Technology* **2019**, *273*, 153–158.

[48] M. Auersvald, B. Shumeiko, D. Vrtiška, P. Straka, M. Staš, P. Šimáček, J. Blažek, D. Kubička, *Fuel* **2019**, *238*, 98–110.

[49] J. X. Wang, J. P. Cao, X. Y. Zhao, S. N. Liu, X. Y. Ren, M. Zhao, X. Cui, Q. Chen, X. Y. Wei, *Bioresource Technology* **2019**, *278*, 116–123.

[50] M. Olazar, R. Aguado, J. Bilbao, A. Barona, *AIChE Journal* **2000**, *46*, 1025–1033.

[51] K. Iisa, R. J. French, K. A. Orton, M. M. Yung, D. K. Johnson, J. ten Dam, M. J. Watson, M. R. Nimlos, *Energy & Fuels* **2016**, *30*, 2144–2157.

[52] M. Bertero, G. De La Puente, U. Sedran, *Energy and Fuels* **2011**, *25*, 1267–1275.

[53] L. Zhu, K. Li, H. Ding, X. Zhu, *Fuel* **2018**, *211*, 704–711.

[54] D. Chen, J. Zhou, Q. Zhang, X. Zhu, *Renewable and Sustainable Energy Reviews* **2014**, *40*, 69–79.

[55] S. Kotrel, H. Knözinger, B. C. Gates, *Microporous and Mesoporous Materials* **2000**, *35-36*, 11–20.

[56] A. Corma, J. Planelles, J. Sánchez-Marín, F. Tomás, *Journal of Catalysis* **1985**, *93*, 30–37.

[57] M. Boronat, P. M. Viruela, A. Corma, *Journal of the American Chemical Society* **2004**, *126*, 3300–3309.

[58] A. G. Gayubo, A. T. Aguayo, A. Atutxa, R. Aguado, M. Olazar, J. Bilbao, *Industrial & Engineering Chemistry Research* **2004**, *43*, 2610–2618.

[59] A. G. Gayubo, A. T. Aguayo, A. Atutxa, R. Aguado, M. Olazar, J. Bilbao, *Industrial and Engineering Chemistry Research* **2004**, *43*, 2619–2626.

[60] J. D. Adjaye, N. N. Bakhshi, *Fuel Processing Technology* **1995**, *45*, 185–202.

[61] A. D. R. Pinho, M. B. B. De Almeida, F. L. Mendes, V. L. Ximenes, *Pure and Applied Chemistry* **2014**, *86*, 859–865.

[62] W. Nabgan, T. A. Tuan Abdullah, R. Mat, B. Nabgan, Y. Gambo, M. Ibrahim, A. Ahmad, A. A. Jalil, S. Triwahyono, I. Saeh, *Renewable and Sustainable Energy Reviews* **2017**, *79*, 347–357.

[63] A. Arandia, A. Remiro, V. García, P. Castaño, J. Bilbao, A. G. Gayubo, *Catalysts* **2018**, *8*, 322–346.

[64] X. Hu, G. Lu, *Applied Catalysis B: Environmental* **2010**, *99*, 289–297.

[65] S. Thaicharoensutcharittham, V. Meeyoo, B. Kitiyanan, P. Rangsunvigit, T. Rirksomboon, *Catalysis Today* **2011**, *164*, 257–261.

[66] A. C. Basagiannis, X. E. Verykios, *Applied Catalysis A: General* **2006**, *308*, 182–193.

[67] C. Rioche, S. Kulkarni, F. C. Meunier, J. P. Breen, R. Burch, *Applied Catalysis B: Environmental* **2005**, *61*, 130–139.

[68] F. Bimbela, J. Ábrego, R. Puerta, L. García, J. Arauzo, *Applied Catalysis B: Environmental* **2017**, *209*, 346–357.

[69] B. Valle, B. Aramburu, A. Remiro, J. Bilbao, A. G. Gayubo, *Applied Catalysis B: Environmental* **2014**, *147*, 402–410.

[70] A. G. Gayubo, B. Valle, A. T. Aguayo, M. Olazar, J. Bilbao, *Journal of Chemical Technology and Biotechnology* **2010**, *85*, 132–144.

[71] Z. Li, E. Jiang, X. Xu, Y. Sun, R. Tu, *Renewable Energy* **2020**, *146*, 1991–2007.

[72] M. Saidi, F. Samimi, D. Karimipourfard, T. Nimmanwudipong, B. C. Gates, M. R. Rahimpour, *Energy Environ. Sci.* **2014**, *7*, 103–129.

[73] X. Zhang, W. Tang, Q. Zhang, Y. Li, L. Chen, Y. Xu, C. Wang, L. Ma, *Fuel* **2018**, *215*, 825–834.

[74] P. L. Cruz, E. Montero, J. Dufour, *Fuel* **2017**, *196*, 362–370.

[75] K. S. Arias, M. J. Climent, A. Corma, S. Iborra, *Energy Environ. Sci.* **2015**, *8*, 317–331.

[76] R. N. Olcese, M. Bettahar, D. Petitjean, B. Malaman, F. Giovanella, A. Dufour, *Applied Catalysis B: Environmental* **2012**, *115-116*, 63–73.

[77] D. J. Rensel, S. Rouvimov, M. E. Gin, J. C. Hicks, *Journal of Catalysis* **2013**, *305*, 256–263.

[78] G. W. Huber, J. N. Chheda, C. J. Barret, J. A. Dumesic, *Science* **2005**, *308*, 1446–1450.

[79] T. P. Vispute, G. W. Huber, *Green Chemistry* **2009**, *11*, 1433–1445.

[80] A. H. A. Zacher, M. V. M. Olarte, D. D. M. Santosa, D. C. Elliott, S. B. Jones, *Green Chemistry* **2014**, *16*, 491–515.

[81] M. Al-Sabawi, J. Chen, S. Ng, *Energy and Fuels* **2012**, *26*, 5355–5372.

[82] P. M. Mortensen, J. D. Grunwaldt, P. A. Jensen, K. G. Knudsen, A. D. Jensen, *Applied Catalysis A: General* **2011**, *407*, 1–19.

[83] J. Sun, A. M. Karim, H. Zhang, L. Kovarik, X. S. Li, A. J. Hensley, J. S. McEwen, Y. Wang, *Journal of Catalysis* **2013**, *306*, 47–57.

[84] A. Witsuthammakul, T. Sooknoi, *Catalysis Science and Technology* **2015**, *5*, 3639–3648.

[85] J. Wang, Y. Zhang, M. Zhang, Z. Wang, M. Zhang, *Catalysis Today* **2018**, *314*, 164–169.

[86] P. Kumar, S. R. Yenumala, S. K. Maity, D. Shee, *Applied Catalysis A: General* **2014**, *471*, 28–38.

[87] P. M. D. Souza, R. C. Rabelo-neto, L. E. P. Borges, G. Jacobs, B. H. Davis, D. E. Resasco, F. B. Noronha, *ACS Catalysis* **2017**, *7*, 2058–2073.

UNIVERSIDAD
DE MÁLAGA

[88] M. Marafi, E. Furimsky, *Energy and Fuels* **2017**, *31*, 5711–5750.

[89] X. Li, G. Chen, C. Liu, W. Ma, B. Yan, J. Zhang, *Renewable and Sustainable Energy Reviews* **2017**, *71*, 296–308.

[90] J. He, C. Zhao, J. A. Lercher, *Journal of Catalysis* **2014**, *309*, 362–375.

[91] E. A. Roldugina, E. R. Naranov, A. L. Maximov, E. A. Karakhanov, *Applied Catalysis A: General* **2018**, *553*, 24–35.

[92] D. C. Elliott, T. R. Hart, G. G. Neuenschwander, L. J. Rotness, M. V. Olarte, A. H. Zacher, Y. Solantausta, *Energy and Fuels* **2012**, *26*, 3891–3896.

[93] A. Sanna, T. P. Vispute, G. W. Huber, *Applied Catalysis B: Environmental* **2015**, *165*, 446–456.

[94] Y. Huang, L. Wei, X. Zhao, S. Cheng, J. Julson, Y. Cao, Z. Gu, *Energy Conversion and Management* **2016**, *115*, 8–16.

[95] W. Nan, C. R. Krishna, T. J. Kim, L. J. Wang, D. Mahajan, *Energy and Fuels* **2014**, *28*, 4588–4595.

[96] Y. Luo, V. K. Guda, E. B. Hassan, P. H. Steele, B. Mitchell, F. Yu, *Energy Conversion and Management* **2016**, *112*, 319–327.

[97] M. Snåre, I. Kubičková, P. Mäki-Arvela, K. Eränen, D. Y. Murzin, *Industrial and Engineering Chemistry Research* **2006**, *45*, 5708–5715.

[98] C. Newman, X. Zhou, B. Goundie, I. T. Ghampson, R. A. Pollock, Z. Ross, M. C. Wheeler, R. W. Meulenberg, R. N. Austin, B. G. Frederick, *Applied Catalysis A: General* **2014**, *477*, 64–74.

[99] K. A. Resende, C. A. Teles, G. Jacobs, B. H. Davis, D. C. Cronauer, A. Jeremy Kropf, C. L. Marshall, C. E. Hori, F. B. Noronha, A. J. Kropf, C. L. Marshall, C. E. Hori, F. B. Noronha, *Applied Catalysis B: Environmental* **2018**, *232*, 213–231.

[100] A. Gutierrez, R. K. Kaila, M. L. Honkela, R. Slioor, A. O. Krause, *Catalysis Today* **2009**, *147*, 239–246.

[101] A. Gutiérrez, J. M. Arandes, P. Castaño, M. Olazar, J. Bilbao, *Fuel Processing Technology* **2012**, *101*, 64–72.

[102] X. Li, X. Luo, Y. Jin, J. Li, H. Zhang, A. Zhang, J. Xie, *Renewable and Sustainable Energy Reviews* **2018**, *82*, 3762–3797.

[103] W. Zhang, Y. Zhang, L. Zhao, W. Wei, *Energy and Fuels* **2010**, *24*, 2052–2059.

[104] M. Patel, A. Kumar, *Renewable and Sustainable Energy Reviews* **2016**, *58*, 1293–1307.

[105] H. Jahromi, F. A. Agblevor, *Energy* **2017**, *141*, 2186–2195.

[106] C. Guo, K. T. V. Rao, Z. Yuan, S. Q. He, S. Rohani, C. C. Xu, *Chemical Engineering Science* **2018**, *178*, 248–259.

[107] L. Nie, P. M. De Souza, F. B. Noronha, W. An, T. Sooknoi, D. E. Resasco, *Journal of Molecular Catalysis A: Chemical* **2014**, *388-389*, 47–55.

[108] C. Zhao, Y. Kou, A. A. Lemonidou, X. Li, J. A. Lercher, *Chemical Communications* **2010**, *46*, 412–414.

[109] T. M. Huynh, U. Armbruster, M. M. Pohl, M. Schneider, J. Radnik, D. L. Hoang, B. M. Q. Phan, D. A. Nguyen, A. Martin, *ChemCatChem* **2014**, *6*, 1940–1951.

[110] D. Raikwar, M. Munagala, S. Majumdar, D. Shee, *Catalysis Today* **2019**, *325*, 117–130.

[111] C. Ranga, V. I. Alexiadis, J. Lauwaert, R. Lødeng, J. W. Thybaut, *Applied Catalysis A: General* **2019**, *571*, 61–70.

[112] Z. Pan, R. Wang, M. Li, Y. Chu, J. Chen, *Journal of Energy Chemistry* **2015**, *24*, 77–86.

[113] Q. Bu, H. Lei, A. H. Zacher, L. Wang, S. Ren, J. Liang, Y. Wei, Y. Liu, J. Tang, Q. Zhang, R. Ruan, *Bioresource Technology* **2012**, *124*, 470–477.

[114] V. N. Bui, D. Laurenti, P. Afanasiev, C. Geantet, *Applied Catalysis B: Environmental* **2011**, *101*, 239–245.

[115] V. M. L. Whiffen, K. J. Smith, *Energy and Fuels* **2010**, *24*, 4728–4737.

[116] D. J. Rensel, J. Kim, V. Jain, Y. Bonita, N. Rai, J. C. Hicks, *Catalysis Science and Technology* **2017**, *7*, 1857–1867.

[117] D. E. Resasco, *Journal of Physical Chemistry Letters* **2011**, *2*, 2294–2295.

[118] X. Zhu, L. Nie, L. L. Lobban, R. G. Mallinson, D. E. Resasco, *Energy and Fuels* **2014**, *28*, 4104–4111.

[119] C. R. Lee, J. S. Yoon, Y.-W. W. Suh, J.-W. W. Choi, J.-M. M. Ha, D. J. Suh, Y.-K. K. Park, *Catalysis Communications* **2012**, *17*, 54–58.

[120] X. Zhang, T. Wang, L. Ma, Q. Zhang, Y. Yu, Q. Liu, *Catalysis Communications* **2013**, *33*, 15–19.

[121] M. J. Yu, S. H. Park, J. K. Jeon, C. Ryu, J. M. Sohn, S. C. Kim, Y. K. Park, *Journal of Nanoscience and Nanotechnology* **2015**, *15*, 527–531.

[122] P. A. Lazaridis, A. P. Fotopoulos, S. A. Karakoulia, K. S. Triantafyllidis, *Frontiers in chemistry* **2018**, *6*, 295.

[123] S. Echeandia, P. L. Arias, V. L. Barrio, B. Pawelec, J. L. G. Fierro, *Applied Catalysis B: Environmental* **2010**, *101*, 1–12.

[124] J. Bedia, R. Barrionuevo, J. Rodríguez-Mirasol, T. Cordero, *Applied Catalysis B: Environmental* **2011**, *103*, 302–310.

[125] I. Hita, T. Cordero-Lanzac, A. Gallardo, J. M. Arandes, J. Rodríguez-Mirasol, J. Bilbao, T. Cordero, P. Castaño, *Catalysis Communications* **2016**, *78*, 48–51.

[126] E. Furimsky, *Applied Catalysis A: General* **2000**, *199*, 147–190.

[127] K. A. Resende, A. H. Braga, F. B. Noronha, C. E. Hori, *Applied Catalysis B: Environmental* **2019**, *245*, 100–113.

[128] M. Auersvald, B. Shumeiko, M. Staš, D. Kubička, J. Chudoba, P. Šimáček, *ACS Sustainable Chemistry and Engineering* **2019**, *7*, 7080–7093.

[129] M. M. Sullivan, A. Bhan, *ACS Catalysis* **2016**, *6*, 1145–1152.

[130] H. Wan, R. V. Chaudhari, B. Subramaniam, *Energy and Fuels* **2013**, *27*, 487–493.

[131] F. E. Massoth, P. Politzer, M. C. Concha, J. S. Murray, J. Jakowski, J. Simons, *Journal of Physical Chemistry B* **2006**, *110*, 14283–14291.

[132] O. I. Şenol, E. M. Ryymin, T. R. Viljava, A. O. Krause, *Journal of Molecular Catalysis A: Chemical* **2007**, *277*, 107–112.

[133] G. S. Foo, A. K. Rogers, M. M. Yung, C. Sievers, *ACS Catalysis* **2016**, *6*, 1292–1307.

[134] R. C. Runnebaum, T. Nimmanwudipong, D. E. Block, B. C. Gates, *Catal. Sci. Technol.* **2012**, *2*, 113–118.

[135] P. A. Alaba, Y. M. Sani, I. Y. Mohammed, W. M. A. Wan Daud, *Reviews in Chemical Engineering* **2016**, *32*, 71–91.

[136] S. Cheng, L. Wei, X. Zhao, J. Julson, *Catalysts* **2016**, *6*, 195–219.

[137] X Xtrine, M. H. Dabrosd, X Xmagnus, Z. Stummannd, X. Højd, X Xpeter, A. Jensend, X.-D. Grunwaldtd, X Xjostein Gabrielsend, M Mortensend, X Xanker, D. Jensend, T. M. Dabros, M. Z. Stummann, M. Høj, P. A. Jensen, J. D. Grunwaldt, J. Gabrielsen, P. M. Mortensen, A. D. Jensen, *Progress in Energy and Combustion Science* **2018**, *68*, 268–309.

[138] I. Hita, T. Cordero-Lanzac, G. Bonura, C. Cannilla, J. M. Arandes, F. Frusteri, J. Bilbao, *Journal of Industrial and Engineering Chemistry* **2019**, *80*, 392–400.

[139] B. Valle, P. Castaño, M. Olazar, J. Bilbao, A. G. Gayubo, *Journal of Catalysis* **2012**, *285*, 304–314.

[140] A. Ibarra, A. Veloso, J. Bilbao, J. M. Arandes, P. Castaño, *Applied Catalysis B: Environmental* **2015**, *182*, 336–346.

[141] D. C. Elliott, H. Wang, R. French, S. Deutch, K. Iisa, *Energy and Fuels* **2014**, *28*, 5909–5917.

[142] D. C. Elliott, H. Wang, M. Rover, L. Whitmer, R. Smith, R. Brown, *ACS Sustainable Chemistry and Engineering* **2015**, *3*, 892–902.

[143] D. C. Elliott, T. R. Hart, G. G. Neuenschwander, L. J. Rotness, A. H. Zacher, *Environmental progress & Sustainable Energy* **2009**, *28*, 441–449.

[144] H. Marsh, F. Rodríguez-Reinoso, *Activated Carbon*, Elsevier B.V., **2006**.

[145] S. Gupta, N. H. Tai, *Journal of Materials Chemistry A* **2016**, *4*, 1550–1565.

[146] X. Zhuang, Y. Wan, C. Feng, Y. Shen, D. Zhao, *Chemistry of Materials* **2009**, *21*, 706–716.

[147] A. H. Van Pelt, O. A. Simakova, S. M. Schimming, J. L. Ewbank, G. S. Foo, E. A. Pidko, E. J. Hensen, C. Sievers, *Carbon* **2014**, *77*, 143–154.

[148] G. Pognon, T. Brousse, L. Demarconnay, D. Bélanger, *Journal of Power Sources* **2011**, *196*, 4117–4122.

[149] R. Berenguer, R. Ruiz-Rosas, A. Gallardo, D. Cazorla-Amorós, E. Morallón, H. Nishihara, T. Kyotani, J. Rodríguez-Mirasol, T. Cordero, *Carbon* **2015**, *95*, 681–689.

[150] M. E. Ramos, P. R. Bonelli, A. L. Cukierman, *Colloids and Surfaces A: Physicochemical and Engineering Aspects* **2008**, *324*, 86–92.

[151] T. Cordero-Lanzac, F. J. García-Mateos, J. M. Rosas, J. Rodríguez-Mirasol, T. Cordero, *Carbon* **2018**, *139*, 599–608.

[152] M. Lallave, J. Bedia, R. Ruiz-Rosas, J. Rodríguez-Mirasol, T. Cordero, J. C. Otero, M. Marquez, A. Barrero, I. G. Loscertales, *Advanced Materials* **2007**, *19*, 4292–4296.

[153] M. Malekshahian, J. M. Hill, *Energy and Fuels* **2011**, *25*, 5250–5256.

[154] V. K. Gupta, B. Gupta, A. Rastogi, S. Agarwal, A. Nayak, *Journal of Hazardous Materials* **2011**, *186*, 891–901.

[155] J. Alvarez, G. Lopez, M. Amutio, J. Bilbao, M. Olazar, *Industrial and Engineering Chemistry Research* **2015**, *54*, 7241–7250.

[156] A. R. Mohamed, M. Mohammadi, G. N. Darzi, *Renewable and Sustainable Energy Reviews* **2010**, *14*, 1591–1599.

[157] J. M. Rosas, J. Bedia, J. Rodríguez-Mirasol, T. Cordero, *Fuel Processing Technology* **2010**, *91*, 1345–1354.

[158] M. Calzado, M. Valero-Romero, P. Garriga, A. Chica, M. Guerrero-Pérez, J. Rodríguez-Mirasol, T. Cordero, *Catalysis Today* **2015**, *257*, 229–236.

[159] Y. Shen, *Renewable and Sustainable Energy Reviews* **2015**, *43*, 281–295.

[160] F. J. García-Mateos, PhD thesis, University of Malaga, **2017**.

[161] M. J. Bleda-Martínez, D. Lozano-Castelló, E. Morallón, D. Cazorla-Amorós, A. Linares-Solano, *Carbon* **2006**, *44*, 2642–2651.

[162] F. Rodríguez-Reinoso, M. Molina-Sabio, *Carbon* **1992**, *30*, 1111–1118.

[163] J. M. Rosas, R. Berenguer, M. J. Valero-Romero, J. Rodríguez-Mirasol, T. Cordero, *Frontiers in Materials* **2014**, *1*, 29.

[164] M. J. Valero-Romero, F. J. García-Mateos, J. Rodríguez-Mirasol, T. Cordero, *Fuel Processing Technology* **2017**, *157*, 116–126.

[165] A. C. Lua, T. Yang, *Journal of Colloid and Interface Science* **2004**, *274*, 594–601.

[166] D. Y. Ryu, T. Shimohara, K. Nakabayashi, J. Miyawaki, J. I. Park, S. H. Yoon, *Journal of Industrial and Engineering Chemistry* **2019**, *80*, 98–105.

[167] W. Liu, J. Xiao, Q. Xu, X. Liu, S. Zhong, H. Huang, M. Zheng, S. R. Kirk, D. Yin, *RSC Advances* **2019**, *9*, 185–191.

[168] O. Sufiani, H. Tanaka, K. Teshima, R. L. Machunda, Y. A. Jande, *Separation and Purification Technology* **2020**, *247*, 116998.

[169] R. Elazari, G. Salitra, A. Garsuch, A. Panchenko, D. Aurbach, *Advanced Materials* **2011**, *23*, 5641–5644.

[170] A. M. M. Puziy, O. I. I. Poddubnaya, A Martínez-Alonso, F Suárez-García, J. M. D. Tascón, *Carbon* **2002**, *40*, 1507–1519.

[171] J. Palomo, J. J. Ternero-Hidalgo, J. M. Rosas, J. Rodríguez-Mirasol, T. Cordero, *Fuel Processing Technology* **2017**, *156*, 438–445.

[172] T. Cordero-Lanzac, J. M. Rosas, F. J. García-Mateos, J. J. Ternero-Hidalgo, J. Palomo, J. Rodríguez-Mirasol, T. Cordero, *Carbon* **2018**, *126*, 65–76.

[173] M. Jagtoyen, F. Derbyshire, *Carbon* **1998**, *36*, 1085–1097.

[174] B. L. Browning, *The chemistry of wood*, Robert E. Krieger Pub. Co, NY, **1975**.

[175] C. Huang, A. M. Puziy, T. Sun, O. I. Poddubnaya, F. Suárez-García, J. M. D. Tascón, D. Hulicova-Jurcakova, *Electrochimica Acta* **2014**, *137*, 219–227.

[176] J. Figueiredo, M. Pereira, M. Freitas, J. Órfão, *Carbon* **1999**, *37*, 1379–1389.

[177] J. M. Rosas, J. Bedia, J. Rodríguez-Mirasol, T. Cordero, *Fuel* **2009**, *88*, 19–26.

[178] J. M. Rosas, R. Ruiz-Rosas, J. Rodríguez-Mirasol, T. Cordero, *Carbon* **2012**, *50*, 1523–1537.

[179] D. W. McKee, C. L. Spiro, E. J. Lamby, *Carbon* **1984**, *22*, 285–290.

[180] S. Oh, N. Rodriguez, *Journal of Materials Research* **1993**, *8*, 2879–2888.

[181] X. Wu, L. R. Radovic, *Carbon* **2006**, *44*, 141–151.

[182] M. M. Alam, M. A. Hossain, M. D. Hossain, M. A. Johir, J. Hossen, M. S. Rahman, J. L. Zhou, A. T. Hasan, A. K. Karmakar, M. B. Ahmed, *Processes* **2020**, *8*, 203.

[183] O. Ioannidou, A. Zabaniotou, *Renewable and Sustainable Energy Reviews* **2007**, *11*, 1966–2005.

[184] Y. Boutillara, J. L. Tombeur, G. De Weireld, P. Lodewyckx, *Chemical Engineering Journal* **2019**, *372*, 631–637.

[185] M. Li, R. Xiao, *Fuel Processing Technology* **2019**, *186*, 35–39.

[186] Y. Guo, C. Tan, J. Sun, W. Li, J. Zhang, C. Zhao, *Chemical Engineering Journal* **2020**, *381*, 122736.

[187] K. Zhou, W. Ma, Z. Zeng, X. Ma, X. Xu, Y. Guo, H. Li, L. Li, *Chemical Engineering Journal* **2019**, *372*, 1122–1133.

[188] I. I. Laskar, Z. Hashisho, J. H. Phillips, J. E. Anderson, M. Nichols, *Separation and Purification Technology* **2019**, *212*, 632–640.

[189] G. Z. Kyzas, G. Bomis, R. I. Kosheleva, E. K. Efthimiadou, E. P. Favvas, M. Kostoglou, A. C. Mitropoulos, *Chemical Engineering Journal* **2019**, *356*, 91–97.

[190] D. Mohan, C. U. Pittman, *Journal of Hazardous Materials* **2006**, *137*, 762–811.

[191] W. Yin, C. Zhao, J. Xu, J. Zhang, Z. Guo, Y. Shao, *Colloids and Surfaces A* **2019**, *560*, 426–433.

[192] G. P. Mashile, A. Mpupa, A. Nqombolo, K. M. Dimpe, P. N. Nomngongo, *Journal of Water Process Engineering* **2020**, *33*, 101011.

[193] F. García-Mateos, R. Ruiz-Rosas, M. Marqués, L. Cotoruelo, J. Rodríguez-Mirasol, T. Cordero, *Chemical Engineering Journal* **2015**, *279*, 18–30.

[194] A. Şavk, H. Aydın, K. Cellat, F. Şen, *Journal of Molecular Liquids* **2020**, *300*, 112355.

[195] V. C. Hoang, K. N. Dinh, V. G. Gomes, *Carbon* **2020**, *157*, 515–524.

[196] B. Braunchweig, D. Hibbitts, M. Neurock, A. Wieckowski, *Catalysis Today* **2013**, *202*, 197–209.

[197] F. Béguin, V. Presser, A. Balducci, E. Frackowiak, *Advanced Materials* **2014**, *26*, 2219–2251.

[198] P. Schlee, O. Hosseinaei, D. Baker, A. Landmér, P. Tomani, M. J. Mostazo-López, D. Cazorla-Amorós, S. Herou, M. M. Titirici, *Carbon* **2019**, *145*, 470–480.

[199] F. Béguin, E. Frackowiak, *Carbons for electrochemical energy storage and conversion systems*, CRC Press, Taylor & Francis Group, **2015**.

[200] D. Salinas-Torres, R. Ruiz-Rosas, E. Morallón, D. Cazorla-Amorós, *Frontiers in Materials* **2019**, *6*, 1–24.

[201] R. Tang, M. Yamamoto, K. Nomura, E. Morallón, D. Cazorla-Amorós, H. Nishihara, T. Kyotani, *Journal of Power Sources* **2020**, *457*, 228042.

[202] D. Hulicova-Jurcakova, M. Seredych, G. Q. Lu, N. Kodiweera, P. E. Stallworth, S. Greenbaum, T. J. Bandosz, *Carbon* **2009**, *47*, 1576–1584.

[203] X. Zhao, S. Wang, Q. Wu, *Electrochimica Acta* **2017**, *247*, 1140–1146.

[204] M. Akhairi, S. Kamarudin, *International Journal of Hydrogen Energy* **2016**, *41*, 4214–4228.

[205] F. J. García-Mateos, T Cordero-Lanzac, R Berenguer, E Morallón, D Cazorla-Amorós, J Rodríguez-Mirasol, T Cordero, *Applied Catalysis B: Environmental* **2017**, *211*, 18–30.

[206] J. Bedia, R. Ruiz-Rosas, J. Rodríguez-Mirasol, T. Cordero, *Journal of Catalysis* **2010**, *271*, 33–42.

[207] M. Kimi, M. M. H. Jaidie, S. C. Pang, *Journal of Physics and Chemistry of Solids* **2018**, *112*, 50–53.

[208] H. Dai, Y. P. Qiu, H. B. Dai, P. Wang, *ACS Sustainable Chemistry and Engineering* **2018**, *6*, 9876–9882.

[209] A. S. Oliveira, J. A. Baeza, D. Garcia, B. Saenz de Miera, L. Calvo, J. J. Rodriguez, M. A. Gilarranz, *Renewable Energy* **2020**, *148*, 889–896.

[210] M. Martin-Martinez, J. J. Rodriguez, R. T. Baker, L. M. Gómez-Sainero, *Chemical Engineering Journal* **2020**, *397*, 125479.

[211] E. Mäkelä, R. Lahti, S. Jaatinen, H. Romar, T. Hu, R. L. Puurunen, U. Lassi, R. Karinen, *ChemCatChem* **2018**, *10*, 3269–3283.

[212] J. Bedia, J. M. Rosas, J. Rodríguez-Mirasol, T. Cordero, *Applied Catalysis B: Environmental* **2010**, *94*, 8–18.

[213] T. Cordero-Lanzac, I. Hita, A. Veloso, J. Arandes, J. Rodríguez-Mirasol, J. Bilbao, T. Cordero, P. Castaño, *Chemical Engineering Journal* **2017**, *327*, 454–464.

[214] E. Lam, J. H. T. Luong, *ACS Catalysis* **2014**, *4*, 3393–3410.

[215] C. Sepúlveda, K. Leiva, R. García, L. R. Radovic, I. T. Ghampson, W. J. Desisto, J. L. Fierro, N. Escalona, *Catalysis Today* **2011**, *172*, 232–239.

[216] J. Wildschut, M. Iqbal, F. H. Mahfud, I. M. Cabrera, R. H. Venderbosch, H. J. Heeres, *Energy & Environmental Science* **2010**, *3*, 962–970.

[217] Y. Elkasabi, C. A. Mullen, A. L. Pighinelli, A. A. Boateng, *Fuel Processing Technology* **2014**, *123*, 11–18.

[218] A. A. Dwiatmoko, L. Zhou, I. Kim, J.-W. W. Choi, D. J. Suh, J.-M. M. Ha, *Catalysis Today* **2016**, *265*, 192–198.

[219] I. Kim, A. A. Dwiatmoko, J. W. Choi, D. J. Suh, J. Jae, J. M. Ha, J. K. Kim, *Journal of Industrial and Engineering Chemistry* **2017**, *56*, 74–81.

[220] M. Marafi, A. Stanislaus, *Resources Conservation and Recycling* **2008**, *53*, 1–26.

[221] M. Breysse, P. Afanasiev, C. Geantet, M. Vrinat, *Catalysis Today* **2003**, *86*, 5–16.

[222] M. Stöcker, *Angewandte Chemie - International Edition* **2008**, *47*, 9200–9211.

[223] M. Tschulkow, T. Compernolle, S. Van den Bosch, J. Van Aelst, I. Storms, M. Van Dael, G. Van den Bossche, B. Sels, S. Van Passel, *Journal of Cleaner Production* **2020**, *266*, 122022.

[224] S. I. Mussatto, J. Moncada, I. C. Roberto, C. A. Cardona, *Bioresource Technology* **2013**, *148*, 302–310.

[225] M. C. Gutiérrez, J. M. Rosas, M. A. Rodríguez-Cano, I. López-Luque, J. Rodríguez-Mirasol, T. Cordero, *Energy Conversion and Management* **2019**, *182*, 201–214.

[226] S. Iştan, S. Ceylan, Y. Topcu, C. Hintz, J. Tefft, T. Chellappa, J. Guo, J. L. Goldfarb, *Energy Conversion and Management* **2016**, *127*, 576–588.

[227] N. Kaur, G. Singh, M. Khatri, S. K. Arya, *Journal of Cleaner Production* **2020**, *256*, 120607.

[228] A. Corma, G. W. Huber, L. Sauvanaud, P. O'Connor, *Journal of Catalysis* **2007**, *247*, 307–327.

[229] M. Bertero, U. Sedran, *Catalysis Today* **2013**, *212*, 10–15.

[230] M. Bertero, G. D. L. Puente, U. Sedran, *Renewable Energy* **2013**, *60*, 349–354.

[231] N. Thegarid, G. Fogassy, Y. Schuurman, C. Mirodatos, S. Stefanidis, E. F. Iliopoulou, K. Kalogiannis, A. A. Lappas, *Applied Catalysis B: Environmental* **2014**, *145*, 161–166.

[232] A Ibarra, E. Rodriguez, U. Sedran, J. M. Arandes, J. Bilbao, *I&EC Research* **2016**, *55*, 1872–1880.

[233] Á. Ibarra, I. Hita, M. J. Azkoiti, J. M. Arandes, J. Bilbao, *Journal of Industrial and Engineering Chemistry* **2019**, *78*, 372–382.

[234] J. Lu, A. Heyden, *Journal of Catalysis* **2015**, *321*, 39–50.

[235] J. Zhou, W. An, Z. Wang, X. Jia, *Catalysis Science & Technology* **2019**, *9*, 4314–4326.

[236] Y. He, Y. Bie, J. Lehtonen, R. Liu, J. Cai, *Fuel* **2019**, *239*, 1015–1027.

[237] P. Arora, E. L. Grennfelt, L. Olsson, D. Creaser, *Chemical Engineering Journal* **2019**, *364*, 376–389.

[238] A. Iino, A. Cho, A. Takagaki, R. Kikuchi, S. Ted Oyama, *Journal of Catalysis* **2014**, *311*, 17–27.

[239] P. J. Becker, N. Serrand, B. Celse, D. Guillaume, H. Dulot, *Fuel* **2016**, *165*, 306–315.

[240] Z. Till, T. Varga, J. Sója, N. Miskolczi, T. Chován, *Chemical Engineering Journal* **2019**, *375*, 121920.

[241] B. Browning, I. Pitault, F. Couenne, T. Jansen, M. Lacroix, P. Alvarez, M. Tayakout-Fayolle, *Chemical Engineering Journal* **2018**, *377*, 119811.

[242] B. K. Srinivas, K. K. Pant, S. K. Gupta, D. N. Saraf, I. R. Choudhury, M. Sau, *Chemical Engineering Journal* **2019**, *358*, 504–519.

[243] J. Pu, D. Laurenti, C. Geantet, M. Tayakout-Fayolle, I. Pitault, *Chemical Engineering Journal* **2020**, *386*, 121969.

[244] T. Cordero-Lanzac, A. T. Aguayo, A. G. Gayubo, P. Castaño, J. Bilbao, *Chemical Engineering Journal* **2018**, *331*, 818–830.

[245] I. Hita, PhD thesis, University of the Basque Country, **2015**.

[246] A. R. Fernandez-Akarregi, J. Makibar, G. Lopez, M. Amutio, M. Olazar, *Fuel Processing Technology* **2013**, *112*, 48–56.

[247] J. Bedia, R. Ruiz-Rosas, J. Rodríguez-Mirasol, T. Cordero, *AIChe Journal* **2010**, *56*, 1557–1568.

[248] J. Bedia, J. M. Rosas, J. Márquez, J. Rodríguez-Mirasol, T. Cordero, *Carbon* **2009**, *47*, 286–294.

[249] P. Castaño, D. van Herk, M. T. Kreutzer, J. A. Moulijn, M. Makkee, *Applied Catalysis B: Environmental* **2009**, *88*, 213–223.

[250] I. Hita, E. Rodríguez, M. Olazar, J. Bilbao, J. M. Arandes, P. Castaño, *Energy & Fuels* **2015**, *29*, 5458–5466.

[251] J. F. Moulder, W. F. Stickle, P. E. Sobol, K. D. Bomben, *Handbook of X-ray Photoelectron Spectroscopy*, **1995**.

[252] I. Hita, R. Palos, J. M. Arandes, J. M. Hill, P. Castaño, *Fuel Processing Technology* **2016**, *144*, 239–247.

[253] D. van Herk, P. Castaño, M. Quaglia, M. T. Kreutzer, M. Makkee, J. A. Moulijn, *Applied Catalysis A: General* **2009**, *365*, 110–121.

[254] G. Elordi, M. Olazar, P. Castaño, M. Artetxe, J. Bilbao, *Industrial and Engineering Chemistry Research* **2012**, *51*, 14008–14017.

[255] A. Ochoa, B. Aramburu, M. Ibáñez, B. Valle, J. Bilbao, A. G. Gayubo, P. Castaño, *ChemSusChem* **2014**, *7*, 2597–2608.

[256] P. Castaño, A. Gutiérrez, I. Hita, J. M. Arandes, A. T. Aguayo, J. Bilbao, *Energy and Fuels* **2012**, *26*, 1509–1519.

[257] A. Oasmaa, E. Kuoppala, A. Ardiyanti, R. H. Venderbosch, H. J. Heeres, *Energy and Fuels* **2010**, *24*, 5264–5272.

[258] R. H. Venderbosch, A. R. Ardiyanti, J. Wildschut, A. Oasmaa, H. J. Heeres, *Journal of Chemical Technology and Biotechnology* **2010**, *85*, 674–686.

[259] A. Gutiérrez, J. M. Arandes, P. Castaño, A. T. Aguayo, J. Bilbao, *Energy and Fuels* **2011**, *25*, 3389–3399.

[260] I. Hita, A. T. Aguayo, M. Olazar, M. J. Azkoiti, J. Bilbao, J. M. Arandes, P. Castaño, *Energy & Fuels* **2015**, *29*, 7542–7553.

[261] P. Tian, Y. Wei, M. Ye, Z. Liu, *ACS Catalysis* **2015**, *5*, 1922–1938.

[262] C. V. Loricera, P Castaño, A Infantes-Molina, I Hita, A Gutiérrez, J. M. Arandes, J. L. G. Fierro, B Pawelec, *Green Chemistry* **2012**, *14*, 2759–2770.

[263] C. Lievens, D. Mourant, M. He, R. Gunawan, X. Li, C. Z. Li, *Fuel* **2011**, *90*, 3417–3423.

[264] C. A. Mullen, G. D. Strahan, A. A. Boateng, *Energy and Fuels* **2009**, *23*, 2707–2718.

[265] M. Ibáñez, B. Valle, J. Bilbao, A. G. Gayubo, P. Castaño, *Catalysis Today* **2012**, *195*, 106–113.

[266] C. H. Bartholomew, *Applied Catalysis A: General* **2001**, *212*, 17–60.

[267] M. Guisnet, P. Magnoux, *Applied Catalysis A: General* **2001**, *212*, 83–96.

[268] K. M. Sundaram, U. Mukherjee, M. Baldassari, *Energy and Fuels* **2008**, *22*, 3226–3236.

[269] T. Cordero-Lanzac, R. Palos, J. M. Arandes, P. Castaño, J. Rodríguez-Mirasol, T. Cordero, J. Bilbao, *Applied Catalysis B: Environmental* **2017**, *203*, 389–399.

[270] R. Palos, A. Gutiérrez, J. M. Arandes, J. Bilbao, *Fuel* **2018**, *216*, 142–152.

[271] A. G. Marshall, R. P. Rodgers, *Accounts of Chemical Research* **2004**, *37*, 53–59.

[272] E. A. Smith, Y. J. Lee, *Energy and Fuels* **2010**, *24*, 5190–5198.

[273] M. Staš, J. Chudoba, M. Auersvald, D. Kubička, S. Conrad, T. Schulzke, M. Pospíšil, *Journal of Analytical and Applied Pyrolysis* **2017**, *124*, 230–238.

[274] E. Furimsky, *Industrial and Engineering Chemistry Product Research and Development* **1983**, *22*, 34–38.

[275] H. S. Cerqueira, C. Sievers, G. Joly, P. Magnoux, J. A. Lercher, *Industrial & Engineering Chemistry Research* **2005**, *44*, 2069–2077.

[276] R. Y. Nsimba, C. A. Mullen, N. M. West, A. A. Boateng, *ACS Sustainable Chemistry and Engineering* **2013**, *1*, 260–267.

[277] A. E. Pütün, E. Apaydin, E. Pütün, *Energy* **2002**, *27*, 703–713.

[278] P. Das, T. Sreelatha, A. Ganesh, *Biomass and Bioenergy* **2004**, *27*, 265–275.

[279] S. Zou, Y. Wu, M. Yang, C. Li, J. Tong, *Energy Environ. Sci.* **2010**, *3*, 1073–1078.

[280] M. C. Edelman, M. K. Maholland, R. M. Baldwin, S. W. Cowley, *Journal of Catalysis* **1988**, *111*, 243–253.

[281] E. M. Ryymin, M. L. Honkela, T. R. Viljava, A. O. I. Krause, *Applied Catalysis A: General* **2010**, *389*, 114–121.

[282] O. D. Mante, F. A. Agblevor, S. T. Oyama, R. McClung, *Fuel* **2014**, *117*, 649–659.

[283] O. D. Mante, F. A. Agblevor, *Green Chemistry* **2014**, *16*, 3364–3377.

[284] H. Y. Zhang, Y. G. Wang, P. Z. Zhang, X. C. Lin, Y. F. Zhu, *Journal of Fuel Chemistry and Technology* **2013**, *41*, 1085–1091.

[285] R. L. Tong, Y. G. Wang, X. Zhang, H. Y. Zhang, J. Z. Dai, X. C. Lin, D. P. Xu, *Journal of Fuel Chemistry and Technology* **2015**, *43*, 1461–1469.

[286] T. Cordero-Lanzac, R. Palos, I. Hita, J. M. Arandes, J. Rodríguez-Mirasol, T. Cordero, J. Bilbao, P. Castaño, *Applied Catalysis B: Environmental* **2018**, *239*, 513–524.

[287] I. Hita, A. Gutiérrez, M. Olazar, J. Bilbao, J. M. Arandes, P. Castaño, *Fuel* **2015**, *145*, 158–169.

[288] J Wildschut, F. H. Mahfud, R. H. Venderbosch, H. J. Heeres, *Industrial and Engineering Chemistry Research* **2009**, *48*, 10324–10334.

[289] I. Hita, P. Deuss, G. Bonura, F. Frusteri, H. Heeres, *Fuel Processing Technology* **2018**, *179*, 143–153.

[290] L. Negahdar, A. Gonzalez-Quiroga, D. Otyuskaya, H. E. Toraman, L. Liu, J. T. B. H. Jastrzebski, K. M. Van Geem, G. B. Marin, J. W. Thybaut, B. M. Weckhuysen, *ACS Sustainable Chemistry & Engineering* **2016**, *4*, 4974–4985.

[291] D. C. Perera, J. W. Hewage, N. De Silva, *Computational and Theoretical Chemistry* **2015**, *1064*, 1–6.

[292] B Valle, A. G. Gayubo, A. T. Aguayo, M Olazar, J Bilbao, *Energy and Fuels* **2010**, *24*, 2060–2070.

[293] E. Kantarelis, W. Yang, W. Blasiak, *Fuel* **2014**, *122*, 119–125.

[294] B. Valle, A. G. Gayubo, A. Alonso, A. T. Aguayo, J. Bilbao, *Applied Catalysis B: Environmental* **2010**, *100*, 318–327.

[295] S. Brunauer, P. H. Emmett, E. Teller, *Journal of the American Chemical Society* **1938**, *60*, 309–319.

[296] M. M. Dubinin, *Carbon* **1987**, *25*, 593–598.

[297] I. Hita, T. Cordero-Lanzac, F. J. García-Mateos, M. J. Azkoiti, J. Rodríguez-Mirasol, T. Cordero, J. Bilbao, *Applied Catalysis B: Environmental* **2019**, *259*, 118112.

[298] J. Makibar, A. R. Fernandez-Akarregi, M. Amutio, G. Lopez, M. Olazar, *Fuel Processing Technology* **2015**, *137*, 283–289.

[299] A. Izadbakhsh, F. Khorasheh, *Chemical Engineering Science* **2011**, *66*, 6199–6208.

[300] R. D. Skeel, M. Berzins, *SIAM Journal on Scientific and Statistical Computing* **1990**, *11*, 1–32.

[301] A. Ochoa, B. Valle, D. E. Resasco, J. Bilbao, A. G. Gayubo, P. Castaño, *ChemCatChem* **2018**, *10*, 2311–2321.

[302] A. T. Aguayo, A. G. Gayubo, J Ereña, A Atutxa, J Bilbao, *Industrial and Engineering Chemistry Research* **2003**, *42*, 3914–3921.

[303] P. Magnoux, H. S. Cerqueira, M. Guisnet, *Applied Catalysis A: General* **2002**, *235*, 93–99.

[304] A. G. Gayubo, A. T. Aguayo, A. L. Morán, M. Olazar, J. Bilbao, *AIChE Journal* **2002**, *48*, 1561–1571.

[305] J. Corella, *Industrial and Engineering Chemistry Research* **2004**, *43*, 4080–4086.

[306] S. Li, S. Zhang, Z. Feng, Y. Yan, *Environmental progress & Sustainable Energy* **2014**, *33*, 1373–1379.

Appendix A

Related publications

UNIVERSIDAD
DE MÁLAGA

UNIVERSIDAD
DE MÁLAGA

Applied Catalysis B: Environmental 203 (2017) 389–399

Contents lists available at ScienceDirect

Applied Catalysis B: Environmental

journal homepage: www.elsevier.com/locate/apcatb

Stability of an acid activated carbon based bifunctional catalyst for the raw bio-oil hydrodeoxygenation

Tomás Cordero-Lanzac[a], Roberto Palos[a], José M. Arandes[a], Pedro Castaño[a,*], José Rodríguez-Mirasol[b], Tomás Cordero[b], Javier Bilbao[a]

[a] *Department of Chemical Engineering, University of the Basque Country UPV/EHU, P.O. Box 644-48080, Bilbao, Spain*
[b] *Universidad de Málaga, Department of Chemical Engineering, Campus de Teatinos s/n 29010, Málaga, Spain*

ARTICLE INFO

Article history:
Received 13 June 2016
Received in revised form 4 October 2016
Accepted 8 October 2016
Available online 11 October 2016

Keywords:
Bio-Oil upgrading
Biofuels
Pt-Pd bifunctional catalyst
Activated carbon
Coke deactivation

ABSTRACT

The performance (activity, selectivity and stability) of a Pt-Pd catalyst supported on a phosphorus-containing activated carbon (ACP) has been studied in the hydrodeoxygenation (HDO) of raw bio-oil, and compared with another bifunctional catalyst prepared with a FCC (Fluid Catalytic Cracking) catalyst as acid support. Experiments have been carried out in a fixed bed reactor under the following conditions: 400–450 °C; 65 bar; space time, 0.18 $g_{cat}\ h\ g^{-1}_{bio\text{-}oil}$; H_2:bio-oil ratio, 20 cm^3_{H2} (STP) $cm^{-3}_{bio\text{-}oil}$; time on stream, 0–10 h. The catalyst reaches a pseudo-steady state at 450 °C after 6 h of time on stream, preserving a constant activity as a consequence of the simultaneous formation and hydrocracking of the deposited coke. In these conditions, the yield of C_{5+} hydrocarbons is 20 wt%. This organic liquid fraction mainly contains aromatics, and thus, it may require an additional mild hydrocracking treatment for its valorization as fuel. On the other hand, the gas fraction obtained can be used directly as fuel, and the aqueous liquid fraction (with a high concentration of methanol, 58 wt%) is interesting as co-feedstock with methanol in a methanol to olefins (MTO) unit.

© 2016 Elsevier B.V. All rights reserved.

1. Introduction

Fast pyrolysis of lignocellulosic biomass is an attractive process to obtain fuels and raw materials. An advantage of this route in relation to the other ones from biomass, is that it can be carried out in geographically delocalized units, and its liquid product (bio-oil) can be valorized at large scale in refinery units. Moreover, fast pyrolysis technology has been extensively developed and it allows for obtaining up to 75 wt% of bio-oil in relatively simple units and involving production costs lower than the required ones for competing technologies based on other thermochemical routes [1–3].

Bio-oil contains hundreds of organic compounds mostly in low concentrations (acids, alcohols, aldehydes, esters, ketones, and a large proportion (20–30 wt%) of lignin-derived phenols) [4], with a significant amount of water (up to 50 wt%). Its main properties (poor stability, low heating value, poor volatility, corrosiveness, high viscosity) exclude its direct usage as internal combustion engine fuel. This drawback has encouraged several transformation routes for enhancing its composition [5,6]. Main strategies are: (i) bio-oil cracking-deoxygenation; associated with pyrolysis, using an acid catalyst (usually a zeolite) in situ in the pyrolysis reactor [7,8], or in a fixed bed reactor coupled on-line in order to transform pyrolysis reactor effluents [9,10]; (ii) bio-oil hydrodeoxygenation (HDO); even though it requires a high H_2 consumption and working at relatively harsh conditions, it allows for obtaining a product with enhanced quality for fuel applications [11,12]. Reactions that take place in the HDO process are [13]: hydrogenolysis of the C–O bond (forming water as a byproduct), dehydration, decarboxylation, hydrogenation of unsaturated compounds and hydrocracking (C–C bond cleavage through a carbocation mechanism).

It is widely assumed that, the large scale bio-oil valorization route requires using the existing refinery infrastructure, co-feeding the bio-oil with the standard feedstock to fluid catalytic cracking (FCC) or to hydroprocessing units [3,14,15]. Considering the versatility of the FCC unit and its presence in most refineries, this route has been extensively studied, particularly using bio-oil model compounds, or its fractions or the pretreated bio-oil (hydrogenated) [16–19]. The results obtained from the cracking of vacuum gas oil (VGO) and raw bio-oil mixture (20 wt%) under FCC conditions, have shown the advantages of co-feeding bio-oil due to the existence of mechanistical synergies between oxygenates and hydrocarbons [20]. On the other hand, this route offers the following disadvan-

---

* Corresponding author.
E-mail address: pedro.castano@ehu.eus (P. Castaño).

http://dx.doi.org/10.1016/j.apcatb.2016.10.018
0926-3373/© 2016 Elsevier B.V. All rights reserved.

UNIVERSIDAD
DE MÁLAGA

Applied Catalysis B: Environmental 239 (2018) 513–524

Contents lists available at ScienceDirect

Applied Catalysis B: Environmental

journal homepage: www.elsevier.com/locate/apcatb

Revealing the pathways of catalyst deactivation by coke during the hydrodeoxygenation of raw bio-oil

Tomás Cordero-Lanzac[a], Roberto Palos[a], Idoia Hita[a,b], José M. Arandes[a], José Rodríguez-Mirasol[c], Tomás Cordero[c], Javier Bilbao[a], Pedro Castaño[a,*]

[a] *Department of Chemical Engineering, University of the Basque Country (UPV/EHU), PO Box 644-48080, Bilbao, Spain*
[b] *Chemical Engineering Department, University of Groningen, Nijenborgh 4, 9747 AG, Groningen, The Netherlands*
[c] *Universidad de Málaga, Department of Chemical Engineering, Andalucia Tech., Campus de Teatinos s/n, 29010, Málaga, Spain*

ARTICLE INFO

Keywords:
Hydrodeoxygenation (HDO)
Bio-oil
Metal supported catalyst
Catalyst deactivation
Coke formation
Mechanisms

ABSTRACT

Virtually all processes aiming for fuels and chemicals from biomass entail no less than one step for removing oxygen by hydrodeoxygenation (HDO). The bottleneck of HDO is the formation of deactivating carbonaceous species on the catalyst surface. In this work, we have studied the deactivation pathways of catalysts based on noble metal nanoparticles (Pt-Pd) supported on mildly acid supports during the HDO of raw bio-oil. At conditions of accelerated deactivation, monitoring the evolution with time on stream of hydrocarbon and oxygenated compounds in the reaction medium, the intermediates on the catalyst surface and the nature-location of deactivating species, two parallel deactivation routes have been revealed: the deposition of (i) thermal or pyrolytic lignin from alkylmethoxy phenols, on the catalyst mesopores and favored at low temperature, and; of (ii) aromatic coke from polycyclic aromatic hydrocarbons, starting on the catalyst micropores through condensation reactions and promoted by acidic sites and high temperature. Nevertheless, catalyst deactivation can be controlled within limits at harsh temperature conditions (450 °C) due to the preferential HDO of alkyl(methoxy) phenols into aromatics and the formation-hydrocracking steady state of the aromatic precursors of coke.

1. Introduction

Bio-oil (liquid product of biomass fast pyrolysis) is getting great attention as an alternative source to petroleum for a more sustainable production of fuels and platform chemicals [1]. Nevertheless, oxygen removal through hydrodeoxygenation (HDO) is a required operation in order to stabilize it before its storage [2], and make the most of its great potential as a fuel [3] or as a feedstock in new or conventional refinery units [4–6]. Essentially, all biomass-derived streams for producing fuels and chemicals show similar HDO requirements. The HDO of bio-oil is commonly carried out over Ni, Mo or W supported catalysts [7–13]. However, noble metal-based catalysts (Pt, Pd, Rh or Ru) [14–20], as well as supported bimetallic catalysts [21,22], show higher activity for HDO and allow for using less severe operational conditions. In these works in the literature, the use of both neutral (α-alumina) and acid (activated carbon, γ-alumina, silica-alumina) supports (thus forming metallic or bifunctional catalysts) have been reported for the preparation of the catalysts.

One of the main drawbacks of this reaction is the catalyst deactivation due to the formation of carbonaceous deposits (coke), which also causes operational difficulties [23–28]. This formation of coke is related to the thermal instability and repolymerization of the phenolic components of bio-oil. In this regard, the use of noble metal-based catalysts (especially Pt catalysts) is recommended for attenuating the deactivation since they promote the hydrocracking of coke precursors [24]. Moreover, recent works have shown interesting results of HDO using a two-stage process formed by sequenced mild and deep HDO [29–31]. In both cases, noble metals are commonly used (mainly in the first stage where deactivation is of critical importance and low temperatures are required) and the positive effect of stabilizing the bio-oil in a prior step was demonstrated to favor the production of liquid hydrocarbons in the second one. This configuration has been deeply investigated by the group of Elliott [29–31] attaining hydrocarbon yields of ca. 50 wt%, which evidences its attractiveness. Other authors have proposed modifications in the pyrolysis stage (catalytic pyrolysis [32–34] or hydropyrolysis [35,36], among others) in order to improve the stability of the feedstock and the operability of HDO.

Another significant hurdle is the high content of water in the reaction medium due to its presence in the raw bio-oil (> 50 wt%) [28,37] and its formation during the HDO reaction. In addition to their

UNIVERSIDAD
DE MÁLAGA

---

* Corresponding author.
E-mail address: pedro.castano@ehu.eus (P. Castaño).

https://doi.org/10.1016/j.apcatb.2018.07.073
Received 27 May 2018; Received in revised form 23 July 2018; Accepted 27 July 2018
Available online 29 July 2018
0926-3373/ © 2018 Elsevier B.V. All rights reserved.

UNIVERSIDAD
DE MÁLAGA

Applied Catalysis B: Environmental 259 (2019) 118112

Contents lists available at ScienceDirect

Applied Catalysis B: Environmental

journal homepage: www.elsevier.com/locate/apcatb

Enhanced production of phenolics and aromatics from raw bio-oil using HZSM-5 zeolite additives for PtPd/C and NiW/C catalysts

Idoia Hita[a,*], Tomás Cordero-Lanzac[a], Francisco J. García-Mateos[b], M. Josune Azkoiti[a], José Rodríguez-Mirasol[b], Tomás Cordero[b], Javier Bilbao[a]

[a] Department of Chemical Engineering, University of the Basque Country (UPV/EHU), PO Box 644-48080, Bilbao, Spain
[b] Universidad de Málaga, Department of Chemical Engineering, Andalucia Tech., Campus de Teatinos s/n, 29010 Málaga, Spain

ARTICLE INFO

Keywords:
Hydrodeoxygenation
Activated carbon catalyst
Zeolite
Aromatics
Phenolics

ABSTRACT

This study delves into the performance of a Pt-Pd and a Ni-W catalyst supported on a phosphorus-containing activated carbon (ACP) in the hydrodeoxygenation (HDO) of raw bio-oil, as well as the enhancement of phenolic and aromatic product yields produced by incorporating physically mixed HZSM-5 zeolites (20 wt%) of different Si/Al ratio (15 and 140 in zeolites Z15 and Z140, respectively) in the catalytic bed. The HDO runs have been conducted in a fixed bed reactor at: 450 °C; 65 bar; space time, 0.15 $g_{cat}\ h\ g_{bio\text{-}oil}^{-1}$; 90 ml min^{-1} H_2; and time on stream up to 6 h. After a fast initial deactivation due to coke deposition the catalysts reached a pseudosteady state at which the carbon product yields are higher than in fresh catalyst conditions. The NiW catalyst provided yields of 42.3 wt% liquid carbon products (in a dry bio-oil basis), yielding 5.3 wt% phenolic and 12.3 wt% aromatic product yields. The NiW + Z140 combination was the most efficient catalyst (with a 47.3 wt% carbon production, including 6.8 wt% phenolics and 15.5 wt% aromatics) as a consequence of this low-acidity zeolite promoting the synergy with the dehydrogenation activity of metallic sites by favoring the acid-catalyzed cracking reactions of the bio-oil oxygenates, while simultaneously limiting gas product and coke formation. Two types of coke were detected, of thermal origin and catalytic coke, with the formation of the latter being dependent on the acidity of the zeolite.

1. Introduction

Biomass-derived feedstock is attracting great research interest due to the foreseeable midterm depletion of fossil resources and increasing strict environmental policies. Specifically, fast pyrolysis of biomass offers promising possibilities given its limited environmental impact, and great potential for the valorization of the resulting products at an industrial refinery scale, particularly the liquid fraction which is known as bio-oil [1,2].

Bio-oil is a highly complex mixture of water (up to 50%, depending on the biomass source [3]) and a wide array of organic oxygenates which originate from the depolymerization of holocellulose (comprising cellulose and hemicellulose) and lignin. A detailed classification of the oxygenates present in bio-oil would distinguish phenols, ketones, acids, esters, aldehydes, alcohols, furans, anhydrous-sugars, nitrogen-containing compounds, and carboxylic acids [4]. Its low stability, high viscosity, corrosiveness and difficulty of storage prevent its wider application as a fuel and, therefore, the necessity to adequate its composition has boosted the research of a number of upgrading routes (i.e. steam reforming [5,6], catalytic cracking and hydroprocessing [7]). The hydrodeoxygenation (HDO) approach outstands for providing stabilized bio-oil with enhanced fuel applications [8], and high-quality products, as phenolics and aromatics. The main sets of reactions that take place in the HDO of bio-oil are: C—O bond hydrogenolysis, dehydration, decarboxylation, hydrogenation of unsaturated components and C—C bond cleavage [9].

So far, HDO has primarily been explored over conventional sulfided transition metals comprising Ni, Mo, Co, W and/or combinations of these. Nonetheless, the high tendency towards coke formation of these catalysts, as well as the necessity to add an external sulfur source to the reaction media for their activation, direct catalyst preference towards noble metal-based catalysts (i.e. Ru, Rh, Pd, Pt, or bimetallic combinations) which, in addition, provide a higher activity at milder operation conditions [7]. The addition of a second metal can avoid problems with Pd sintering [10]. On the other hand, PtPd catalysts perform stably during hydroprocessing, with a higher hydrogenation activity that the monometallic Pt and Pd counterparts [11].

Given the complexity of unraveling the catalytic conversion of real

---

[*] Corresponding author.
E-mail address: idoia.hita@ehu.eus (I. Hita).

https://doi.org/10.1016/j.apcatb.2019.118112
Received 18 December 2018; Received in revised form 17 July 2019; Accepted 22 August 2019
Available online 23 August 2019
0926-3373/ © 2019 Elsevier B.V. All rights reserved.

UNIVERSIDAD
DE MÁLAGA

Chemical Engineering Journal 400 (2020) 124679

Contents lists available at ScienceDirect

Chemical Engineering Journal

journal homepage: www.elsevier.com/locate/cej

Adaptable kinetic model for the transient and pseudo-steady states in the hydrodeoxygenation of raw bio-oil

Tomás Cordero-Lanzac[a,b], Idoia Hita[a,c], Francisco J. García-Mateos[b], Pedro Castaño[a,c], José Rodríguez-Mirasol[b], Tomás Cordero[b,*], Javier Bilbao[a]

[a] Department of Chemical Engineering, University of the Basque Country (UPV/EHU), PO BOX 644-48080 Bilbao, Spain
[b] Universidad de Málaga, Andalucia Tech, Department of Chemical Engineering, Campus de Teatinos, s/n, 29010 Málaga, Spain
[c] Multiscale Reaction Engineering, KAUST Catalysis Center (KCC), King Abdullah University of Science and Technology (KAUST), Thuwal 23955-6900, Saudi Arabia

HIGHLIGHTS

- Two kinetic stages are observed in the HDO of raw bio-oil on a bifunctional catalyst.
- Transient and pseudo-steady states are modeled with a lump-based kinetic model.
- A selective deactivation model predicts the evolution with time of HDO.
- Deposition of solid products is predicted at the beginning of the transient state.
- A simplification of the model reproduces the data in the pseudo-steady state.

GRAPHICAL ABSTRACT

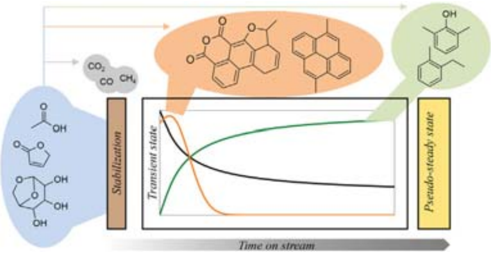

ARTICLE INFO

Keywords:
Bio-oil hydrodeoxygenation
Kinetic model
Activated carbon
Bifunctional catalyst
Thermal lignin
Coke

ABSTRACT

The hydrodeoxygenation (HDO) of raw bio-oil is an attractive route for the production of fuels and chemicals from biomass. For the sake of advancing towards the implantation of HDO at larger scale, an adaptable kinetic model is presented for this process. A CoMo bifunctional catalyst supported on an activated carbon has been used. The P-functionalities of the activated carbon support provide the catalyst with enhanced acidic features. The HDO runs have been carried out in a continuous packed bed reactor at 425–475 °C. Two subsequent reaction stages have been observed during the experimental runs: a transient and a pseudo-steady state. In the former stage, the catalyst is partially deactivated whereas in the latter, an apparent constant activity is reached. The model decodes the complex reaction network of HDO with seven lumps and eleven reaction steps. The proposed model accounts for the evolution with time of the reaction medium composition in the transient state, considering the reactions involved in the gas phase and the ones of solid product deposition and catalyst deactivation. Important contributions of decarboxylation/decarbonylation/decomposition and repolymerization pathways towards CO/CO_2/CH_4 and thermal lignin are observed. The model also estimates the product distribution in the pseudo-steady state, in which the net deposition of solid products and the catalyst deactivation are negligible. In this state, the catalyst shows a partially inhibited conversion of phenolic compounds and the maximum yield of aromatics, which are the most interesting value-added chemicals. The proposed kinetic model could play a key role in the design of reactors for the HDO process at higher scale.

---

[*] Corresponding author.
E-mail address: tomas.cordero@ehu.eus (T. Cordero).

https://doi.org/10.1016/j.cej.2020.124679
Received 17 December 2019; Received in revised form 3 March 2020; Accepted 5 March 2020
Available online 12 March 2020
1385-8947/ © 2020 Elsevier B.V. All rights reserved.